POLITECNICO DI MILANO

School of Industrial and Information Engineering

Master Degree in Materials Engineering and Nanotechnology

Linear sp carbon chains-polymer nanocomposites by Pulsed Laser Ablation in Liquid

Supervisor: Prof. Carlo S. Casari

Co-supervisor: Dr. Sonia Peggiani

Dr. Anna Facibeni

Master Thesis of:

Stefano Sala

Matr. 905146

Academic Year 2019-2020

Abstract

In the last decades the development of novel carbon nanomaterials has opened up promising perspectives for several nanoengineering applications. More recently, great progresses have been made in the field of Carbon Atomic Wires (CAWs), pure 1D carbon systems arranged in sp-hybridized linear chains in form of cumulenes or polyynes. Even though exceptional properties have been theoretically predicted, the highly reactive *sp* electronic configuration causes critical stability issues, limiting CAWs application in advanced devices. Among the approaches developed to prevent linear chains fast degradation, the incorporation of such nanostructures in polymeric nanocomposites is a very effective strategy. In this thesis work we investigate the synthesis of polyynes by Pulsed Laser Ablation in Liquid (PLAL) and their encapsulation in a poly(methyl methacrylate) (PMMA) matrix. In order to obtain such nanocomposites, we developed an *in situ* synthesis process, which involves the ablation of a graphite target directly in a PMMA solution in acetone, allowing to produce polyynes in a polymeric solution in a single-step process. The presence of dissolved PMMA in the PLAL solvent plays a key role in the stabilization of synthesized polyynes. To demonstrate the successful encapsulation of polyynes in the PMMA matrix and to investigate on their stability improvement, silver nanoparticles have been introduced in the nanocomposite, allowing to characterize the samples by means of surface-enhanced Raman scattering (SERS) measurements. Moreover, the adsorption of polyynes on Ag NPs surface provides a further contribution to their stability enhancement. Two different approaches have been followed in order to add Ag NPs to the nanocomposite: firstly they have been added from an aqueous Ag colloid produced by chemical reduction methods, while in the second method they have been synthesized by PLAL in the PMMA solution before ablating the graphite target, in a sort of "all PLAL"-based nanocomposite. Despite the different nature of used Ag NPs, in both kinds of samples the typical *sp* carbon SERS signals have been detected after 21 weeks after solidification, confirming the stability enhancement of polyynes immobilized in polymeric nanocomposites.

Sommario

Negli ultimi decenni lo sviluppo di nuovi nanomateriali di carbonio ha aperto prospettive promettenti in diverse ambiti di nanoingegneria. Di recente, grandi passi avanti sono stati fatti nel campo dei Carbon Atomic Wires (CAWs), sistemi di carbonio puramente 1D organizzati in catene lineari con ibridazione *sp* in forma di cumuleni e poliine. Sebbene dalle previsioni teoriche i CAWs siano dotati di proprietà eccezionali, il loro uso in dispositivi avanzati è limitato dalla particolare reattività della configurazione elettronica di tipo *sp*, che comporta grosse criticità dal punto di vista della stabilità. Tra le tecniche sviluppate per prevenire la veloce degradazione delle catene lineari, una strategia efficiente consiste nell'incorporazione di tali nanostrutture in nanocompositi polimerici. In questo lavoro di tesi approfondiamo la sintesi di poliine tramite Pulsed Laser Ablation in Liquid (PLAL) e il loro incapsulamento in una matrice di polimetilmetacrilato (PMMA). Al fine di ottenere questi nanocompositi abbiamo sviluppato un processo di sintesi *in situ*, che consiste nell'ablazione laser di un target di grafite direttamente in una soluzione di PMMA e acetone, permettendo di produrre le poliine in una soluzione polimerica tramite un processo single-step. La presenza di PMMA nel solvente usato per la PLAL svolge un ruolo fondamentale nella stabilizzazione delle poliine formate. Per dimostrare il riuscito incapsulamento di poliine nella matrice di PMMA, e per verificarne il miglioramento di stabilità, delle nanoparticelle di argento sono state introdotte nel sistema, permettendo la caratterizzazione dei campioni attraverso misure di spettroscopia Raman amplificata da superfici (SERS). Inoltre, l'adsorbimento di poliine sulla superficie delle nanoparticelle di Ag fornisce un ulteriore contributo nel miglioramento della loro stabilità. Per aggiungere le nanoparticelle di Ag nel nanocomposito sono stati seguiti due approcci diversi: in primo luogo esse sono state aggiunte da un colloide di Ag in soluzione acquosa, preparato tramite un processo di riduzione chimica, mentre in un secondo metodo esse sono state sintetizzate tramite PLAL nella soluzione di PMMA, prima di ablare il target di grafite, in una sorta di nanocomposito "all PLAL"-based. Nonostante la diversa natura delle nanoparticelle di Ag usate, in entrambe le

tipologie di campione i tipici segnali SERS del carbonio *sp* sono stati osservati anche dopo 21 settimane dalla solidificazione, confermando l'aumento di stabilità delle poliine immobilizzate nei nanocompositi polimerici.

Ringraziamenti

Portare a termine questo percorso non è stato affatto semplice, ma dal momento che siamo arrivati alla fine, il primo enorme ringraziamento va alla mia famiglia. Grazie a mamma, papà e Cecilia per il vostro supporto incondizionato in questi anni, per avermi sempre incoraggiato dopo gli insuccessi e per aver gioito con me dopo le vittorie. Grazie anche per avermi sopportato a ridosso degli esami, cercando sempre di stemperare la tensione e facendo in modo che ci dedicassi tutto il tempo necessario, senza farmi mai mancare nulla. Ringrazio mia nonna Mariuccia, un autentico esempio di passione e resilienza, per aver seguito con curiosità e apprensione tutto il mio percorso. Ringrazio infine i miei nonni Gianni, Bambina e Ugo: so quanto sareste fieri di me e sarete sempre nel mio cuore.

Svolgere l'attività sperimentale della tesi magistrale presso il NanoLab è stata un'esperienza formativa a 360 gradi, unica nel suo genere. Per questo motivo ringrazio il mio relatore, il professore Carlo Casari per avermi accolto come tesista, supervisionando l'intera attività sperimentale e indirizzandomi sempre in modo gentile e costruttivo. Grazie ad Anna, che con affetto materno mi ha fatto sentire parte di una grande famiglia sin dal primo giorno in cui ho messo piede in laboratorio, offrendomi i suoi consigli e la sua saggezza in ogni momento. Un enorme grazie va a Sonia, per avermi seguito con infinita pazienza per tutta l'attività sperimentale, mostrandomi con entusiasmo e determinazione la bellezza della ricerca scientifica. Mi ha insegnato a valorizzare i risultati e interpretare con curiosità gli errori, il tutto senza mai perdere il sorriso, nonostante la mia scarsa manualità con la strumentazione del laboratorio! Ci tengo a ringraziarvi anche per l'immensa vicinanza mostrata negli ultimi difficili mesi, il vostro sostegno è stato una fonte di luce indispensabile.

Un ultimo ringraziamento va a tutti gli amici che con affetto mi sono stati vicini in questo viaggio, siete delle persone brillanti e leali, se vi nominassi uno ad uno questa tesi diventerebbe un vero e proprio schedario. Ci tengo però a ringraziare tutti i compagni di classe che hanno reso divertenti alcune interminabili giornate sui banchi, e con cui ho trascorso momenti indimenti-

cabili anche al di fuori delle lezioni. Ultimi ma non per importanza ci sono gli amici di sempre, la Seue Squad, con cui ho sempre avuto la possibilità di sfogarmi e divertirmi, andare allo stadio e ai concerti, viaggiare e partecipare a progetti meravigliosi. Quando torneremo alla normalità, festeggeremo come si deve!

Contents

List of Figures

List of Tables

Introduction

The discovery of low-dimensional carbon systems is one of the cornerstones in the recent development of nanotechnology and advanced materials science. Depending on the hybridization state of their building blocks, i.e., carbon atoms, such nanostructures exist in different allotropic forms, each of which displaying unique properties, which reflect the effects of quantum confinement. Fullerenes, carbon nanotubes and graphene are the most renowned carbon nanosystems and are characterized by a sp^2 hybridization of carbon atoms. The existence of a pure 1D carbon system characterized by a sp configuration, named as carbyne, has been subject of controversy for several years. Its theoretically predicted mechanical, electronic and non-linear optical properties, which are superior to the ones of any other carbon systems, have recently attracted the interest of the scientific community. In the last years, great progresses have been made in the synthesis by chemical and physical methods of short carbon atomic wires (CAWs) made of linearly arranged sp carbon atoms. Depending on the bonding arrangement, CAWs can exist either in a cumulenic or polyynic configuration, characterized by an equalized double bond or alternated single-triple bond structure, respectively. Due to their peculiar electronic distribution, linear sp carbon chains are highly reactive species, extremely susceptible both to external agents like heat, light and humidity and to cross-linking reactions resulting from the interactions between chains, which cause structural reorganization processes towards a more stable sp^2 phase. In order to exploit CAWs exceptional properties in technological applications, improvements in the synthesis and stability features as well as the incorporation in solid-state devices are required. The encapsulation of CAWs in other nanosystems such as carbon nanotubes and Ag nanoisland, as well as in inorganic and organic matrices, has been proven to be an effective way to prevent linear chains fast degradation processes, enhancing their stability up to several weeks and months. In particular, as already developed with other carbon nanostructures, the formation of CAWs in polymeric nanocomposites could be a way to exploit the advantages of polymer solution processing in order to achieve a stability improvement by

the immobilization of linear chains in a polymeric matrix. Moreover, the synthesis of such nanocomposites could be an important possibility to investigate linear sp carbon chains behaviour in solid-state systems, in sight of future nanoengineering applications.

The aim of the experimental activity in this thesis is to investigate the synthesis and stability properties of linear sp carbon chains in poly/methyl methacrylate) (PMMA) nanocomposites, obtained exploiting the wide versatility offered by the physical production technique of Pulsed Laser Ablation in Liquid (PLAL). In order to design a proper synthesis step and to perform an effective characterization of the nanocomposites, the effects of some of the process parameters as well as of the introduction of Ag nanoparticles for Surface-Enhanced Raman Scattering (SERS) purposes have been explored. This thesis work is organized as follows:

- Chapter 1: an historical overview on carbon nanostructures is presented, focusing then on structural, physical and synthesis properties of Carbon Atomic Wires (CAws).

- Chapter 2: the pioneering studies of polyynes-polymer nanocomposites are discussed after a brief overview on the state of the art of carbon-based polymer nanocomposites.

- Chapter 3: the materials and the techniques used for the synthesis and characterization of polyynes-polymer nanocomposites are presented.

- Chapter 4: the experimental results are reported, investigating on the synthesis and stability properties of nanocomposites achieved following two different strategies for the introduction of Ag nanoparticles.

Chapter 1

Carbon Atomic Wires (CAWS)

1.1 Carbon allotropic forms

Carbon, together with helium, hydrogen and oxygen, is one of the most abundant elements in the solar system. Its presence has been widely detected in the sun and in the stars, in the asteroids and in the comets, up to the atmosphere of the planets and in Earth's crust, too. In nature, carbon is the element which provides the basis for life on Earth, being the building block of all essential biological molecules in living organisms such as carbohydrates, lipids, proteins and nucleic acids like DNA and RNA. None of the elements in nature can equal carbon in the extent and versatility of its catenation: over 95% of known chemical compounds are carbon-based, thanks to its tendency to bind to both electropositive and electronegative elements, but also to itself through single, double and triple bonds [1]. Such ability can be exploited in many industrial and technological applications, as in the synthesis of organic compounds like drugs and in the development of synthetic materials like polymers. The extraordinary binding ability of carbon can be understood by looking at its electronic configuration, i.e. the arrangement of the electrons in the atomic orbitals, labelled as $1s^2 2s^2 2p^2$: according to this disposition, in the ground state carbon has only two electrons available for chemical bonds in the valence shell. Actually, this is not what can be observed in nature: in many compounds the $1s^2 2s^2 2p^2$ configuration can not account for certain symmetries, for instance the tetrahedral one, which characterizes methane and diamond, where each carbon atom binds to other four atoms. This phenomenon can be explained from quantum mechanics considerations using the Linear Combination of Atomic Orbitals (LCAO) theory, according to which, when the carbon atom is involved in chemical bonds, new molecular orbitals can be formed by the superposition of atomic orbitals. In this way,

the electronic configuration is altered and new hybrid orbitals are formed by the combination of $2s$ and $2p$ orbitals, allowing different symmetries in carbon compounds. Hybridization is favoured by the low energy difference between the $2s$ and $2p$ orbitals and is responsible for the existence in nature of several allotropes of pure carbon, all having the same composition but displaying completely different materials properties, depending on carbon hybridization state and atomic arrangement. Hybridization, which can be of sp^3-, sp^2- or sp-type, determines the structure and reactivity of carbon allotropic forms, affecting bond strength and coordination of carbon atoms. Different hybridization states allow to produce a wide range of compounds, ranging from condensed matter to molecules and nanostructures [2].

Carbon is present in nature in two solid state allotropes known since ancient times, diamond and graphite, characterized by extended structures with respectively sp^3- and sp^2-hybridized atomic orbitals [3]. In diamond, each carbon atom is sp^3-hybridized and covalently bonds to four others; the hybridization is said to be sp^3 since one s orbital and three p orbitals combine to form four new equivalent hybridized orbitals with identical shape but different spatial orientation. By convention, a directional orbital like the sp^3 one is named as σ orbital, and the involved bond as σ bond. In sp^3 hybridization the arrangement of atoms is tetrahedral with a bond angle of $109°28'$. In this disposition, the structure of the solid diamond lattice can be thought as two interpenetrating face-centered cubic lattices with one displaced by $1/4$ of the diagonal along a cubic cell, alternatively as a FCC unit cell with two atoms per base [4]. Thanks to the arrangement and strength of its covalent bonds, diamond is the hardest material known and is usefully exploited in abrasive applications. Carbon is a very interesting material also in terms of thermal conductivity, where thanks to its covalent bonds and low phonon scattering, it is the best thermal conductor, with a conductivity of about 2200 W/mK, (five times higher than silver). Being involved in sp^3 hybridization, none of the $2p$ orbitals are available to form the delocalized π orbital. Subsequently, diamond has a bandgap of 5.5 eV, resulting the widest band gap semiconductor material. Moreover, diamond is transparent to visible light since no photons with a corresponding energy can be absorbed [5].

Over diamond, the second well-known natural allotrope of carbon is graphite. It is carbon most stable form in nature and is characterized by pure sp^2 hybridization. In graphite, sp^2-hybridized orbitals are formed by the combination of one s orbital with two p orbitals and are organized in a trigonal planar geometry with 120° angles between bonds. In this kind of hybridization three sp^2 hybrid orbitals are formed, while the $2p_z$ orbital remains unhybridized with a free, delocalized electron available to form a π bond, directed perpendicularly to the plane of sp^2 orbitals. As a conse-

quence, in graphite each carbon atom establishes three covalent σ bonds, responsible for the formation of planar hexagonal structures arranged in a layer (graphene sheet), and one π bond involving the delocalized electron, which allows the π-π stacking between parallel layers, which are kept together by a much weaker interaction called van der Waals force [3]. The highly anisotropic structure of graphite results in a high degree of anisotropy in its properties, which vary considerably when measured within or perpendicularly to the plane. Transport properties are particularly affected by the structure: considering electrical resistivity, graphite behaves as a semi-metal, being a conductor within a plane thanks to the delocalized π band, and an insulator in the normal direction, since electrons can not move from one plane to another due to the relatively high distance among them. In the case of thermal resistivity, which is based on phonons, graphite is a good thermal conductor in the direction along the plane and an insulator perpendicularly to the plane, since in that direction the amplitude of lattice vibration is much lower. Moreover, in contrast with diamond's peculiar hardness, graphite is a very soft material with lubricant properties thanks to the weak van der Waals forces between its layers, allowing them to slide past each other. From thermodynamic point of view, at room temperature and atmospheric pressure, graphite is more stable than diamond, due to this, the latter turns into graphite through a very slow process of graphitization [5].

As reported in Fig. 1.1, in the last decades the development of nanotechnology induced researchers to focus their attention on other possible carbon systems, leading to the discovery of low-dimensional carbon structures such as fullerenes, carbon clusters, nanodiamonds, nanotubes and graphene, and opening a great challenge in the study of an elusive, elemental solid composed exclusively of sp-hybridized carbon, named as carbyne. Nowadays, carbon nanostructures are very appealing in many applications thanks to the influence of quantum confinement on their behaviour [6].

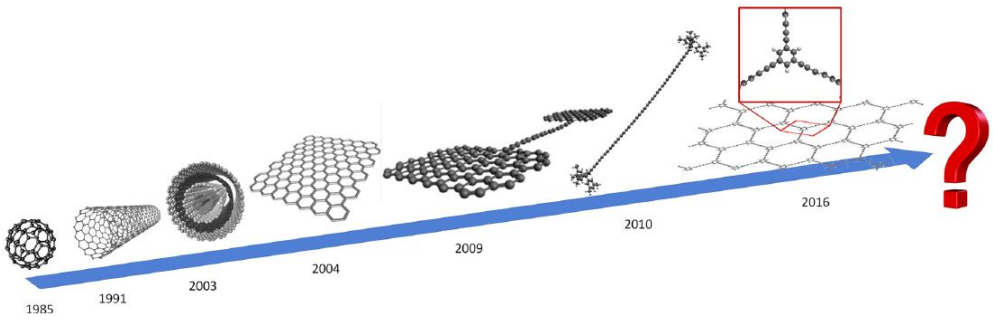

Figure 1.1: Roadmap of most relevant discovered carbon nanostructures [7].

Fullerenes were discovered in 1985 by Kroto, Smalley and Curl, who received a Noble prize in Chemistry for this breakthrough in the research of synthetic materials [8]. The pronounced abundance of C_{60} cluster in their graphite laser vaporization experiment led to the proposal of fullerene structure, confirmed a few years later by means of IR spectroscopy [9]. Fullerenes are 0D systems confined in three directions, characterized by mainly sp^2 hybridization with a small fraction of sp^3 character. The peculiar structure of a carbon-cage molecule is composed of fused pentagonal and hexagonal rings, which can be arranged in several isomers containing a different amount of carbon atoms. Among produced fullerenes, C_{60} (also known as Buckminster Fullerene) is the most stable and abundant one; its structure of truncated icosahedron consists of a spherical network of 60 carbon atoms arranged in twenty hexagons and twelve pentagons, the latter being responsible for the distortion of the structure. Over C_{60}, several other fullerene structures have been isolated, including arrangements of 70, 76, 84 or 90 carbon atoms. Fullerene molecules can be derivatized in several ways, for instance by incorporating guest atoms or molecules within the carbon framework (endohedral fullerenes), or by substituting carbon atoms with different elements (heterofullerene). Furthermore, fullerenes' surface can be functionalized to improve their peculiar electrical properties and solubility in several solvents, giving also the possibility to couple them with other materials to combine their properties, like in the case of exohedral covalent binding between fullerene acceptors and organic donor molecules such as porphyrins in photovoltaic devices [2].

In 1991, soon after the discovery of fullerene molecules, carbon nanotubes have been reported by Iijima in an experiment which concerned evaporated graphite [10]. These new allotropic forms of carbon are considered as quasi-1D systems due to the confinement in two directions. Carbon nanotubes are characterized by a very high aspect ratio, having a diameter typically of the order of nm and lengths of millimetric sizes. CNTs can be open-ended or closed-ended and appear as rolled-up graphene sheets. By means of different preparation conditions CNTs can exist in a single-walled or multi-walled structure, depending on the number of coaxial rolled sheets. As in fullerenes, carbon atoms are characterized mainly by sp^2 hybrid orbitals, with a fraction of sp^3 hybridization responsible for the curvature of graphene sheets. The rolling of graphene layers leads to the formation of three possible tube structures: armchair, zig-zag and chiral. Electronic properties of CNTs are strongly affected by their geometry, indeed they can be either semiconducting or metallic thanks to the presence of contact points between valence and conduction bands (Dirac's Cones) in the band structure, making them suitable for applications in molecular electronics and nanospintronics [11]. Further-

more, CNTs are characterized by a really high mechanical strength, which makes them appealing as a reinforcement in composite materials. These systems have been investigated for several biological applications, too [2].

A further step in the development of synthetic carbon allotropes occurred in 2004, when graphene was isolated by Geim and Novoselov, who also were awarded the 2010 Nobel Prize in Physics thanks to their research on the mechanical exfoliation method and on graphene's electronic properties. Graphene, which for decades has been considered only a theoretical model, is the ultimate 2D material with one atom thickness, consisting of a single sheet of graphite [12]. Atoms in the plane are arranged in the honeycomb geometry, characterized by purely sp^2 hybridization. The strong quantum confinement heavily affects graphene's properties, making it one of the most attractive materials in several fields like digital electronics. Indeed, its unique band structure is characterized by the presence of Dirac's cones, making graphene a gapless material suitable for ambipolar conductivity, with extremely high values of charge carrier mobility and current-carrying capability at room temperature, satisfying the requirements for the realization of graphene-based field effect transistors and transparent conductive electrodes [2]. Over its outstanding electronic behaviour, graphene is characterized by flexibility and excellent mechanical properties, indeed its Young modulus of 1 TPa and intrinsic tensile strength of 130 GPa make it a promising candidate among nanocomposites fillers. In addition to this, chemical functionalization of graphene could be a powerful technique to improve its solubility, processability and stability properties. The combination of *sp*-, sp^2- and sp^3-hybridized carbon atoms allows to think of the presence of many allotropic forms extended in one, two and three dimensions, making the research of synthetic carbon allotropes a field in continuous expansion [13].

1.2 sp Carbon Atomic Wires (CAWs)

During the investigation of carbon allotropes, the absence of a third crystalline solid made purely by *sp*-carbon raised the interest of the scientific community. The existence of carbyne, the hypothetical allotrope of carbon composed entirely of *sp*-hybridized carbon atoms in linear chains, has been under controversy for a long time due to stability reasons [14, 15]. Such compounds may be present in significant amounts in extreme environmental conditions such as interstellar clouds [16]. The study of carbyne is still at the academic level and presents great challenges in terms of compound preparation and stability, although in the recent years great progresses in the synthesis of short, end-capped *sp*-carbon atom wires have been made.

Furthermore, other novel structures containing combinations of *sp*- and sp^2-carbon like graphynes and graphdyines, or of *sp*- and sp^3-carbon like yne-diamond have been theorized and are under increasing investigation.

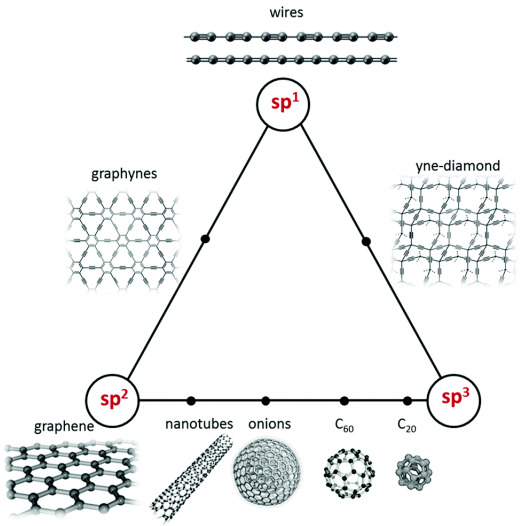

Figure 1.2: Ternary diagram of carbon nanostructures according to their hybridization state [17].

According to the classification in Fig. 1.2, the *sp*-vertex is related to the existence of linear structures and molecules arranged in linear carbon chains, also called carbon atomic wires (CAWs). With a diameter of one atom, CAWs represent the ultimate 1D material [18]. Up to now, any of the attempts to isolate an infinitely long carbon atomic wire did not work. However, different chemical and physical methods to synthesize short *sp*-carbon chains with different chemical endgroups have been developed [19, 20]. From theoretical models, sp carbon wires are characterized by unique vibrational, optic and transport properties, which can be tuned by controlling their structure, length and endgroups and could be exploited in several fields, from molecular electronics to non-linear optics. However, issues in their synthesis and reactivity control must be still overcome in order to use these nanomaterials in real devices. Carbyne's predicted properties are exceptional even compared to other carbon nanostructures, which in turn were thought as the most promising in many applications. Indeed, considering thermal conductivity, Wang and Lin reported values of 80-200 kW/mK, overcoming nanotubes and graphene's ones of one order of magnitude [21]. Depending on bond arrangement, carbyne can behave as a metal or a semiconductor, reaching values of electron mobility of $1.5 \cdot 10^5$ cm^2/Vs [22]. In terms of mechanical properties, Liu et al. showed carbyne should display a specific

stiffness value of $10^9\ Nm/kg$ and a Young's modulus of $32\ TPa$, which largely overcomes graphene, carbon nanotubes and diamond properties [23]. In addition to outstanding mechanical properties, the estimated specific surface is about 13000 m^2/g, four times larger than graphene, making carbyne an excellent material as storage medium or for nanocomposites reinforcement [24]. In order to exploit these outstanding predicted properties, the development of production and stabilization techniques is a real challenge in carbon nanoscience.

1.2.1 Structure of linear carbon chains

The *sp* hybridization typical of carbon atomic wires confers on them a linear arrangement with an angle of 180° between bonds, where each carbon atom binds to other two carbon atoms. In *sp* configuration, the $2s$ orbital combines with one $2p$ orbital in order to produce two *sp* hybrid orbitals, without involving the $2p_y$ and $2p_z$ orbitals, which are responsible for the peculiar π-conjugation of linear chains. As a first approximation, structure and properties of CAWs can be described considering as an ideal model the infinite 1D chain of carbon atoms [25]. Clearly, it is necessary to include the effects of chain's finite length and the presence of different chemical endgroups for a refined description of real systems [26]. Starting from the infinite 1D chain model, following a solid-state physics approach, two different structures are possible, as shown is Fig. 1.3, depending on the established bonds among carbon atoms: polycumulene (or just "cumulene") and polyyne.

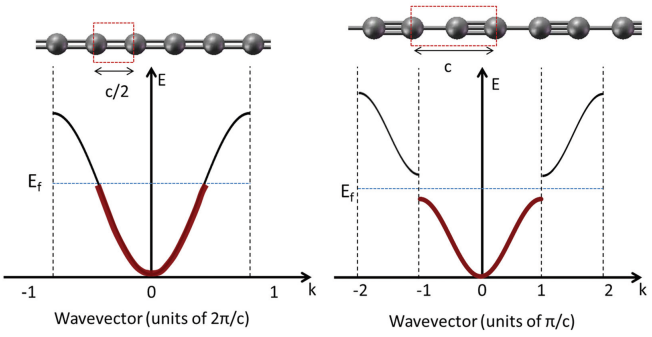

Figure 1.3: Geometric arrangement and band structure of cumulenic (on the left) and polyynic (on the right) infinite chain [17].

In cumulene all carbon atoms are arranged in the linear chain through a series of equivalent double bonds, so it can be described as a 1D crystal with a monoatomic unit cell. This kind of structure is characterized by a metallic

behaviour since the conduction band is half filled, receiving a contribution for each carbon atom of one electron from each of the two $2p$ orbitals. Differently, polyynes are characterized by a sequence of alternating single and triple bonds, so the system can be considered as a 1D crystal with a biatomic unit cell, which provides two electrons in each orbital, resulting in a half Brillouin zone. Subsequently, polyynes show a semiconducting behaviour, having a completely filled valence band separated by an empty conduction band through a bandgap opened at the edges of the Brillouin zone [17]. A direct consequence of electronic delocalization in polyynes is observed in the modification of CC bond lengths. Indeed, triple bonds are slightly longer and single bonds are slightly shorter compared to the typical ones found in acetylene and ethane, respectively.

Bonding arrangement in CAWs can be described by a structural parameter named as bond length alternation (BLA), which takes into account the difference in length between adjacent bonds. It follows that cumulene, being composed of all equalized double bonds, has a BLA value equal to zero, while this parameter is non-zero in the case of polyynes, where the BLA value depends on the degree of π-conjugation that affects the lengths of single and triple bonds [27]. As reported by Milani et al., from DFT pseudopotential computations, BLA strongly affects the band structure of the infinite carbon chain [28].

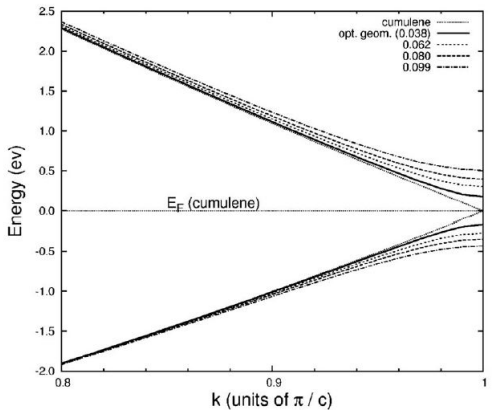

Figure 1.4: Band structure of a linear carbon chain for the cumulenic (BLA$=0$) and polyynic (BLA$\neq 0$) configurations [28].

In Fig. 1.4 it can be observed that as BLA increases starting from 0 (ideal cumulenic case), a metal-to-semiconductor transition occurs, leading to the opening of a band gap at the edges of the Brillouin zone. As the BLA value grows, the difference between the top of the valence band and the bottom of

the conduction band increases, conferring to the system a more pronounced energy gap.

Cumulene is not a stable configuration of linear carbon chains due to the occurrence of Peierls distortion, a phenomenon which affects linear metals and polyconjugated systems, too [29]. According to Peierls effect, by means of BLA modification, cumulene undergoes a transition towards the alternate polyynic structure, which corresponds to the minimum energy configuration. Hence, the equilibrium geometry is characterized by BLA $\neq 0$ and by the presence of a bandgap. Actually, the reason for which it is found the polyynic structure in the most of synthesized CAWs is not referable to only Peierls distortion. In fact, as shown by Yang and Kertesz in a computational analysis, the above-described phenomenon is effective only for long chains (over 52 carbon atoms), in which it counterbalances the opposite contribution of BLA decrease promoted by π-electron delocalization [30]. Due to this, Peierls distortion can be rigorously defined just in the case of ideal infinite chain, whereas is not sufficient alone to justify the main presence of the alternate polyyne-like structure in finite short wires. Indeed, in the case of finite length carbon systems, a fundamental role is played by chemical endgroups, which strongly affect the molecular structure of the chain. In real structures, the chemical nature of chain terminations is the main responsible for BLA modification, influencing the properties of the whole system, ranging from the energy gap to the electrical and vibrational behaviour. For instance, in hydrogen terminated chains, the CH bond requires the establishment of a triple bond in the adjacent CC, leading to an alternate structure. Differently, a CH_2 endgroup promotes double bounds starting at chain termination and proceeding along the whole wire, leading to a cumulenic structure with a BLA tending to zero. In addition to this, fixing endgroups, in longer chains it can be observed an expected increase of π-conjugation, which in turn promotes a decrease in BLA in a more equalized structure [31]. As a result, the nature of chain capping is the main responsible in determining CAWs' structure, which is strictly related to tune electronic, optic and vibrational behaviours of the system. By means of a proper production process, selected endgroups can be conferred on linear chains, allowing to achieve a fine structural control and thus to tune the desired properties [32].

1.2.2 Stability issues

Cumulenes are far less stable than polyynes and far fewer reports can be found in literature, thus in the present work the term "polyynes" will be often used in order to indicate *sp*-linear carbon chains, also due to the fact that polyynes have been the main subject of the experimental section. Linear

carbon chains are highly reactive and unstable structures, due to the peculiar electronic distribution of the system. CAWs are very susceptible to degradation mechanisms such as oxidation when exposed to oxygen and ozone [33]. Another detrimental reaction is polyynes hydrogenation, in which CH bonds are formed leading to a decrease of the sp fraction in the structure [34]. Furthermore, an extremely common phenomenon occurring in CAWs is the crosslinking reaction, a structural reorganization process of the sp-hybridized system towards more stable sp^2 and sp^3 configurations [35]. As it involves interaction among polyynes, it is very difficult to obtain very concentrated solutions hindering crosslinking reactions. Hence, polyynes are very sensitive towards factors which can activate or accelerate degradation processes such as light, heat and moisture, but also reactive compounds like acids and bases [36]. As CAWs are extremely prone to undergo degradation reactions, the development of stabilization techniques is an essential issue to overcome. Up to now, several strategies have been proposed. A possible method consists of acting directly during the synthesis step, where sterically bulky terminations are conferred on chains, hindering wire-wire interactions and the subsequent crosslinking [37]. As a consequence, in addition to the possibility to modify CAWs properties, the design of proper end-capping groups can improve the stability of the system, becoming even more a crucial point for technological applications. Other strategies involve the stabilization of already formed wires. As shown by Casari et al., the use of a silver colloid in solution allows to achieve after solvent evaporation a solid assembly of silver nanoparticles and H-terminated polyynes, characterized by stability under ambient conditions for several weeks [38]. Stabilization has been achieved in nanocomposites, too. This fascinating possibility has been one of the reasons that pushed the curiosity for the development of this thesis work. For instance, silver or gold nanoparticles and polyynes have been embedded in a poly(vinyl alcohol) film as protective polymeric matrix, displaying a SERS signal stable up to six months [39, 40]. In another attempt of stabilization, polyynes were immobilized in an inorganic matrix of dried SiO_2 gel and showed stability for almost four months [41]. In order to confer protection from external agents, linear chains have been inserted in other low-dimensional carbon systems such as carbon nanotubes, too [42]. In sight of technological applications, stability of polyynes and cumulenes is an indispensable requirement and remains one of the greatest objectives in CAWs development.

1.3 Pulsed Laser Ablation in Liquid (PLAL) for polyynes synthesis

By means of properly designed process parameters, production techniques allow to control the structure and to tune CAWs properties [19]. Polyynes synthesis has been investigated through several techniques, which can be classified into two main categories: chemical and physical processes, each of these with its peculiar pros and cons, which will be discussed at the end of this section.

In order to improve the limitations arose in chemical processes, physical methods were developed, among which two main techniques stood out: Submerged Arc Discharge in Liquid (SADL) and Pulsed Laser Ablation in Liquid (PLAL). In the former process an arc discharge between two graphite electrodes is exploited for the formation of a plasma, which is able to produce polyynes consuming the electrodes, while in the latter plasma formation is achieved by means of the high energy density obtained by focusing a laser light typically on a graphite target, from which polyynes are synthesized. In particular, PLAL has been used in the experimental section of this work, being a very promising technique with versatile features. To better understand the formation of polyynes and how process parameters affect the produced structures, the physical mechanism of PLAL will be explained in the following section.

1.3.1 Physics of the process

Pulsed Laser Ablation in Liquid (PLAL) is a very recent physical process which can be used for the synthesis of a wide range of nanomaterials such as polyynes and noble metals nanoparticles [43]. Through PLAL nanomaterials can be produced by focusing laser pulses on a bulk target immersed in a proper liquid solution. Laser ablation leads to fragmentation of the bulk target into nanoparticulates, hence to a physical modification of matter. In addition to this, chemical modifications may occur including the formation of new compounds and phases. Thus, nanomaterials are generated by a hybrid process between top down physical methods (fragmentation of bulk target to nanometric compounds) and bottom up chemical methods (nucleation and growth of nuclei). The selection of appropriate synthesis parameters is an essential point of the fabrication process, in order to maximize the yield and characteristics of nanomaterials. The evolution with time of physical and chemical events in the ablation process has been treated in detail by Amendola and Meneghetti and represented in Fig. 1.5 [44]. The first event in

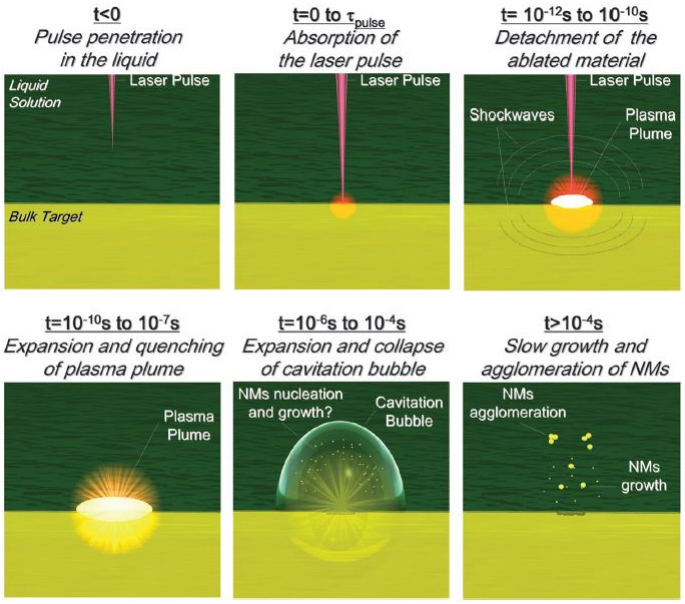

Figure 1.5: Sequence of events occurring during a laser pulse in PLAL [44].

the temporal sequence is laser pulse penetration in the liquid, before it reaches the target. The solvent should be transparent to laser wavelength, so that the energy absorbed by the target results several orders of magnitude higher than the one by the liquid. Particular attention must be paid to the breakdown of the solvent, which must be avoided by working under defocusing conditions. Moreover, to prevent non-linear optical effects like multiphoton absorption by the solvent, a fluence threshold must not be overcome.

As the laser pulse hits the target ($t = 0$), for a time corresponding to pulse duration τ_{pulse}, both optical absorption and laser-matter interaction take place, leading to the different phenomena depending on pulse duration. Here a description related to a nanosecond-pulsed laser is provided, since it is the one used in the experimental part. Differently from ps and fs lasers, a peculiar feature of nanosecond-pulsed lasers is that pulse duration is longer than the electron-lattice thermalization time. In this case, laser ablation can be treated as a thermal process, where thermal evaporation is a dominant mechanism which promotes surface melting [43]. Furthermore, specific thermalization processes such as thermionic emission, boiling, melting, vaporization and photoionization occur [44].

After the absorption of laser pulse, in a time window from 10^{-12} s to 10^{-10} s, detachment of the ablated material occurs. Material removal is promoted by electrons-ions collisions and by the local space-charge fields induced by laser absorption. Moreover, the transfer of kinetic energy from excited

electrons to the lattice leads to the heating of the material, promoting the detachment. A huge temperature gradient is established between the irradiated zone and the rest of the target, so that material removal occurs in a region almost coincident with the laser spot. Depending on process parameters and in particular on pulse duration, different fragmentation processes are possible [44]. In the case of ns lasers, the main mechanism of material detachment is explosive boiling, which occurs when the solid target is superheated reaching the thermodynamic critical temperature [45]. Moreover, a contribution to material detachment is given by coulombic explosion [46]. During the ablation process, the elastic recoil of the material causes the generation of a shockwave in the target and of a specular shockwave into the liquid solution. The propagation of this pressure wave implies density and temperature discontinuities and causes target and liquid heating, thus promoting matter detachment from the crater. As a consequence of high temperature and photoionization processes, the ablated material consists of highly ionized species and expands as a non-equilibrium plasma plume [47].

Material detachment and plasma formation are followed by the expansion and cooling down of the plasma plume in a time interval of 10^{-10}-10^{-7} s from pulse absorption [48]. Plasma is characterized by a temperature of the order of 10^3 K, a pressure of 10^9-10^{10} Pa and a density of 10^{23} atoms per cm^3, with a lifetime of tens of nanoseconds. From the thermodynamic point of view, a non-equilibrium condition is established due to the presence of melted drops and solid fragments, and due to the abrupt thermal alternations between heating by the laser pulse and cooling given by plasma plume expansion and heat exchange with the solvent [47]. A great advantage of performing the ablation in liquid instead of in gas is that the plasma plume is heavily confined onto the crater area by the liquid buffer effect [49]. Thanks to confinement, the hot detached matter of the plasma plume is able to provide a greater fraction of thermal energy to the underlying target, so that a larger portion of the target reaches the energy threshold for material detachment thanks to an additional contribution. As a result, when performing pulsed ablation in liquid, two energetic contributions must be taken into account: the one provided by the laser pulse hitting the target and the energy transfer from the plasma plume to the underlying material. The latter contribution may last for several nanoseconds after the end of laser pulse, becoming very relevant. Hence, in liquid, the cooling rate at the interface between the ablated material and the target is reduced and the ablation yield is improved. It must be noted that on one side the plasma plume releases energy to the target improving the ablation process, on the other hand a fraction of heat is transferred to the surrounding liquid, leading to possible degradation, ionization and pyrolysis of solvent molecules [50]. Another possible effect is “plasma shielding”, which

occurs due to the overlap between the plasma plume and the laser pulse. As a consequence of plasma shielding, a lower fraction of laser energy reaches the target, since part of pulse energy can be absorbed by the plume, with an increase in its energy and lifetime [51].

The quenching of plasma plume involves an energetic release to the external liquid, leading to the generation of a cavitation bubble at times of the order of 10^{-7} s which expands up to about 10^{-4} s with supersonic velocity (greater than 10^{3} m/s), reaching a radius up to the order of millimetres [52]. Temperature, pressure and concentrations of solute and nanomaterials play a fundamental role in determining the expansion of plasma plume and cavitation bubble. While expanding, a decrease of temperature inside the bubble is observed, with a corresponding decrease of internal pressure up to a value lower than the one in the surrounding liquid, leading to the collapse of the cavitation bubble and to the emission of a shockwave. Shockwave emission corresponds to the release of a huge amount of energy, generating values of temperature and pressure similar to the ones reached in the initial plasma plume [44]. These conditions favour further matter detachment from the target and effects in the formed nanostructures such as aggregation and phase transition. After cavitation bubble collapse and shockwave emission, in a time frame after 10^{-4} s from pulse absorption, the system finally reaches the steady state equilibrium and a slow growth of generated nanostructures can be observed.

The actual step of formation of nanomaterials and their spatial distribution still have to be fully understood. A first proposal concerned that already formed nanomaterials were able to travel in front of the expanding bubbles [53]. Subsequently, it has been hypothesized that nanomaterials formation occurs on a time scale of 10^{-6}-10^{-4} s during the expansion of the cavitation bubble, since at the beginning the nanostructures come from the hot plasma region in which the bubbles originate [54]. According to this mechanism, nucleation and condensation of nanomaterials could be promoted by the temperature difference at the interface between the bubble and the external liquid. However, due to the absence of a quantitative analysis of the spatial distribution of nanomaterials, it is possible that a consisting part of structures are already formed and can be found in other regions of the solution.

1.3.2 Synthesis of polyynes

The particular versatility and efficiency of PLAL made it an appealing technique as a new physical method for polyynes production. Laser ablation of graphite targets, coal and carbon clusters has been investigated [19].The

most reliable hypothesis for the growth of hydrogen-capped polyynic chains in PLAL has been presented by Tsuji et al. in 2002 [55]. According to their hypothesis, the formation of polyynes involves the competition between two reaction mechanisms: radical polymerization by consecutive coupling of C_2 radicals produced by laser ablation and termination by hydrogenation at both ends of the chain, where hydrogen atoms are supplied by the solvent.

Since PLAL is relatively recent technique in polyynes production, a complete insight into its features is still uncomplete and different inconsistencies can be found in literature, mainly due to different experimental conditions. Nowadays, several PLAL setups are developing, trying to explore the wide PLAL versality as much as possible. Generally, the main elements of a PLAL apparatus for polyynes production involve a bulk graphite target immersed in a liquid, ready to be hit by a focused ns-pulsed laser, as in the case of the present thesis work. In several cases, the analysis of product by means of HPLC coupled with UV-Vis absorption spectroscopy showed that hydrogen-capped polyynes of different lengths have been produced [55–59]. For instance, as shown in Fig. 1.6, Matsutani and coworkers succeeded in producing very long polyynes up to $C_{30}H_2$ using decalin as solvent [59].

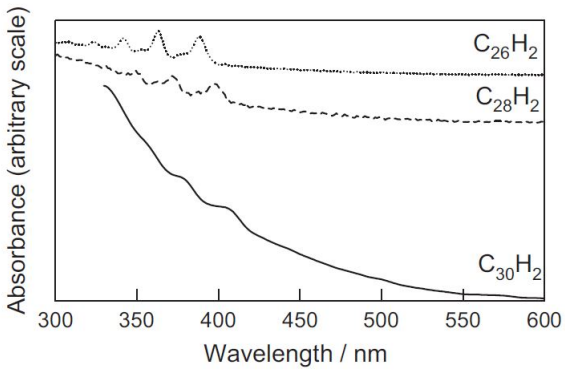

Figure 1.6: UV–Vis spectra of $C_{26}H_2$, $C_{28}H_2$, and $C_{30}H_2$ polyynes produced in decalin and separated using HPLC [59].

Such a high length seems to be related to the use of decalin, which provides a relatively small amount of hydrogen atoms and whose viscosity hinders C_2 radicals diffusion [58]. The choice of solvent is an essential point in process design since it allows to confer on polyynes different terminations, such as hydrogen, cyano- and methyl-cappings, affecting stability and properties of linear chains. Among the most common investigated surrounding liquids in PLAL, one can find water and organic solvents such as alkanes, alcohols, acetonitrile, benzene, toluene, decalin and acetone [60–63].

1.3.3 Advantages of PLAL

Pulsed laser ablation in liquid has been considered one of the most promising techniques for the production of noble metal nanoparticles, thanks to its ability to control their mean size and size distribution and to the high degree of purity of products. Moreover, for what concerns metallic nanoparticles, it is considered as a "green" technique since no stabilizers and other chemicals are required to have an appreciable product.

As introduced at the beginning of this section, in recent years PLAL attracted scientists also for the synthesis of sp carbon linear chains in a wide range of solvents. For what concerns polyynes production, an overview on the historical development of their synthesis processes helps to understand the superior features of PLAL. Chemical techniques were the first developed and involve different chemical transformations, such as polymerization reactions or homo- and hetero-coupling of acetylene precursors (Glaser method). These reactions allow to get appreciable concentrations of polyynes in solution, even with the desired bulky groups at their ends, but unfortunately with a high degree of polydispersion. In addition to this, unreacted reagents and byproducts of reaction may be present, thus making necessary the presence of purification steps in the process design [64].

The development of physical processes such as SADL and PLAL allowed to overcome some limits of chemical methods, including a lower amount of required material, the possibility of plasma confinement by the liquid and the chance of production at the industrial level. In physical methods a higher control of contaminations and purity of products is reached, since in principle no precursors and surfactants are involved in chemical reactions, which caused the generation of unavoidable byproducts [44]. PLAL gained interest thanks to its ease of execution and low costs. Indeed, manual operations are brought to the minimum and costs are significatively reduced, since cheaper and common solvents and targets are required, instead of expensive vacuum chambers and costly chemical precursors [65].

Furthermore, what really makes PLAL an appealing method for polyynes production is its extraordinary versatility. Properties of products are heavily affected by synthesis conditions, which in turn can be easily tuned by modifying the involved parameters. Process parameters can be distinguished into material parameters, such as target, solvent, pressure and temperature, and laser parameters, including wavelength, number, energy and duration of pulse, repetition rate and spot size on target [44]. A huge work of exploration of PLAL parameters has started in the last years, in order to provide as much as possible a complete description of this process, which still has to be completely understood.

1.4 Characterization of sp Carbon

In order to explore CAWs properties and to have an insight into produced chains, different characterization techniques are used in combination with predictions from computational investigations. Most popular linear chains characterization methods are UV-Vis and IR spectroscopy, high performance liquid chromatography (HPLC) and Raman spectroscopy, including surface-enhanced Raman scattering (SERS), too. Of particular interest for this work, both to understand sp carbon properties and to introduce the experimental activity, are UV-Vis and Raman based techniques, based on polyynes absorption and vibrational properties, respectively.

1.4.1 Absorption properties

The peculiar absorption properties of CAWs make ultraviolet-visible (UV-Vis) spectroscopy a powerful tool for polyynes analysis. This characterization technique is based on the absorption of UV and visible light by the molecule. As a result of light-matter interaction, electrons are promoted from ground to excited states, where the absorbed incident wavelength corresponds to the energy difference between the two levels. In a poly-conjugated system, this behaviour is strictly related to the extent of conjugation. The resulting output is an absorption spectrum with different peaks as a function of the incident wavelength, as reported in Fig 1.7.

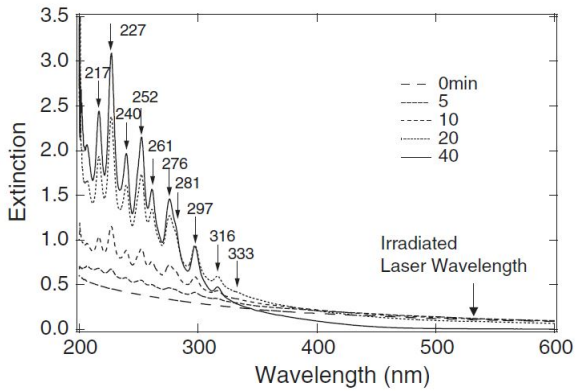

Figure 1.7: UV-Vis spectrum after laser irradiation for various ablation times [66].

A first information given by UV-Vis spectra is the concentration of produced polyynes in dilute solutions, which is related to peaks height. Indeed, the UV-Vis spectrophotometer principle is based on the Lambert-Beer law

(Eq. 1.1), according to which a linear proportionality between the absorbance and the concentration of the absorbing substance exists:

$$A = log_{10}(I_0/I) = \varepsilon Lc \tag{1.1}$$

Where A is the measured absorbance (adimensional), I_0 and I are the intensities of incident and transmitted wavelength respectively, ε is the molar extinction coefficient ($cm^2\ mol^{-1}$), L is the optical path (cm) and c is the concentration ($mol\ cm^{-3}$).

A second information achievable by UV-Vis spectra is related to chain length distributions, which can be investigated by looking at peaks' positions. The interplay between structure (BLA) and electronic properties of polyynes makes UV-Vis spectrometry an effective investigation method. Indeed, the length of linear chains strongly affects the extent of π-conjugation, which is higher for longer polyynes, since more $2p$ orbitals are available for the formation of the π-orbital. Such increase in π-conjugation results in a reduction of the HOMO-LUMO gap, thus a lower incident energy is required for the electronic excitation [7]. As a result, according to the Plank-Einstein relation, $E = h\nu = hc/\lambda$, peaks at longer wavelengths correspond to longer chains, which in turn are characterized by a lower BLA, as described in section 1.2. This has been also experimentally seen by analysing UV-Vis spectra of solutions of polyynes separated in size by means of HPLC (Fig. 1.8).

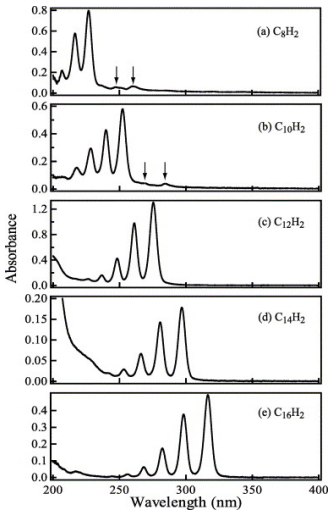

Figure 1.8: Absorption spectra of hydrogen-capped polyynes: (a) C_8H_2, (b) $C_{10}H_2$, (c) $C_{12}H_2$, (d) $C_{14}H_2$, and (e) $C_{16}H_2$ in n-hexane. The small structures indicated by arrows in (a) and (b) are due to impurities [67].

Each absorption spectrum is characterized by a main peak and two secondary peaks in the range of 200-350 nm. A red shift of absorption peaks towards longer wavelengths can be observed with increasing the polyynes length [67]. Furhtermore, as shown by Wakabayashi et al., different end-cappings in polyynes of the same size lead to a modulation of the absorption spectra [68].

1.4.2 Vibrational properties

Vibrational properties of π-conjugated systems like sp-carbon chains are strictly dependent on BLA due to the typical presence of electron-phonon coupling. Consequently, vibrational spectroscopy is able to provide an effective characterization of CAWs. A first insight into CAWs vibrational properties is provided considering the infinite chain model. The phonon dispersion relation of cumulene is given by just three acoustic branches, being modelled as a monoatomic infinite 1D chain. On the other hand, polyynes are represented by a biatomic infinite 1D chain, resulting subsequently characterized by three optical phonon branches, too, as sketched in Fig. 1.9.

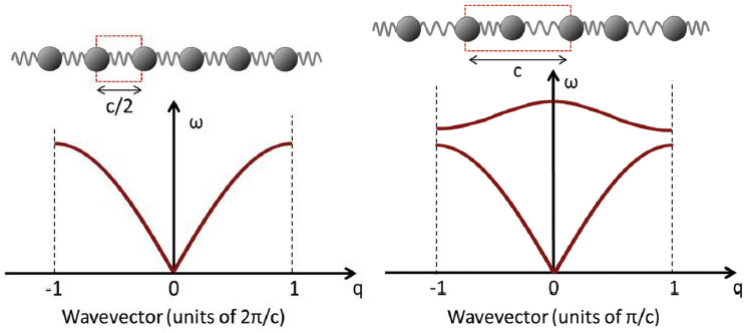

Figure 1.9: Phonon dispersion branches of a bond equalized (cumulene, on the left) and alternate (polyyne, on the right) infinite wire [17].

Through computations based on the tight-binding model, Milani et al. highlighted the extremely sensitive dependence of the longitudinal optical branch (LO) of polyynes on BLA [28]. The infinite chain model provides an interpretation of the peculiar vibrational behaviour of polyynes on the basis of the longitudinal optical (LO) phonon dispersion branches. Once again, effects of chain terminations and other deviations from the ideal structure must be taken into account when dealing with vibrational analysis of real, finite-length chains.

Raman and SERS of polyynes

Raman spectroscopy is based on the inelastic scattering of photons (Raman effect) and allows the determination of vibrational modes of a sample, leading to the identification of molecules characterized by a non-zero change in polarizability. This characterization method is one of the most useful techniques for the analysis of carbon-based structures, being very sensitive to the hybridization state of carbon atoms, chemical bond and local structural order [67]. Even though vibrational frequencies of polyynes are heavily affected by chain terminations, the ones of hydrogen-capped polyynes are only slightly perturbed by terminations, making them suitable for the exploration of CAWs vibrational behaviour. As shown in Fig. 1.10, the peculiar fingerprint of polyynes lies in the 1800-2300 cm^{-1} CC stretching spectral region, which is very exclusive to sp carbon wires, since Raman peaks of all other carbon structures are placed at lower or higher wavenumbers [69].

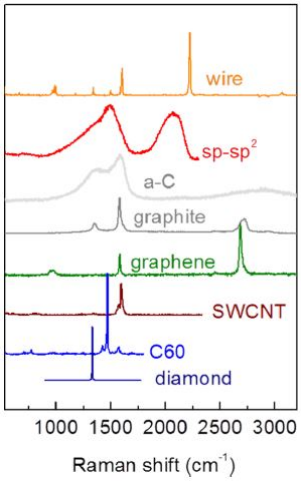

Figure 1.10: Experimental Raman spectra of carbon solids and nanostructures [69].

Polyynes spectra are characterized by essentially two Raman peaks, which have been assigned to different collective stretching vibrations of C-C bonds by means of theoretical analysis and first principle computations. According to the effective conjugation coordinate (ECC) model, the most intense line, also known as "α line", describes the so-called "ECC" mode, correspondent to the $q = 0$ LO phonon of the infinite chain and related to a collective BLA oscillation which involves stretching of all triple bonds and shrinking of all single bonds. A second minor peak, named "β line", has been often observed at lower wavenumbers. The β peak describes a different CC stretching normal mode, which involves just the out-of-phase stretching of triple bonds

and is associated to the $q = \pi/a$ LO phonon of the infinite 1D crystal [70]. Selection rules for carbyne imply that only $q = 0$ modes give rise to a non-negligible Raman signal; however, the selection rule is relaxed in the case of short length chains and further q points are allowed.

In accordance with Kastner computations, Tabata et al. showed that, due to electron-phonon coupling effects, when polyyne chain length increases, the strongest α peak undergoes a red-shift to lower wavenumbers and a growth in intensity, while the β line is affected in a more irregular way, as reported in Fig. 1.11 [67, 71].

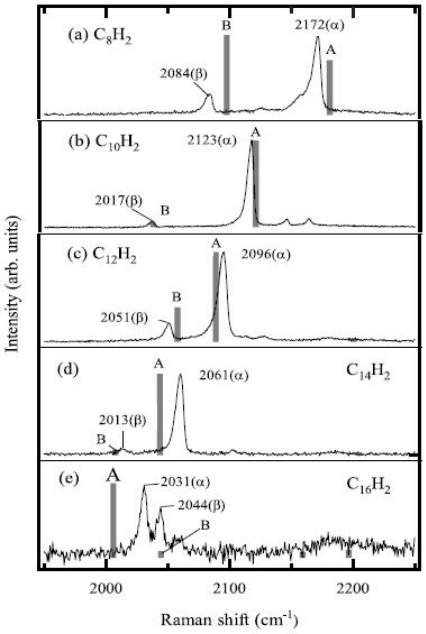

Figure 1.11: Experimental Raman spectra of (a) C_8H_2, (b) $C_{10}H_2$, (c) $C_{12}H_2$, (d) $C_{14}H_2$ and (e)$C_{16}H_2$ compared with DFT calculations of Raman active modes (A and B) [67].

In some cases, the low concentration of produced polyynes ($< 10^{-3}$ M) and strong luminescence signals caused by impurity molecules coming from the production step do not allow the correct detection of Raman signals, which may appear extremely weak or even fully covered [67]. In order to increase the sensitivity of Raman spectroscopy, the surface-enhanced Raman scattering (SERS) technique can be used [72].

SERS is based on the interaction between polyynes and noble metal nanoparticles (Ag and Au), which are added to the sample solution or on a solid surface [69]. The raise in sensitivity given by SERS is related to two main contributions: the first one is known as electromagnetic enhancement

and is based on the effect of surface plasmon resonance. Secondly, in SERS is exploited a chemical enhancement related to the formation of a complex between the polyyne and a metal nanoparticle by charge transfer. Furthermore, the chemical interaction between polyynes and silver nanoparticles can result in NPs agglomeration and even in a substitution of hydrogen capping the polyynes chains with silver. The adsorption of polyynes on metal surface is also proved to increase the system stability [38].

An enhancement factor of 10^6 has been achieved by Lucotti et al, who added a silver colloid to a solution containing H-terminated polyynes [73]. As reported in Fig. 1.12, the SERS spectrum differs from the Normal Raman (NR) from many aspects.

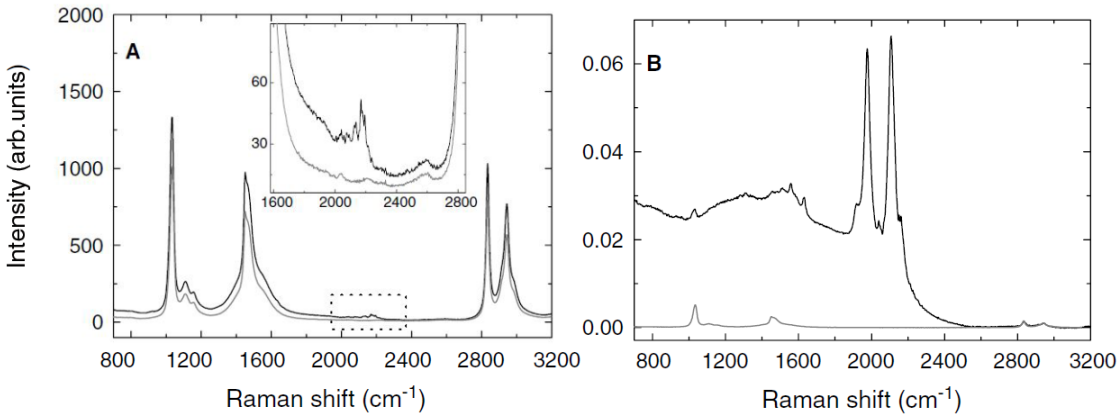

Figure 1.12: (A) Experimental normal Raman spectra of polyyne solution (black line) compared with pure methanol (grey line). Magnification of the 1800-2200 cm^{-1} region is shown in the inset. (B) Experimental SERS spectra of polyyne (black line) and pure methanol (grey line) solutions [73].

Besides the remarkable enhancement of *sp* carbon signal, a red shift of the most intense line can be observed, together with the appearance of new peaks below 2000 cm^{-1}, which were not observed in normal Raman measurements. As reflected by DFT simulations, the red shift of alpha line is related to the formation of Ag substituted polyynes. On the other hand, the appearance of new peaks at lower wavenumbers might be related either to the Raman signal of cumulenic chains or, more probably, to the SERS signal provided by formation of longer polyynes starting from shorter chains, favoured by the adsorption onto silver particles [73].

1.5 Future applications of polyynes

Provided that synthesis processes and stability issues can be fully explored and overcome, polyynes may be introduced as a game-changer nanostructure in various technological applications. Indeed, as introduced in section 1.2, the increasing interest for the development of *sp* carbon chains has been driven by the prediction of their excellent and tuneable mechanical, transport and non-linear optic properties.

The simulated values of tensile, bending and torsional stiffness conferred by chain structure allow to expect an amazing role of CAWs as structural elements in molecular mechanics or as nanoropes [74]. By means of a structural modulation, a high degree of control in electronic properties can be achieved. Thus, CAWs are very appealing in nanoelectronics applications as mono-dimensional conducting materials, thanks to the peculiar double degenerate π-conjugation along the chain and to the presence of Dirac's cones (typical feature of graphene). Polyynes may be exploited as molecular wires thanks to their cylindrical charge distribution, high charge carrier mobility and quantized conductance [75]. Furthermore, in a very recent work, a p-type field-effect transistor (FET) has been produced exploiting cumulenic wires as active material [76]. Being characterized by an extremely high surface area, linear chains may be used as host material for applications in which is required a powerful hydrogen storage medium [24]. Polyyne-based materials could be applied in supermultiplexing techniques, which allow the simultaneous measurement of several distinctive species.

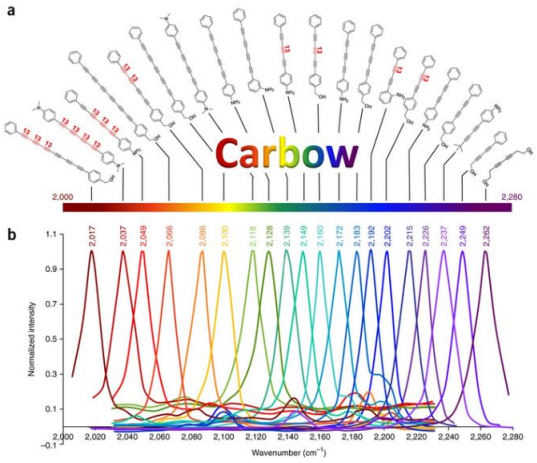

Figure 1.13: (a) Chemical structures of 20 polyynes with distinct Raman frequencies, which are termed Carbon rainbow (i.e., Carbow). (b) Raman peaks of Carbow in the silent spectral window [77].

Through the engineering of conjugation length, chain terminations and bond-selective isotope doping, Hu et al. achieved the so-called carbon rainbow, or "carbow" (Fig. 1.13), made of 20 separated Raman frequencies, with the possibility of imaging, screening and diagnostics in photonics and biomedicine [77].

In addition to this, *sp* carbon wires can be combined with other low-dimensional carbon structures with different hybridizations, such as graphynes and graphdyines, opening an entire new world to investigate [78]. More and more possible applications of sp-carbon chains are going to be found in the years to come, meanwhile at the research level several strategies and as much critical issues are being explored.

Chapter 2

Polymer-Carbon nanocomposites

2.1 Carbon-based polymer nanocomposites

Polymers are extremely versatile materials which have revolutionized the technological habits of the twentieth century. Even though polymers are characterized by unique properties like low density, flexibility and processability, their values of strength and impact strength are inadequate for advanced engineering applications. Different strategies have been developed in order to improve polymer mechanical performances, such as polymer blends and reinforced polymer composites. The use of organic and inorganic fillers in polymer composites has allowed to enhance the desired properties, unfortunately with a loss of processability given by the unavoidably high filler loading.

In the last decades the advent of nanotechology and the progresses in the field of synthetic materials made it possible to develop a new class of composite materials named as polymer nanocomposites. In these advanced materials the polymeric matrix is reinforced using nanofillers, which confer the desired properties with lower filler loading, better processability and lower costs. The use of fillers at the nanoscale instead of bulk carbon black, silica or metal particles allows to enhance toughness without sacrificing stiffness, thanks to the extremely high surface area between the reinforcing material and the matrix. By means of nanofillers, over mechanical characteristics, an improvement in transport properties, oxidative stability and self-estinguishing behaviour can be achieved. Furthemore, a very interesting feature of nanocomposites is the possibility to improve nanofillers stability through a correct design of the nanocomposite [79].

Carbon nanostructures like nanofibers, nanotubes and graphene are some of the most appealing nanofillers to investigate. The possibility to combine their record-breaking properties to the ones of a polymer matrix has been explored in sight of possible advanced applications [80]. Furthemore, together with the recent progresses in their synthesis, the concept of encapsulation of short sp carbon wires in a polymeric film took shape.

2.1.1 State of the art in nanocomposites production

In order to enclose low-dimensional carbon structures in polymeric matrices, several techniques have been developed. Although the synthesis of sp carbon wires in nanocomposites is still at its very early stages, many aspects and issues that arose in the fabrication of composites with other carbon nanostructures can be taken into account in the design of novel synthesis routes of solution processing for polyynes-polymer nanocomposites. In terms of polymeric processing and of interaction between carbon nanofillers and polymeric matrix, the development of polymer nanocomposites embedding other carbon nanostructures may be of particular interest. Indeed, for what concerns the solution processing of carbon-based polymer nanocomposites, different solution techniques have been developed, among which solution blending, melt mixing and *in situ* polymerization are the most relevant for the embedding of carbon nanotubes, carbon nanofibers and graphene in a polymeric matrix [79, 81, 82]. Firstly, preprocessing may be required before proceeding with the above-listed strategies, in order to prepare the nanofillers to be processed on the macroscopic scale. In particular, they can undergo purification, deagglomeration and chemical functionalization steps, with the aim to improve their dispersion and interaction with the matrix [83].

Solution blending involves three steps: carbon nanostructures are firstly dispersed in a suitable solvent, then mixed with the polymeric solution at room or higher temperatures and finally the nanocomposite is achieved by precipitation or film casting followed by solvent evaporation. Solution blending is a common process when dealing with polymers like poly(methyl methacrylate) (PMMA) and polyethylene (PE); it is effective with samples of small sizes and can be designed through several experimental parameters [81, 84]. The choice of a suitable solvent able to dissolve the polymer and promote nanofillers dispersion is a crucial point. Unfortunately, it is difficult to achieve homogeneous dispersions and agglomeration of nanostructures, which is promoted by a slow solvent evaporation. Furthermore, residual solvent and unreacted fractions may contaminate the final product. These issues can be partially improved by the reduction of evaporation time using either spin casting on a rotating substrate or drop casting on an already hot

substrate; moreover, the use of surfactants may help to prevent nanofillers agglomeration and promote their dispersion [85].

Melt mixing is another well-developed fabrication process. This technique concerns the formation of a viscous liquid by melting polymer pellets, followed by the application of shear forces to promote nanofillers dispersion and, as in the case of solution blending, solidifcation and solvent evaporation to achieve film formation [83]. Although this technique is very simple, low-cost and applicable on the industrial scale for the synthesis of carbon nanofillers-polymer nanocomposites, the presence of shear stresses at high temperatures would be detrimental for reactive and unstable nanostructures such as sp carbon linear chains.

A third common fabrication method is represented by the *in situ* polymerization, where polymerization is promoted by means of thermal treatments or light exposure, after having dispersed the carbon nanostructures in a solution containing the required monomer. This technique allows to deal with polymers which are not suitable for solution blending and melt mixing, like conducting polymers like polythiophene (PT) and poly(3,4-ethylenedioxythiophene) (PEDOT) and thermosetting polymers such as epoxy resins. Together with a good dispersion of high loadings in the liquid monomer, a strong covalent bonding between filler and matrix can be achieved [85]. On the other hand, the progressive increase of viscosity and the restricted extent of reaction are limiting factors which must be taken into account. Furthermore, in sight of polyynes encapsulation, several process parameters should be optimized to hinder CAWs degradation.

2.1.2 Properties of polymer-carbon nanocomposites

A great challenge in nanocomposite development is to succeed in the implementation of the remarkable properties of carbon nanostructures in systems at the macroscale, combining the choice of materials and the proper processing methods. For instance, in terms of mechanical properties, the high specific surfaces of nanofillers allow to improve the phenomenon of load-transfer by the matrix, allowing to combine high flexibility and strength with high stiffness, which could not be achieved using traditional carbon fillers. For what concerns transport properties, an exceptional enhancement could be achieved both in electrical and thermal conductivity, by the introduction of extremely low nanofillers content thanks to their large aspect ratio. In particular, intrinsically conducting polymers can display a further increase in strength, conductivity and thermal degradation resistance [83].

Properties of polymer nanocomposites strongly depend on how well fillers are dispersed. Indeed, agglomeration effects may arise, leading to structural

irregularities, crystallization defects and inhomogeneous properties in the solid material. In order to hinder aggregation of nanofillers, different dispersion approaches have been developed. For instance, mechanical methods (shear mixing), chemical additives (surfactants), electric fields and solution ultrasonication can be used [79]. If on one hand dispersion is a fundamental requirement in nanocomposite, on the other hand it may be challenging to achieve the desired degree without affecting nanofillers integrity, as reported in Fig. 2.1 for the case of CNTs embedding.

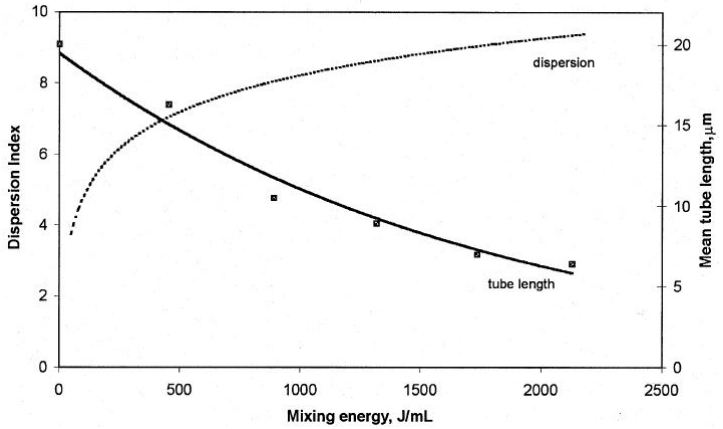

Figure 2.1: MWNT dispersion and tube breakage in shear mixing [86].

Regarding nanofillers dispersion, a second crucial point to consider to understand nanocomposites properties is the interaction between nanostructures and polymeric matrix. For instance the load transfer between matrix and filler plays a key role in the enhancement of mechanical properties and it is related to the interfacial shear stresses between them. The most important contributions in the interfacial interaction are micro-mechanical interlocking, chemical bonding and van der Waals bonding [87]. Functionalization of nanofillers with proper moieties and the use of surfactants can have beneficial effects in improving the interfacial bonding [85, 88].

The performances of a nanocomposite can be effectively enhanced by conferring a certain degree of alignment on nanofillers. With this aim, several routes have been explored, such as electric and magnetic fields, electrospinning and liquid crystalline phase-induced methods [89]. Transport properties are particularly affected by such control, which allows to provide percolated pathways for electron transfer, making the composites electrically conductive [90, 91]. More in general, different works show that a good degree of alignment of carbon nanofibres, carbon nanotubes and graphene in polymer matrices allows to greatly improve mechanical, electrical, thermal, optical

and super-hydrophobic properties of nanocomposites [89–93]. Thanks to the property advantages provided by nanomaterial additives in comparison to both their conventional filler counterparts and base polymers, polymer nanocomposites are suitable for plenty of advanced engineering applications [94]. For instance, they can be exploited in the development of novel photovoltaic cells, supercapacitors and transparent conductive coatings, or in the fields of electromagnetic interference shielding, sensors and optoelectronics devices [95–97].

2.2 Polyynes-based nanocomposites

While synthesis methods, properties enhancement and possible engineering applications have been already widely explored for polymer nanocomposites which encapsulate other carbon nanostructures, the embedding of CAWs in polymeric matrices is still an almost unexplored concept in literature. Indeed, synthesis of CAWs is a field in recent and continuous expansion, hence very few works on the encapsulation of polyynes in solid state systems, and even fewer in polymeric films, have been carried on. However, in sight of technological applications, to build polyyne-based devices, the synthesis of carbon wires in solid state systems is a fundamental and challenging research goal. Furthermore, the immobilization in solid matrices has been proven to be an effective strategy to overcome the typical stability issues of carbon atomic wires. The embedding of polyynes in solid nanocomposites has been explored using different materials. For instance, the presence of polyynes has been proven in electrochemically prepared carbonaceous solids like fluoropolymers [98]. Moreover, it has been demonstrated by means of SERS spectroscopy the adsorption of polyynes on Ag NPs aggregates, leading to the formation of a solid system after solvent evaporation [38]. Furthermore, Sana et al. achieved a nanocomposite by pouring a polyynic solution in the pores of an anodized alumina matrix. The peculiar nanoporous structure of alumina conferred a high stability to the system, preventing the cross-linking degradation reactions by hindering the interaction between linear chains [99]. Another interesting study has been conducted by Matsutani et al., who synthesized polyynes within a transparent SiO_2 dried gel by means of sol-gel methods [41]. As it can be seen by the absorption spectra reported in Fig. 2.2, formation of polyynes in the gel and stability up to 14 weeks have been achieved.

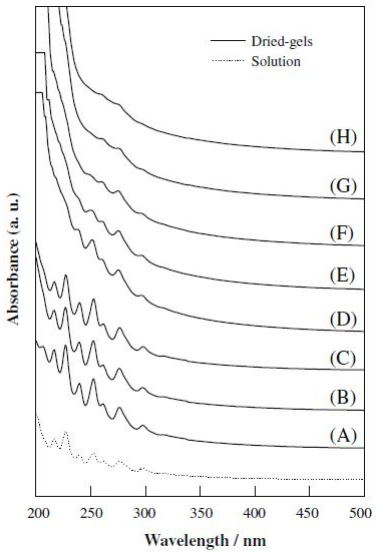

Figure 2.2: UV–Vis spectra of a polyyne-containing SiO2 dried gel measured at different keeping times: immediately (A), 3 days (B), 7 days (C), 18 days (D), 4 weeks (E), 6 weeks (F), 10 weeks (G) and 14 weeks (H) after preparation. The dotted line is for the polyyne solution [41].

2.2.1 Encapsulation of CAWs in polymeric nanocomposites

Over the above-mentioned nanocomposites, polyynes have been encapsulated in polymeric films, too. In 2011 Okada et al. reported the synthesis of a poly(vinyl alcohol) composite film containing polyynes adsorbed on Ag nanoparticle aggregates [39]. The choice of PVA as polymeric matrix for polyynes nanocomposites is promoted by its good solubility in several solvents and its transparency down to the UV wavelength of 220 nm (240 nm if present in high concentrations), easing the synthesis and characterization steps. The presence of Ag nanoparticles allows to characterize the material by means of surface-enhanced Raman scattering (SERS) measurements, and contributes to improve the stability of the nanocomposite. In this pioneer experiment, a solution of polyynes, achieved by pulsed laser ablation of graphite powder in methanol, was mixed in a volume rario of 1:4 with an Ag colloidal solution, prepared by laser ablation of a silver plate in distilled water. PVA granules were dissolved in the mixture increasing the temperature at 373 K up to reach a 8 wt.% PVA solution, then a free-standing composite film has been achieved by casting the solution on a glass substrate. A first proof of polyynes encapsulation has been provided by the comparison of UV-Vis absorption spectra of the Ag/Polyyne/PVA film and of Ag/PVA

alone. As reported in Fig. 2.3, in absence of sp carbon chains, the peculiar narrow surface plasmon resonance (SPR) band of Ag nanoparticles can be observed at 425 nm. The presence of polyynes in the nanocomposite results in a broadening and shift to higher wavelengths of the SPR band, given by the agglomeration of Ag nanoparticles promoted by polyynes.

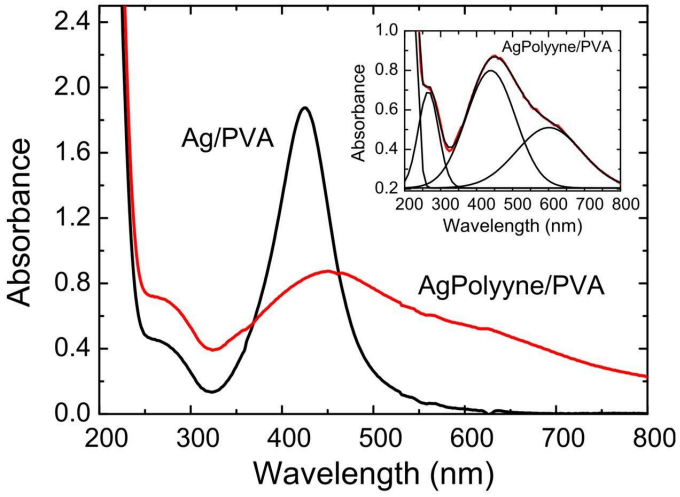

Figure 2.3: UV-Vis absorption spectra for Ag/PVA and Ag/Polyyne/PVA films [39].

In 2015, An and coworkers succeded in the immobilization of polyynes adsobed on Au nanoparticle aggregates into PVA films [40]. In this experiment, a concentrated solution of polyynes produced by arc discharge in methanol was first mixed with Au colloids prepared by chemical reduction methods. Then, the polymer nanocomposite has been obtained following the route proposed by Okada in the realization of the Ag/Polyyne/PVA film [39]. As in the case of Ag NPs, polyynes promoted the agglomeration of GNPs, leading to the formation of hot spots in the sample, in which an increased SERS signal could be observed. Gold has been chosen as SERS enhancer material thanks to its advantages with respect to other metal nanoparticles, such as high homogeneity, long-term stability, chemical inertia and biocompatibility. On the other hand, the use of Au colloids instead of Ag colloreids leads to lower intensity of Raman signals of polyynes.

The encapsulation of polyynes in polymeric nanocomposites has been achieved also in a more recent work by Sata et al. [100]. Nanocomposites were synthesized by dipping hard PVA films in solutions of size-separated polyynes, achieved by pulsed laser ablation of carbon particles in methanol and separated by means of high performance liquid chromatography (HPLC). In this work, it has been shown that stretching the PVA film, the alignment of

trapped *sp* carbon chains was promoted. Indications on the molecular alignment of polyynes have been achieved investigating the angular dependence of absorption intensity of linearly polarized UV light.

Furthermore, Peggiani et al. took a step forward in nanocomposites synthesis by developing a new, one-step *in situ* technique which allows to make the most of PLAL advantages. This promising synthesis route involves the laser ablation of a graphite target directly in a suitable solvent which contains the dissolved polymer, allowing to get the polymeric nanocomposites by solvent evaporation after having casted the PLAL solution on a flat substrate. In this way, nanocomposite properties can be tuned by simply changing the surrounding liquid and ablation parameters [101]. In this work, in order to detect polyynic signals by SERS, an aqueous Ag colloid has been mixed to the solution after PLAL, and a Ag/polyynes/PVA film has been obtained after solvent evaporation. In Fig. 2.4 the SERS spectra of these nanocomposites are reported, focusing on the effect of PVA concentration in the PLAL solvent.

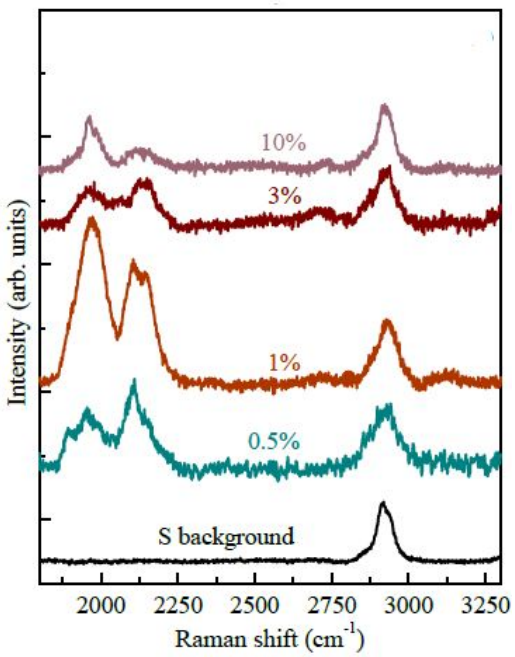

Figure 2.4: SERS spectra of Ag/Polyyne/PVA by *in situ* PLAL at different polymer concentrations [101].

2.2.2 Stability enhancement of polyynes in a polymeric matrix

The fast degradation of CAWs is a very critical issue in the development and application of these structures. Polyynes are usually relatively stable in suitable solvents, however a significant stability enhancement can be observed also when immobilized in solid state matrices. Indeed, the adsorption on metal nanoparticles, together with the encapsulation in solid polymeric nanocomposites, prevents polyynes from interacting among themselves, hindering the detrimental cross-linking reactions, and confers a higher protection against the exposure to external aggressive agents. Over the synthesis of polymeric nanocomposites, the experiments of both Okada and An involved the investigation of polyynes stability with time.

With the purpose of proving the formation and subsequent stability of polyynes in the Ag/Polyyne/PVA composite, Okada et al. studied how the SERS and UV-Vis absorption spectra of the sample evolved over time [39]. These measurements are reported in Fig. 2.5.

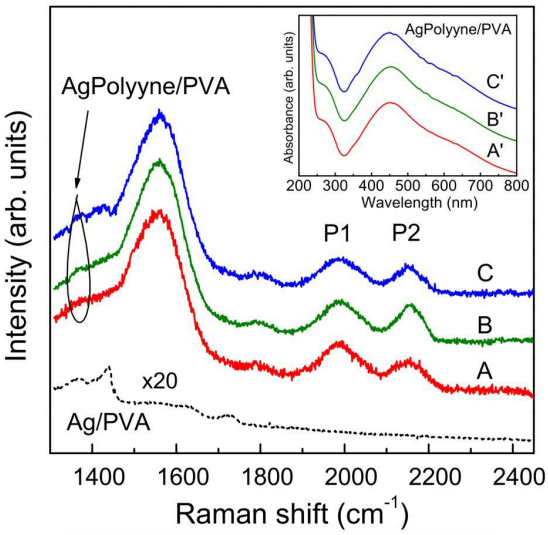

Figure 2.5: SERS spectra of Ag/Polyyne/PVA film recorded as prepared (A), after a week (B) and a month (C). The inset shows the corresponding time evolution of the UV-Vis absorption spectrum [39].

Considering the SERS characterization of the Ag/Polyyne/PVA film, in the 1800-2200 cm^{-1} region, typical of the CC stretching modes, two SERS features, P1 and P2, can be clearly observed. Being absent in the spectrum of Ag/PVA film (dotted line in the figure), these two bands confirm the successful immobilization of polyynes in the PVA matrix. Since polyynes

were not separated in size before encapsulation, the contributions to the two peaks from chains with different lengths are difficult to assign. The peak appearing at 1560 cm^{-1} has been selected to normalize the intensities of different spectra. It can be noted that the relative intensities of the two polyynic peaks in the spectra taken as prepared, after a week and after a month (A, B and C respectively) are substantially unchanged. As a result, the encapsulation of polyynes in the nanocomposites has conferred a good enhancement in stability of CAWs at least up to a month. This has been validated also by the recording of UV-Vis spectra at different storage times, consistent to the ones of SERS measurements (A', B' and C' respectively). Indeed, as shown in the inset of Fig. 2.5, the shape of the absorption spectra after one week and a month do not differ significatively from the measurement taken as the film was prepared.

A similar stability study has been carried on by An et al. after the synthesis of the above-mentioned Au/Polyyne/PVA film [40]. Also in this case, by means of SERS characterization, the two peculiar polyynic bands have been detected in 1900-2200 cm^{-1} region. As reported in Fig. 2.6 (a), stability was proven by the presence of the α and β peaks up to six months.

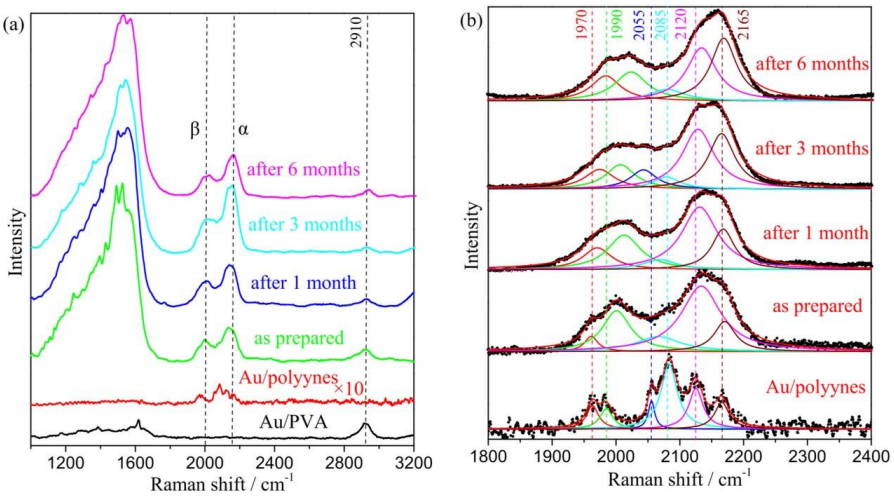

Figure 2.6: (a) Time evolution of SERS spectra of Au/Polyynes/PVa film. (b) Lorentz fits of α and β modes in the SERS spectra [40].

By means of Lorentz fit (Fig. 2.6 (b)), it can be noted that the relatively high processing temperature (353 K) leads to a shift in the bands of the film with respect to the ones in the Au/Polyyne system, probably given by an increasing chemical reaction between Au NPs and polyynes when temperature is increased. In addition to the shift of position, also the intensity of different contributions to the SERS peaks changed with time. Indeed,

by looking at the polyyne to PVA intensity ratios, different behaviours over time were detected, as plotted in Fig. 2.7. As a result, polyynes of different lengths, which contribute to the SERS bands with peculiar wavenumbers, are characterized by a different stability.

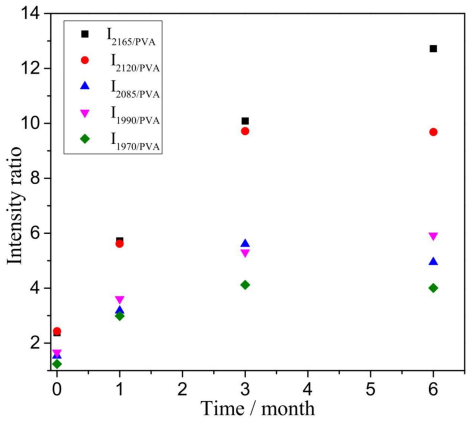

Figure 2.7: Evolution with time of polyyne to PVA intensity ratios [40].

In the same work, by means of HPLC, polyynes were separated in size and used in the synthesis of different nanocomposites ($C_{2n}H_2$ with $n = 4, 5, 6$). This allowed to assign more precisely SERS peaks of the nanocomposite containing polyynes with an unknown length distribution and to study in deep the thermal stability of chains with different length when are encapsulated in the PVA film. The SERS spectra of separated polyynes in solution and in nanocomposites are shown in Fig. 2.8.

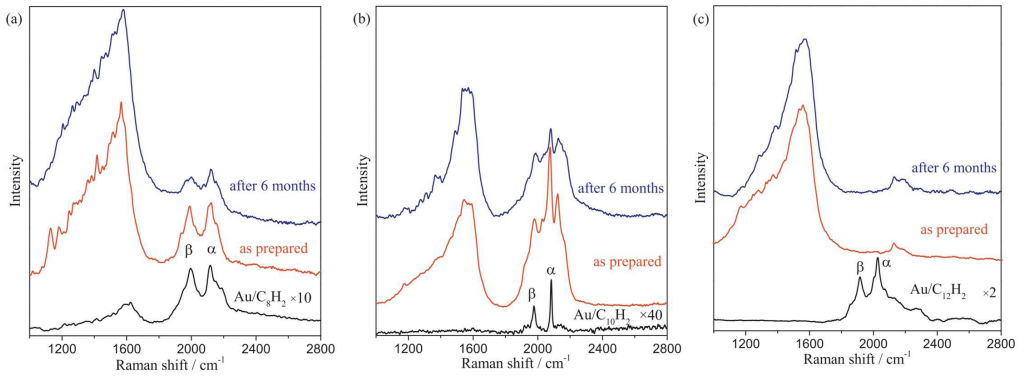

Figure 2.8: SERS spectra of (a) C_8H_2, (b) $C_{10}H_2$ and (c) $C_{12}H_2$ under different conditions: in Au colloids and in PVA films as prepared and after 6 months [40].

It can be observed that in the case of C_8H_2, the positions of SERS peaks in solution and in film are almost unchanged, thus short polyynes display a good thermal stability. As polyynic length increases to $n = 5, 6$, a blue shift of the two peculiar peaks is displayed. In accordance with Tabata, bands shifted at higher wavenumbers are peculiar of shorter polyynes [67]. As a result, in the encapsulation in the PVA film, longer polyynes show a lower thermal stability and undergo a partial dissociation, promoting the formation of shorter polyynes, which are also characterized by a higher stability over time.

Among the presented studies, the *in situ* synthesis of polyynes-PVA nanocomposites by PLAL of a C target in a polymeric solution has given outstanding results in terms of stability. Indeed, Peggiani et al. reported the presence of polyynic signals even after 11 months after film solidification, as displayed by the SERS spectra in Fig. 2.9.

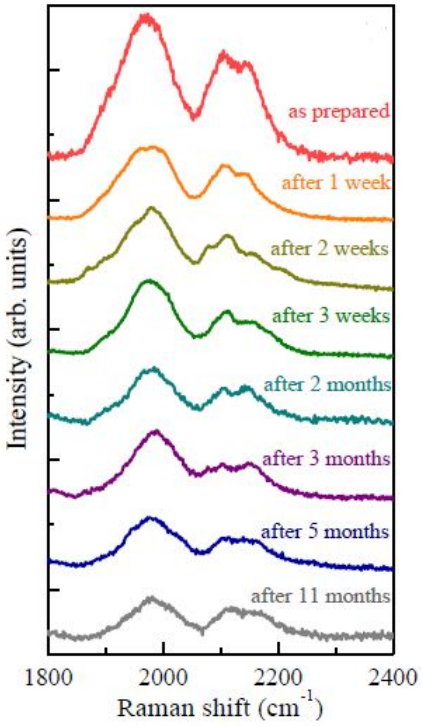

Figure 2.9: Stability study of polyynes-based PVA nanocomposites by *in situ* synthesis process [101].

In the few works conducted so far, the development of PVA nanocomposites has revealed to be an effective strategy both to encapsulate polyynes within solid state systems and to improve the stability of carbon wires. Many

aspects of polyynes/polymer systems still need to be explored, such as the proper combination between materials and synthesis techniques, which could further improve the stability of carbon atomic wires and ease their characterization.

2.3 Ag NPs in polyynes-polymer nanocomposites

A fundamental element in polyynes/polymer nanocomposites is the presence of noble metal nanoparticles, such as Ag and Au. As already discussed, this third component in nanocomposites has a double key role. Indeed, nanoparticles act as a SERS enhancer medium, providing both a chemical and an electromagnetic contribution in the enhancement of signal in the characterization by vibrational spectroscopy, making possible the analysis of low-concentrated species like polyynes [72]. Polymer matrices are able to hinder both oxidation and coalescence of embedded NPs, providing a long-time stability. Furthermore, Ag interaction with polyynes leads to an improved stabilization of carbon wires [38]. As a result, the encapsulation of metallic nanoparticles is an essential step in the synthesis of polymer nanocomposites containing sp carbon linear chains. From now on, in accordance with the aim of this thesis, Ag NPs will be considered among metallic nanoparticles.

2.3.1 Encapsulation of Ag NPs in polymer nanocomposites

In order to insert Ag NPs in polymeric nanocomposites, colloidal solutions of Ag nanoparticles are often used and mixed with polymeric solutions, followed by film casting. A very common method for the production of Ag colloids involves the chemical reduction of Ag ions in solution [102]. However, in this synthesis technique surfactants are always required and chemical byproducts may be present. In addition to their cost and difficult removal, these compounds lead to detrimental effects in NPs applications. For instance, borate and citrate ions can be present on the surface of Ag NPs and the SERS enhancement may be negatively affected [103]. A further disadvantage in the chemical production of Ag colloids for polymer nanocomposites is the limitation provided by the solvent, usually water, which may be incompatible with a certain range of polymers, preventing the correct mixing and casting operations [104].

A valid alternative to the chemical synthesis may be provided by the

pulsed laser ablation in liquid (PLAL) physical technique. As introduced in section 1.3, over being an effective method for polyynes synthesis, PLAL allows to synthesize inorganic nanoparticles in an extremely wide range of solvents, including liquid polymers [105]. Indeed, a laser beam can be focused to ablate a bulk inorganic target immersed in a liquid monomer or a polymer-containing organic solvent, leading to the embeddingt of nanoparticles into the polymer matrix. This route allows to combine in a one-step process the great advantages of PLAL (simplicity, costs and versatility) to a high yield of extremely pure product, avoiding the contamination by stabilizers, matrix binders and reducing agents needed in chemical strategies [106].

The formation of encapsulated nanoparticle-polymer composites reflects the physical mechanism of PLAL: nanoparticles are crystallized within the cavitation bubble in a microsecond time scale, then the collapse of the bubble leads to the release of NPs into the solvent, with subsequent adsorption of polymer chains onto the NPs surface [107]. After laser ablation, nanocomposite films can be achieved by solvent drying when the solution is casted onto a flat substrate [108].

A good control on ablation efficiency and on stability, dispersion and size distribution of nanoparticles in the composite can be achieved by tuning polymer, laser and process parameters [109]. Indeed, as reported in Fig. 2.10, the proper selection of polymer in the PLAL solution promotes fewer agglomerates and smaller particles, thanks to steric stabilization and growth quenching phenomena.

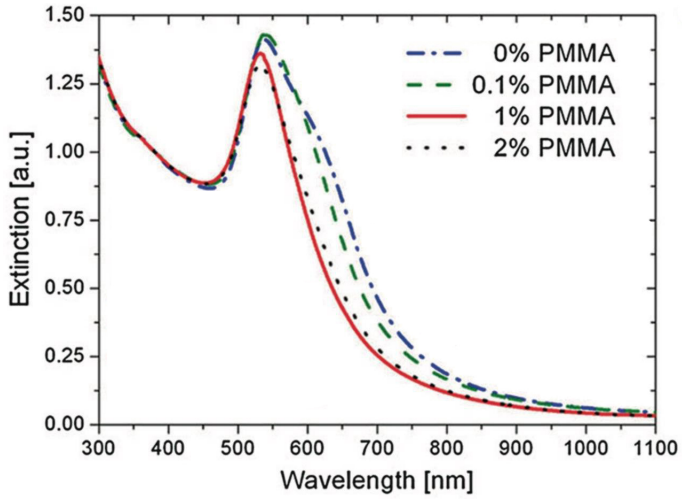

Figure 2.10: Extinction spectra of Au nanoparticles in MMA with different concentrations of dissolved PMMA for an ablation time of 6 min [106].

As a result, both dispersion and mass productivity are heavily affected by

polymer concentration in the organic solvent. An optimal polymer wt% in solution must be found, below which agglomeration of NPs would be promoted and above which liquid's viscosity would increase reducing the production rate [110]. Furthermore, the ablation process itself allows to confer a good control on nanoparticles size, including the achievement of a very narrow size distribution. Indeed, since the absorption coefficient of metal NPs is strictly dependent on their size, the ablation mechanism becomes selective only for those clusters which are able to absorb the laser wavelength. Indeed, those particles with dimensions such that are able to absorb the laser wavelength are completely eliminated, while the ones which do not absorbe the laser light undergo a reshaping process [111]. In addition to this, a contribution to size selectivity is provided by the phenomenon of particles evaporation, whose rate is proportional to $exp(1/d)$. In this way, a more monodisperse solution of NPs can be achieved by laser ablation.

As it can be seen in Fig. 2.11, laser parameters such as wavelength and ablation time have different effects on NPs size and ablated mass. Using the fundamental laser wavelength (1030 nm) a higher concentration of particles is produced, moreover a linear decline in hydrodynamic particle size and a linear increase in ablation rate occur. On the other hand, employing the second harmonic wavelength (515 nm), losses of excitation light lead to a gradual saturation of ablated mass and to an exponential decrease of hydrodynamic particle size due to fragmentation processes.

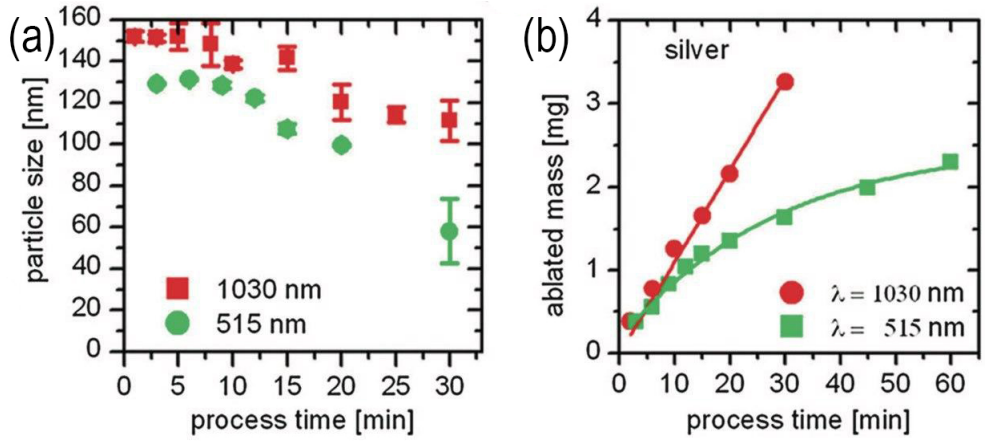

Figure 2.11: Ag particle size (a) and cumulative ablated mass (b) as a function of process time and laser wavelength [106].

The possibility to tune NPs properties by acting on PLAL parameters allows a better control in sight of the addition and exploitation of silver nanoparticles in polyynes-polymer nanocomposites. A glimpse on the inter-

play between nanoparticles and polyynes allows to better understand the role and the advantages of Ag in such systems.

2.3.2 Interaction between Ag NPs and polyynes

The presence of Ag NPs in polyynes-polymer nanocomposites leads to a modification of the system from the physical and chemical points of view, resulting in different optical and reactivity properties [112]. In particular, by the combination of UV-Vis and Raman measurements with transmission electron microscopy, it is possible to understand the nature of the interaction among polyynes and Ag NPs, which allows to detect appreciable SERS peaks during nanocomposites characterization and has a contribution to polyynic stabilization.

The stability enhancement observed in polyynes-polymer nanocomposites is furtherly promoted by the presence of Ag NPs. Indeed, the adsorption of polyynes on nanoparticles surface results in the formation of complexes with a higher stability of Ag-terminated linear chains in solution [113]. The key role played by silver in stabilization of polyynes may consist in the formation of a bonding which helps to stabilize the reactive electronic configuration of *sp* linear chains, preventing the driving force which promotes the typical cross-linking reactions which imply a reorganization towards a more stable sp^2 electronic arrangement [38]. As a result, even in absence of a polymer matrix, CAWs stability is improved when immobilized in solid state Ag NPs assemblies after solvent evaporation, as shown in Fig. 2.12.

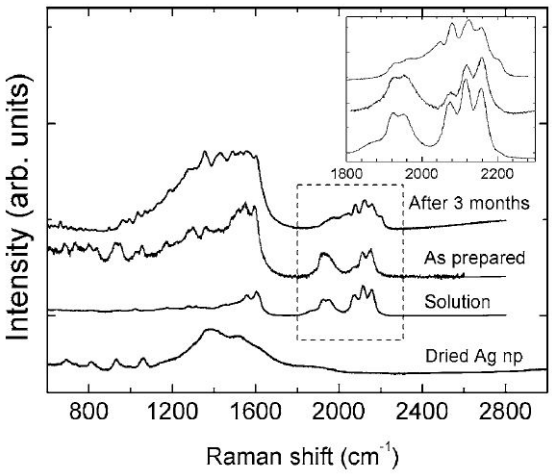

Figure 2.12: SERS spectra of polyynes in solution and in the solid Ag nanoparticle assembly [38].

2.3 Ag NPs in polyynes-polymer nanocomposites

The analysis of UV-Vis spectra of polyynes/Ag systems reveals that the presence of polyynes promotes aggregation phenomena among Ag NPs in the liquid environment [114]. From the absorption spectra reported in Fig. 2.13, it can be noted that in absence of polyynes the NPs solution shows the expected surface plasmon absorption peak at about 397 nm.

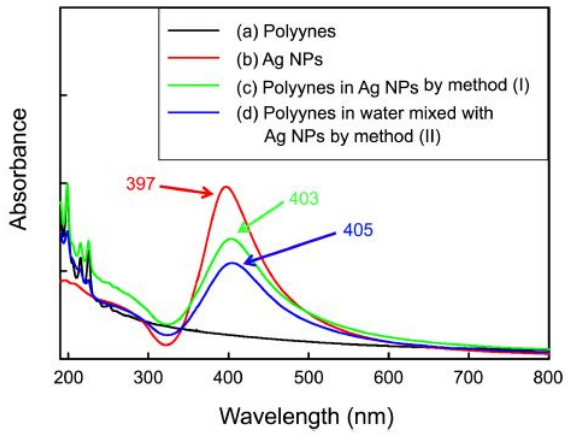

Figure 2.13: UV-Vis absorption spectra of (a) polyynes in deionized water, (b) silver nanoparitcle solution, (c) Ag-polyyne solution prepared by graphite ablation in Ag NPs solution and (d) Ag-polyyne solution prepared by mixing polyyne solution with Ag NPs solution [114].

When interacting with polyynes, a modification in the spectral position and shape can be observed, both in the case of polyynes produced by laser ablation directly in a solution containing the Ag colloid and of polyynic solution added to the Ag colloid. Indeed, these two spectra show a red shift in the SPR peak, together with a broadening and decrease in intensity compared to the original Ag NPs solution, which is an indication of Ag aggregation. Furthermore, in the Ag-polyyne systems, the strong interband transitions of silver nanoparticles in the 200-350 nm range covers polyynic peaks [112]. The agglomeration effect provided by polyynes to Ag NPs has been observed in polymeric nanocomposites, too. The remarkable SERS enhancement of polyynic signal in the recorded Raman spectra allows to prove the aggregation of Ag nanoparticles with adsorbed polyynes. Furthermore, the aggregation of Ag NPs has been observed by means of transmission electron microscopy (TEM), as reported in Fig 2.14.

In absence of polyynes, Ag nanoparticles are well isolated in the polymeric film and few particles are included in the selected TEM area. On the other hand, in Ag/Polyyne/PVA nanocomposites the agglomeration driven by polyynes allows to observe a larger number of particles in the TEM area.

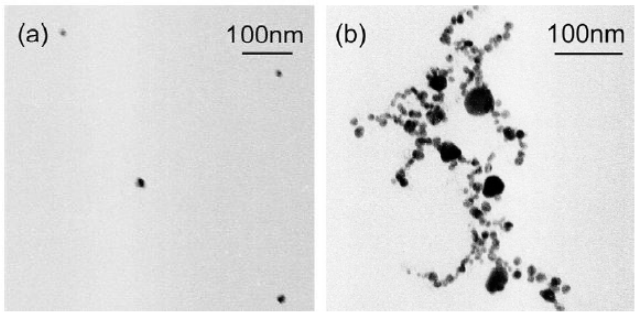

Figure 2.14: TEM images of (a) Ag/PVA and (b) Ag/Polyyne/PVA films [39].

The development of a synthesis method suitable for the encapsulation of polyynes in polymeric nanocomposites, with the further incorporation of metallic nanoparticles to enhance the vibrational signals and to confer stability on the system, remains a great open challenge in science of materials and nanofabrication. The exploration of pulsed laser ablation in liquid (PLAL) features can be a way to move forward towards the achievement of the desired dispersion, size control and morphological properties of the polymeric nanocomposites.

Chapter 3

Materials and experimental methods

In this chapter the synthesis and characterization techniques involved in the experimental activity of this thesis work are introduced. Pulsed laser ablation in liquid (PLAL) has been the leading method for the production of sp-carbon linear chains. The encapsulation of polyynes in a polymeric matrix and the subsequent solidification of a nanocomposite film have been investigated following different strategies. For characterization and stability purposes, Ag nanoparticles produced by different routes have been embedded in the samples. The presence and stability of carbon wires in the nanocomposites over time have been assessed by means of surface-enhanced Raman scattering (SERS) spectroscopy. UV-Vis spectroscopy allowed to achieve information on Ag nanoparticles size distribution and concentration in the samples. Additional information on NPs morphology and dispersion has been provided, when possible, by scanning electron microscopy (SEM).

3.1 Synthesis of samples

3.1.1 Materials

In terms of materials, the production of polyynes by means of pulsed laser ablation in liquid (PLAL) involved the selection of proper targets as carbon sources and of suitable solvents as liquid media. In all the performed ablations of this thesis work the use of a bulk graphite planar target has been involved for the synthesis of polyynes. As presented in Fig. 3.1(a), this type of target is characterized by a disk-like shape, with a thickness of 2 mm and a diameter of 8 mm. The choice of such planar geometry has been promoted

by the selection of the solvent volume (always 2 mL) and of a suitable glass container, able to confer the desired liquid height above the target. Furthermore, such target dimensions almost match with the vial bottom, allowing to reduce as much as possible the unwanted target displacements when it is hit by incident laser pulses.

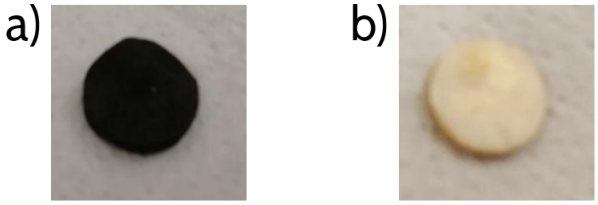

Figure 3.1: (a) graphite and b) Ag planar targets.

In this experimental activity pulsed laser ablation in liquid has been used as a physical method to synthesize silver nanoparticles, too. To do this, a solid Ag target has been used. As it can be seen in Fig. 3.1(b), for the same above-mentioned ablation requirements and advantages provided by graphite target dimensions, the geometrical features of the selected Ag target involved the shape of a planar disk with a thickness of 2 mm and a diameter of 8 mm. Over the use of Ag NPs by *in situ* PLAL, another kind of Ag NPs has been exploited, i.e. NPs coming from a 10^{-3} M aqueous Ag colloid. These NPs have been synthesized by Dr. Anna Facibeni following the Lee-Meisel chemical reduction process, exploiting silver nitrate ($AgNO_3$) as chemical precursor and sodium citrate as reducing agent and surfactant to prevent the coalescence of NPs [115]. Their UV-Vis absorption spectrum is displayed in Fig. 3.2.

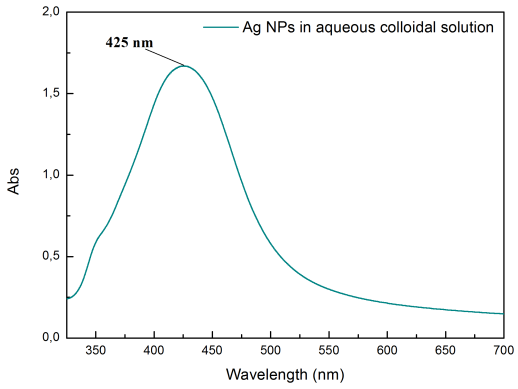

Figure 3.2: UV-Vis absorption spectrum of aqueous Ag colloid.

3.1 Synthesis of samples

A good polymeric matrix for the synthesis of polyynes-based nanocomposites needed to satisfy certain requirements in terms of processing (solubility, filmability and non-toxicity) and characterization (transparency at UV-Vis spectroscopy, absence of Raman features in the sp-region and compatibility with Ag nanoparticles for SERS purposes). In this thesis work, the investigated polymer was poly(methyl methacrylate) (PMMA), a transparent, thermoplastic and non-conducting polymer, with a glassy temperature interval between 100-130°C. PMMA presents some critical issues of filmability, however it is particularly compatible with silver nanoparticles, allowing a good interaction when Ag NPs are added in the polymeric nanocomposite. In Fig. 3.3 the Raman and UV-Vis absorption spectra of PMMA are reported. As it can be seen, in the UV-Vis spectrum the absorption band starts below 300 nm, overlapping with polyynic signals. However, Raman features are absent in the spectral region typical of polyynes (1800-2300 cm^{-1}), allowing the detection of sp carbon chains by means of vibrational spectroscopy.

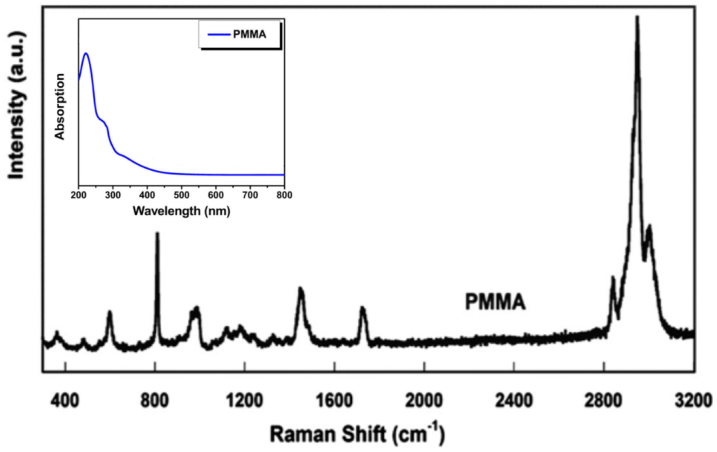

Figure 3.3: Raman spectrum of PMMA. In the inset is reported the corresponding UV-Vis absorption profile.

Good solvents for this polymer are toluene, dichloromethane (DCM), dimethylformammide (DMF) and acetone. The latter has been selected as suitable solvent for PMMA in this thesis work. The chemical structure of methyl methachrylate, poly(methyl methachrylate) and acetone are reported in Fig. 3.4.

The nanocomposites synthesis step in this thesis work has been conducted on the basis of a novel concept developed by Dr. Sonia Peggiani and Dr. Anna Facibeni. In their work, by means of an *in situ* approach, polyynes have been synthesized directly in a polymeric solution through the pulsed

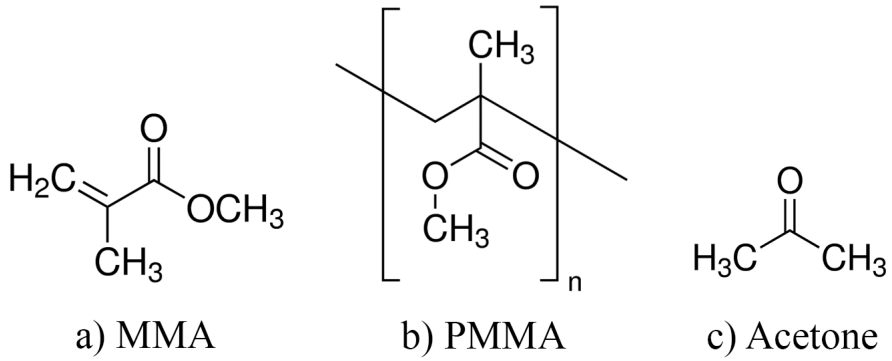

Figure 3.4: Chemical structure of a) methyl methachrylate, b) poly(methyl methachrylate) and c) acetone.

laser ablation of graphite in a liquid solvent with dissolved polymer [101]. Following this strategy, ablations were performed both in acetone and in polymeric solutions of PMMA 2 wt.% and 5 wt.% in acetone, allowing to achieve a nanocomposite solution in a one-step ablation process, with a contribution of steric stabilization by the polymer in the PLAL solvent. These liquid media have been the same used also for the synthesis by PLAL of Ag NPs. Density and refractive index of used solvents affect the polyynes generation mechanism and the fluence reaching the target, respectively. Their values are reported in table 3.1, from which the correct values for polymeric solutions have been computed.

Solvent	*Density* (g/cm^3)	*Refractive index*
Acetone	0,79	1,3590
PMMA 2 wt.% in acetone	0,795	1,3617
PMMA 5 wt.% in acetone	0,804	1,3644

Table 3.1: Properties of used solvents.

Both acetone and PMMA pellets, which have been dissolved in solution, have been purchased by Sigma Aldrich. Used solvents were characterized by a purity degree greater than 99.9%, in order to avoid unwanted ablation byproducts, affect the interactions between nanocomposite components and provide interference signals in the characterization phases. Since organic solvents with relatively low boiling points were involved as liquid media for laser ablation, we immersed the PLAL vial in a beaker filled with water. This allowed to cool down the liquid to hinder evaporation and to reduce flammability issues.

3.1.2 PLAL apparatus

All ablations have been performed using a Quantel Q-Smart 850 Nd:YAG (neodymium-doped yttrium aluminum garnet) solid-state nanosecond pulsed laser, whose apparatus is shown in Fig. 3.5. After being generated, the laser pulse travels up to a mirror inclined at 45°. The role of the mirror is to deviate the laser towards the focal lens, where the beam is directed towards the vial containing the target in the liquid medium. The handling systems of x-y-z stages are connected to a computer by means of controllers and a Python code was implemented to move the stages. In our case, a spiral motion with a constant velocity of 4 mm/s was imposed by the code, allowing to ablate the target in the most possible uniform way in order to prevent localized degradation areas. Furthermore, the system movimentation might provide a small degree of stirring to the PLAL solution, reducing the agglomeration and precipitation of generated nanomaterials.

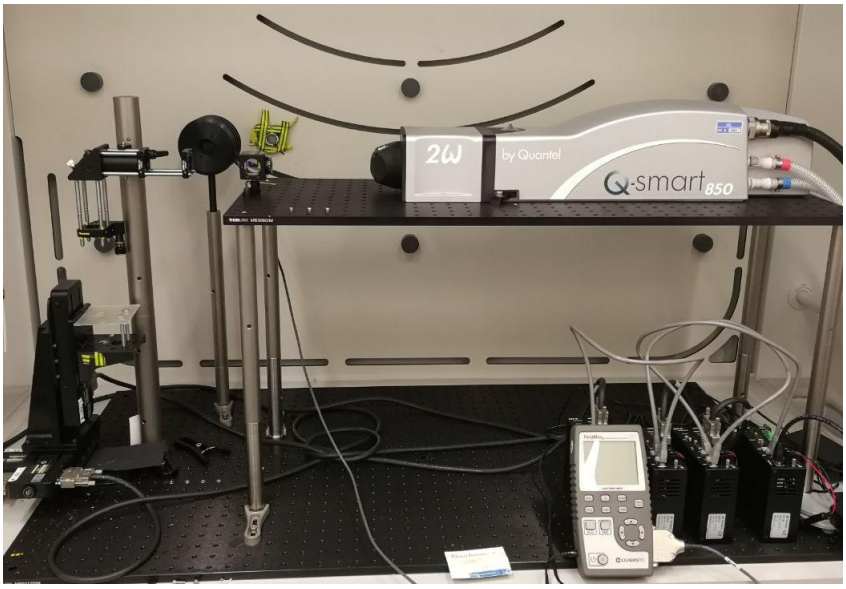

Figure 3.5: Apparatus of the Nd:YAG laser used for PLAL.

Among laser parameters, a constant repetition rate of 10 Hz and a pulse duration of 5 ns have been used. Even though the instrument allows to use three different wavelenghts (355 nm, 532 nm and 1064 nm), the green wavelength (532 nm) has been used in the synthesis of all samples, being the most exploited in polyynes generation, except from a set of ablations performed with the fundamental wavelength (1064 nm), achieved by the disassembly of the second harmonic generation module. A beam attenuator, located between the laser head and the second harmonic generation module, is used to

tune the energy per laser pulse. The maximum achievable energy was 850 mJ with the fundamental wavelength. However, in this experimental activity, the attenuator was fixed to an energy lower than the highest achievable, equal to 54 ± 1 mJ/pulse, checked before each ablation using a power meter placed in a deviated optical path before reaching the mirror. This lower energy value has been chosen in order to get a higher safety control over liquid splashing phenomena, able to provide at the same time enough energy for a correct target ablation. These critical issues have been hindered also by working in defocusing conditions, i.e., with lens-target distance slightly different from the actual focal length. The actual energy delivered to the target has been controlled through the introduction of a parameter identified as laser fluence (J/cm^2), which corresponds to the ratio between laser energy and spot size on the target and allows to take into account the setup features that affect the laser focal properties, such as the lens-target distance, the height of liquid and the refractive index of the solvent. In particular, since the laser energy per pulse was fixed, laser fluence could be easily decreased by modifying the distance between the focusing lens and the target, moving to a even more defocused condition.

3.2 Characterization of samples

3.2.1 Raman and SERS spectroscopy

Useful information on polyynes presence, thus the successful encapsulation in PMMA films has been provided by the use of Raman and surface-enhanced Raman scattering (SERS) vibrational spectroscopy. The experimental setup of a Raman spectrometer is shown in Fig. 3.6.

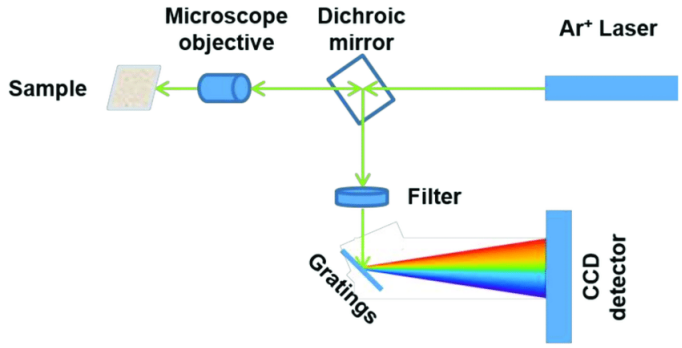

Figure 3.6: Experimental setup of a Raman spectrometer.

The emitted monochromatic beam is allowed to reach the sample after

having passed through an optical system of lenses, beam splitters and mirrors. After the cut-off of the elastic (Rayleigh) component of the backscattered light by means of a filter and the separation of the inelastically scattered light into its components by a proper diffraction grating, the signal reaches the charge-couple-detector (CCD) of the instrument, allowing the recording of the Raman spectrum. Two different Renishaw InVia micro Raman spectrometers have been used for the vibrational analysis of nanocomposites. The first instrument, equipped with a Ar^+ laser source, allowed the emission of a 457 nm (blue) and 514.4 nm (green) laser light, while the second one, characterized by the presence of a diode-pumped solid-state laser and an automatic translator x-y-z of micrometric resolution, offered a 532 nm (green) and 660 nm (red) wavelength for sample analysis. In order to exploit SERS enhancement from Ag NPs, green light has been always used. Actually, the 457 nm (blue) laser wavelength would be closer to the SPR peak of Ag NPs, however due to luminescence effects it is difficult to detect polyynic signals. Using the green light allows a lower luminescence effect is observed, allowing a proper characterization of polyynes, since in any case a good matching with wavelength and SPR peak is achieved, thanks to the peak broadening promoted by the presence of polyynes.

In order to characterize liquid samples with the 514.4 nm laser wavelength, the selected power was of 10 mW and the objective lens was the 5x one, while with solid films these parameters were 2 mW and 50x, respectively. A great advantage provided by the 532 nm Raman was the capability to automatically achieve map acquisitions, a particularly useful feature for solid samples. Indeed, the output result of a Raman assessment strongly depends on the investigated area, in particular when SERS enhancement is provided by Ag NPs dispersed in the sample, and it is not a trivial challenge to repeat measurements in the same points of a solid sample, even though a centimeter scale on its borders was introduced. As a result, only the acquisition of spectra in slightly different points could provide a reliable description of the vibrational behaviour of the sample.

The new instrument allowed to perform map acquisitions. In fact, it was possible to perform many sequential measurements around a chosen point in a user-defined grid, focusing the analysis where the sp-carbon signal was more intense and providing a more complete insight of the local differences of inelastic scattering measurements. Due to the strong dependence on the investigated points, the tens of spectra acquired during the map acquisition mode allowed to provide a statistical description of the investigated area. In this way, maps were automatically achieved in a relatively fast way, since 200 accumulations of 0.05 s each were used for every collected spectrum, hindering sample degradation with a laser power of 8.75 mW.

3.2.2 UV-Vis spectroscopy

UV-Vis absorption measurements have been conducted using a Shimadzu UV-1800 spectrophotometer. In such instrument a halogen and a deuterium lamp are used combinedly for the analysis of liquid and solid samples. The working mechanism of the spectrophotometer for UV-Vis characterization is schematized in Fig. 3.7.

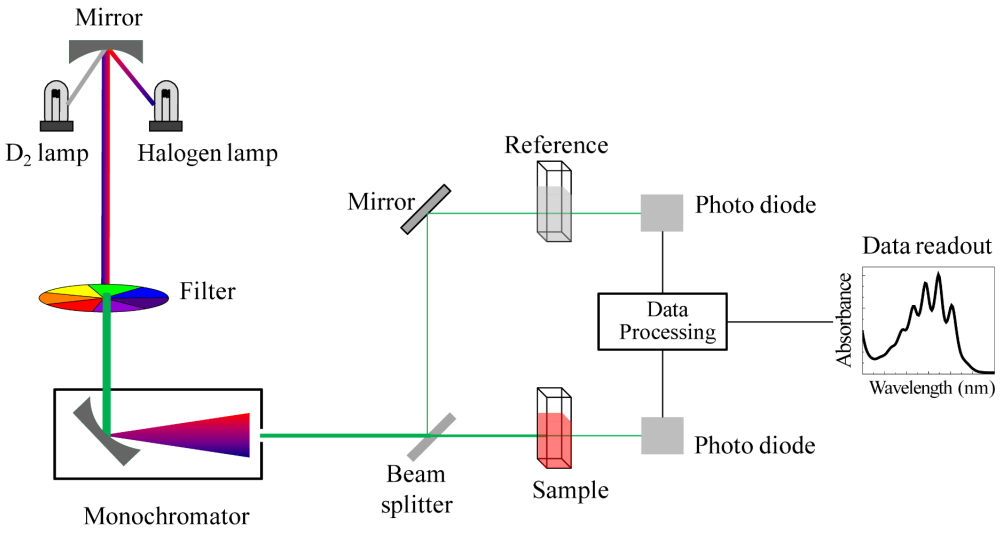

Figure 3.7: Working mechanism of a UV-Vis absorption spectrophotometer.

The emitted light passes through a filter and a monochromator before reaching an optical system of mirrors and splitters, which allow to divide the beam towards two quartz cuvettes: the first containing the solution to analyze and the second with a reference solution. The optical path provided by the cuvette, which is a fundamental parameter of Lambert Beer law (Eq. 1.1), was of 10 mm. The spectrophotometer used in this experimental activity has always been set to absorbance mode, and the recording of a reference baseline was always required before analyzing the sample. Absorption measurements within a range of wavelengths of 190-1100 nm were allowed. In our case we limited the range to 700 or 900 nm, since the UV-Vis characterization has been used to detect the position and the intensity of the SPR band of Ag NPs in solution only, usually located around 405 nm. Indeed, even though UV-Vis absorption spectroscopy is a valid technique in the assessment of both size and concentration of polyynes in solution, measurements are affected by the cut-off frequencies of used solvents and, unfortunately, the ones chosen in this work (Tab. 3.1) completely cover the polyynic absorption bands region (200-350 nm).

3.2.3 Scanning electron microscopy

The instrument used in scanning electron microscopy was a Zeiss Supra 40 Field Emission Scanning Electron Microscope (FE-SEM). By means of such apparatus, a characterization of Ag NPs morphology, size and dispersion in the sample has been achieved. In Fig. 3.8 are reported the components of a scanning electron microscope.

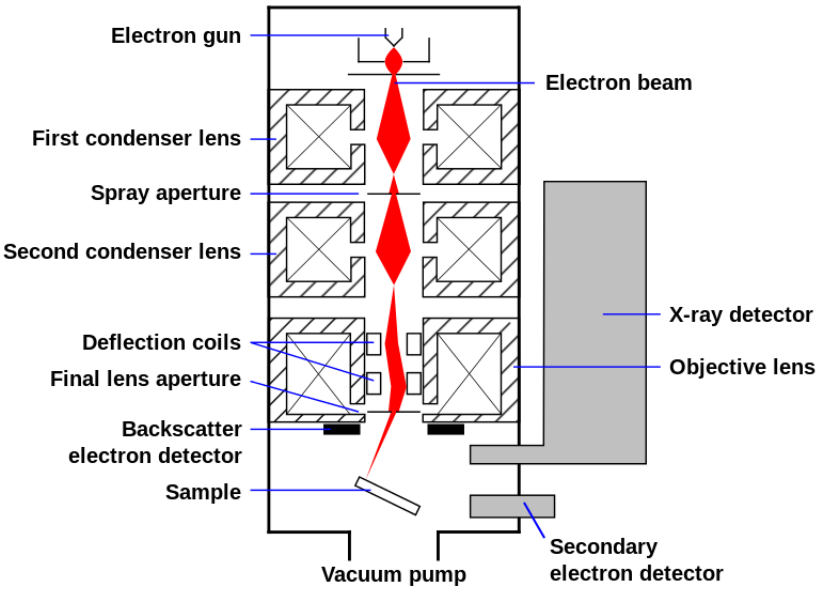

Figure 3.8: Scanning Electron Microscope (SEM) components.

By means of field emission phenomenon, a beam of highly energetic electrons is generated by the electron gun. The beam is directed towards the sample dried on a Si substrate, after having passed through a system of electrostatic and electromagnetic lenses which allow to achieve a focused and collimated beam. Two different detectors are placed to receive information from the two peculiar signals of SEM analysis: backscattered electrons and secondary electrons. The former are the ones emitted by the electron gun and reflected back after elastic collisions with the nuclei of deep regions of the sample, while the latter, which come from a more surface area of the sample, originate from sample atoms, due to inelastic interactions between the electron beam and the sample. These two signals carry different types of information: backscattered electrons are highly sensitive to the atomic number of sample atoms involved in the scattering event, providing details about sample composition, since atoms of larger radii provide higher signals, which appear brighter in the elaborated image. On the other hand, sec-

ondary electrons allow to achieve a precise analysis of sample topography. The combination of both types of signal allows a more complete inspection of the sample.

In order to achieve a correct imaging in scanning electron microscopy, the samples need to be electrically conductive, otherwise they tend to charge, leading to artifacts in the characterization. For this reason, in the analysis of certain speciments containing PMMA, which is not a conducting polymer, the application of an Ag paste on sample borders was required to confer on the sample a sufficient degree of electrical conductivity.

Chapter 4

Experimental results

In this chapter the results achieved during the experimental activity are reported. Even though the synthesis of polyynes-polymer nanocomposites had been already investigated [39, 40, 100, 101], the encapsulation of polyynes in a PMMA matrix was still an unexplored path. As a consequence, different approaches and synthesis parameters have been explored in order to properly synthesize such nanocomposites and to perform an effective characterization, able to prove the successful encapsulation of polyynes in a PMMA film for the first time. The chapter is divided into two sections, each of which involves the synthesis and stability investigation of polyynes-PMMA nanocomposites, presenting two different strategies for the introduction of Ag nanoparticles, i.e., both by the addition from an aqueous Ag colloid and by the synthesis with laser ablation in a sort of "all PLAL"-based process, consequently affecting the synthesis and characterization properties of the nanocomposite. The surface-enhanced Raman scattering (SERS) effect promoted by the presence of silver nanoparticles has been proven to be a fundamental element in the vibrational analysis of CAWs. Indeed, even though the produced polyynes are not concentrated enough to provide a Raman signal, such species are able to strongly couple with the introduced Ag NPs, which promote a remarkable enhancement for the detection of peaks in the typical sp region (1800-2300 cm^{-1}).

4.1 Nanocomposites of polyynes in a PMMA matrix with Ag NPs from aqueous colloid

The synthesis routes explored to achieve a polyynes-PMMA nanocomposite with the presence of Ag NPs in form of aqueous colloidal solution achieved by chemical reduction methods is discussed in this section. After having found a

proper method to encapsulate polyynes in the polymer nanocomposite and to include the Ag colloid, the sample with optimized features has been selected to perform a stability study, which lasted several weeks, in order to evaluate the polyynic stabilization improvement in the solid state nanocomposite.

4.1.1 Synthesis of polyynes-PMMA nanocomposites with Ag NPs from aqueous colloid

The first attempt of polyynes-PMMA nanocomposite synthesis involved the pulsed laser ablation of a bulk graphite planar target directly in a 2 mL solution of PMMA 5 wt.%. in acetone, following the successful route proposed by Peggiani et al., who succeeded in the *in situ* synthesis of polyynes in an aqueous solution containing PVA at different wt.% and achieved a nanocomposite film after water evaporation [101]. Before that work, polyynes have never been synthesized directly in polymeric solutions, but in water and organic solvents only [60–63]. In our experiment, the ablation time was set to 15 min and the laser fluence to 2 J/cm^2, at which splashing and flammability issues of the polymeric solvent have been prevented. After having performed the laser ablation, the resulting solution has been drop casted and left to dry over a glass slide at room temperature, in order to achieve a solid nanocomposite. The evaporation of acetone from the PLAL solution promoted the formation of a free-standing transparent film of PMMA, in which polyynes have been synthesized. In order to prove the formation of polyynes, proper characterization techniques needed to be performed. Since UV-Vis absorption bands of PMMA overlap with polyynic signals, Raman spectroscopy has been chosen as characterization method to detect polyynes presence. In order to perform such vibrational analysis, the film has been peeled off from the glass slide and placed over a silicon substrate, previously cleaned by means of ultrasonication baths in acetone and in water.

The Raman spectrum of the achieved polyynes-PMMA transparent film is represented in Fig. 4.1, where it has been compared to a reference spectrum of a PMMA film, solidified from a solution of PMMA 5 wt.% acetone. The two Raman spectra have been achieved after having performed repeated measurements in different areas of the samples. In both spectra a Raman peak at 2951 cm^{-1}, which is a typical feature of PMMA, corresponding to the CH stretching vibrational mode [116]. Differently from the vibrational profile of PMMA only, the spectrum of PMMA film encapsulating polyynes presents a broad band peaked around 1602 cm^{-1}, corresponding to the G-band of amorphous carbon. The presence of amorphous carbon in the system could derive both by PMMA degradation during the ablation step and by

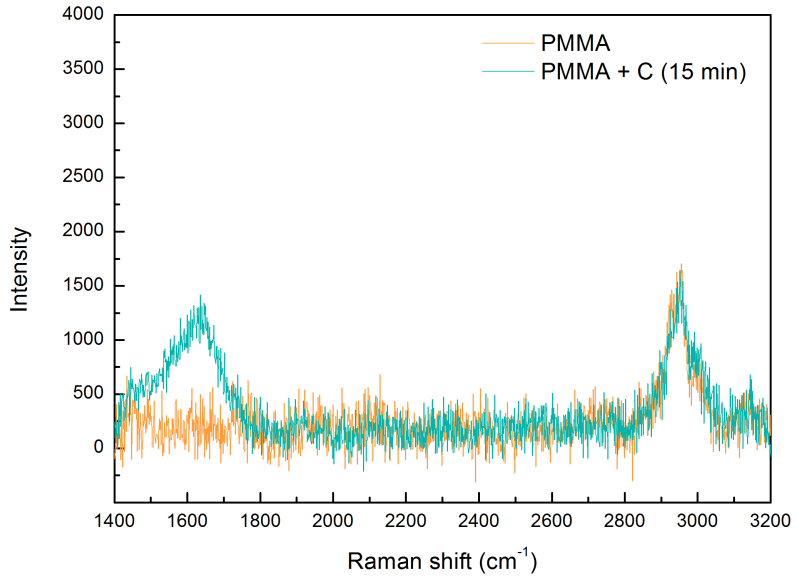

Figure 4.1: Raman spectrum of transparent solid PMMA film containing polyynes compared to the one of PMMA only.

the formation of a sp^2 carbon fraction from graphite target ablation. On the other hand, *sp* Raman features are missing in the spectrum of the film achieved after graphite ablation, in which polyynes should have been detected. In order to observe Raman signals, polyynes must be present in a higher concentration, which has still to be reached by means of PLAL. As a result, surface-enhanced Raman scattering (SERS), which allows to enhance signals of very low-concentrated species, needed to be used in the vibrational characterization, in order to demonstrate the polyynes presence in the polymeric film. To do that, the introduction of Ag nanoparticles as SERS enhancement media has been required. In principle, the available NPs were the ones in form of 10^{-3} M aqueous Ag colloid from the Lee-Meisel chemical reduction route. However, the direct mixing of such NPs in the polymeric solution, as done in the synthesis of polyynes-PVA nanocomposites [101], was not a trivial step, due to the high insolubility of PMMA in water. Thus, different ways to add the aqueous Ag colloid to the nanocomposite have been explored.

By means of scanning electron microscopy (SEM), morphological details of these Ag NPs have been achieved, allowing to better estimate their size distribution. In order to perform this characterization technique, a layer of

Ag colloid has been deposited onto a Si substrate, then it has been left to dry at 323 K to promote water evaporation. Two SEM images aquired at different magnifications are shown in Fig. 4.2, where uniformly distributed NPs with a diameter between 40-60 nm could be clearly distinguished.

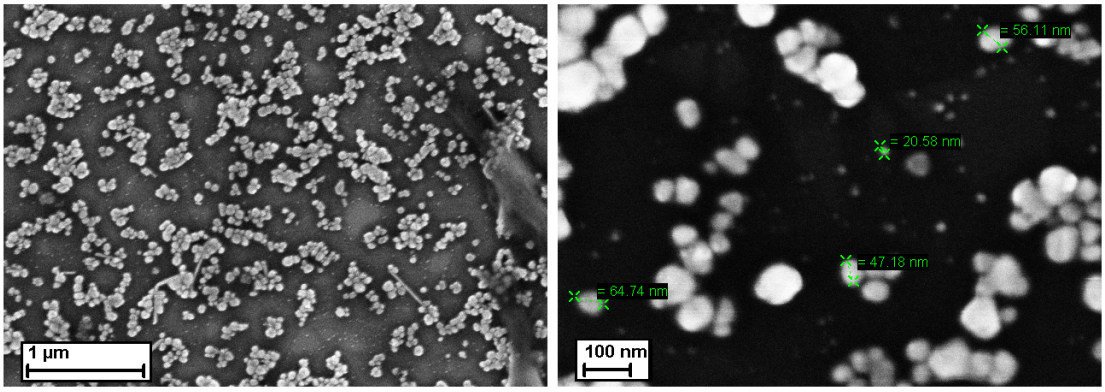

Figure 4.2: SEM images of Ag NPs dried on a Si substrate after water evaporation.

The introduction of Ag NPs to allow SERS measurements was not a trivial step in the synthesis of the nanocomposite. A first way to achieve such embedding concerned to exploit the behaviour of PMMA in water to obtain a solid material. In this method, drops of the aqueous Ag colloid were spilled directly in the solution of PMMA 5 wt.% in acetone in which the C target had been previously ablated for 15 min with a laser fluence of 2 J/cm^2. Doing so, due to PMMA insolubility, a phase separation phenomenon occurred and a wet mass of PMMA with encapsulated polyynes and entrapped Ag NPs could be collected and left to dry to achieve a solid nanocomposite. Differently from the above-mentioned transparent film without Ag NPs obtained by acetone evaporation, in this way a white, thick and brittle sample has been achieved, with brownish areas which could be an indication of Ag NPs presence. As a reference, a solid PMMA-Ag nanocomposite without polyynes has been synthesized by spilling the Ag colloid in a PMMA 5 wt.% in acetone solution, in order to compare the SERS profiles and to correctly assign the detected bands.

The Raman spectra of the two last-mentioned samples (Ag/polyynes/ PMMA and Ag/PMMA), achieved exploiting PMMA insolubility, are reported in Fig. 4.3, where they have been compared to the Raman spectra of

the original transparent films without Ag NPs (polyynes/PMMA and PMMA alone).

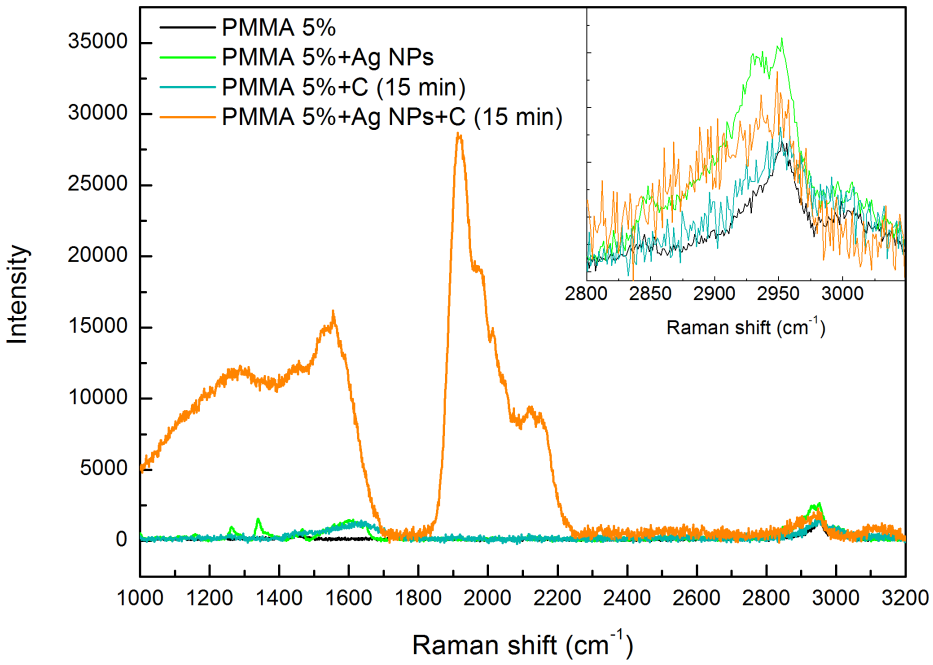

Figure 4.3: Raman spectra of solid nanocomposites with Ag NPs by PMMA insolubility. In the inset a zoom of the peak 2951 cm^{-1} is reported.

Over the presence of a broad band below 1600 cm^{-1}, related to the interaction between Ag NPs and sp^2 carbon, a strong SERS band with different peaks can be detected in the typical polyynic region of the nanocomposite sample containing both Ag NPs from the aqueous Ag colloid and polyynes: a principal peak is located around 1950 cm^{-1} and a broad shoulder at 2115 cm^{-1}, both of them presenting some features on the top. The observed signals can be considered an indication of polyynes successful encapsulation in the nanocomposite, being completely absent in the other reported spectra. As a result, the SERS effect provided by the introduction of Ag NPs in the sample has been necessary in order to detect polyynes: indeed, the ablation parameters for the synthesis of polyynes were the same used for the transparent film without the Ag presence, however, sp signals have been detected only in the nanocomposite with entrapped Ag NPs. Thus, the *in situ* pulsed laser ablation of the graphite target in the polymeric solution succeeded in

the synthesis of polyynes. Furthermore, this solidification technique, which involved the addition of the aqueous Ag colloid to the PLAL solution followed by PMMA precipitation, allowed to successfully introduce the Ag NPs to the nanocomposite.

A further consideration on the SERS effect promoted by the Ag NPs from aqueous Ag colloid can be done. In the inset of Fig. 4.3 a zoom of the region around the PMMA peak at 2951 cm^{-1} is reported. Even though Ag NPs were able to exceptionally enhance the sp carbon signals, this can not be said for this vibrational mode. Indeed, peak intensities are practically unchanged in all the samples, and the presence of Ag leads just to a more rumorous features. The reasons of the absence of SERS enhancement to the PMMA peak at 2951 cm^{-1} may reside in the nanocomposite solidification process and in the Ag NPs nature. Indeed, the SERS effect strongly depends on the adsorption of macromolecular chains on Ag NPs and the chemical coupling among them, which are features affected by nanocomposite solidification process and by the presence of surfactants or other chemical species on NPs surface.

Even if the solidification technique based on PMMA insolubility allowed to obtain a solid polyynes-PMMA nanocomposite with entrapped Ag nanoparticles, a second synthesis route has been developed, in order to overcome some limits of this method. Indeed, the obtained nanocomposites were not in form of a thin film but in small and thick PMMA fragments. With such morphology, the application of a grating in order to perform measurements in the same points after different weeks was not possible. Indeed, even though attempts to achieve thinner films with that method have been performed by pressing the wet mass before drying, no appreciable improvements have been observed. Furthermore, a critical issue with these samples was the highly uncontrolled Ag NPs dispersion in the sample, which was affected by the collection of the separated PMMA when the aqueous Ag colloid was introduced in the system.

Following a completely different solidification method, a homogeneous thin film has been achieved. In this more controlled route, a layer of Ag NPs has been firstly deposited on an accurately cleaned Si substrate, then water evaporation has been promoted by placing the sample in an oven at 323 K. After that, the solution coming from PLAL has been drop casted and left do dry over the solidified Ag NPs layer on the Si substrate. In this way, the PMMA solution with synthesized polyynes could come into contact with a more uniform layer of dried Ag NPs, avoiding the direct contact with water. This method allowed to achieve a solid nanocomposite by exploiting water and acetone evaporation in two separate steps. Moreover, differently from the previous solidification method, the PMMA concentration in the PLAL

solvent has been lowered from 5 wt.% to 2 wt.%. Over the reduction of viscosity of the system, the main reason which lead to such decision was the higher readiness and velocity of polymer dissolution. However, strong polyynic signals have been observed also by using the PMMA 2 wt.% solution, allowing to maintain that concentration for the rest of the experimental activity.

Following this route, two nanocomposites have been produced by the solidification over Si/Ag substrates of PLAL solutions, in which the C targer has been ablated at different ablation times (5 and 15 min) with a fluence of 2.02 J/cm^2 in a PMMA 2 wt.% acetone solution. In Fig. 4.4 the SERS spectra of these two solid samples are reported, compared with the spectrum of the Si/Ag substrate achieved after water evaporation from the Ag colloid.

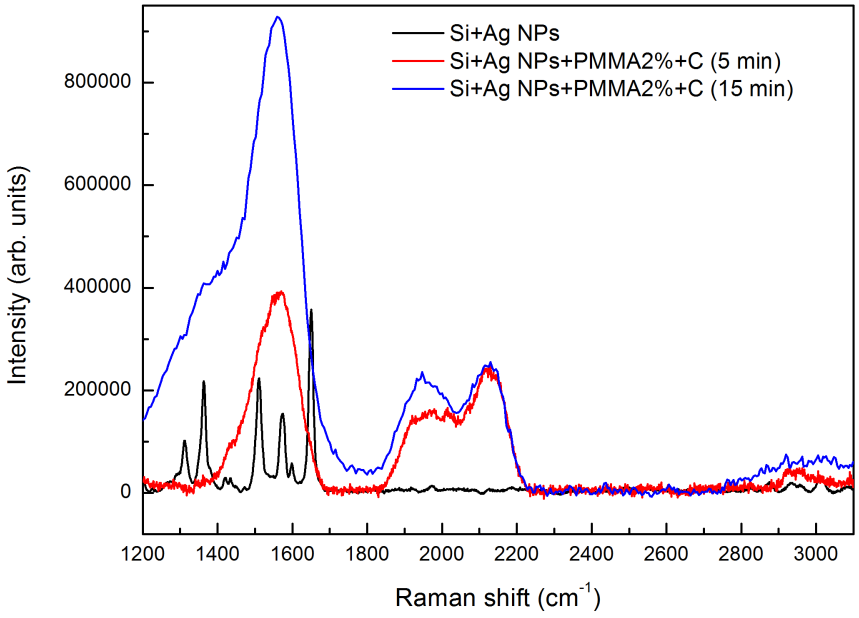

Figure 4.4: SERS spectra of polyynes-PMMA nanocomposites casted over a Si substrate with dried Ag NPs.

The presence of NPs added by the new solidification strategy provided a SERS effect in the vibrational analysis of the two nanocomposites, allowing to detect a sp band consisting of two strong peaks located around 2135 cm^{-1} and 1965 cm^{-1}. The former peak is related to the ECC vibrational mode of polyynes, which consists of a collective CC stretching of linear chains, while

the latter, located at lower wavenumbers, describes a different CC stretching normal mode, related to the out-of-phase stretching of triple bonds. In both samples containing PMMA and polyynes, an intense band at 1570 cm^{-1} can be observed, related to the presence of sp^2 carbon in the system. Furthermore, in these two spectra, a rumorous and broad band instead of the CH stretching peak of PMMA can be observed, even after having performed SERS measurements in different areas of the sample. As already discussed, this may be related to the poor interaction of macromolecular chains and Ag NPs from the aqueous Ag colloid, due to the presence of chemical species on Ag NPs surface. Moreover, since the PMMA peak is completely absent compared to the above-mentioned case, a key role could have been played by the solidification method, related to the deposition of separated layers of Ag and PMMA in different times, which could prevent an effective chemical coupling between the polymer and Ag NPs. In order to observe the differences in shape between the polyynic peaks of the two nanocomposites, the intensities of the peak at higher wavenumbers have been equalized. As a result, polyynes were successfully encapsulated also in these two kind of samples, which allowed a better control on sample morphology and on Ag distribution in the film. While the sp band at higher wavenumbers was identical in shape and position for both films, the nanocomposite in which C was ablated for 5 min displayed a relatively less defined and broader sp peak at lower wavenumbers, compared to the sample ablated for 15 min. For this reason, the latter polyynes-PMMA nanocomposite has been chosen to perform a stability study over time, in order to assess the possible stabilization provided by the encapsulation in the nanocomposite film.

4.1.2 Stability of polyynes-PMMA nanocomposites with Ag NPs from aqueous colloid

The polyynes-PMMA film solidified over a Si substrate with dried Ag NPs, obtained by the ablation of C (15 min) in PMMA 2 wt.% acetone, displayed the best SERS and morphological features among the synthesized ones. Due to this, the stability of polyynes embedded in such thin polymeric film has been investigated over time. In order to provide an accurate characterization, the Raman spectrometer equipped with a diode-pumped λ=532 nm laser has been used, thanks to the possibility to exploit its peculiar map aquisition mode. By means of the automatic translator of micrometric resolution, the point in the sample which showed particularly strong sp peaks has been selected for the study. Then, the vibrational analysis has been performed, defining a grid to be scanned by the laser around the chosen point. In

order to analyze always the same area of the sample at distance of several weeks, a centimeter scale has been placed around the film, allowing to identify univocally the investigated point. This has been made easy by the thin and homogeneous morphology of the nanocomposite, achieved following the improved solidification method. The investigated sample is reported in Fig. 4.5.

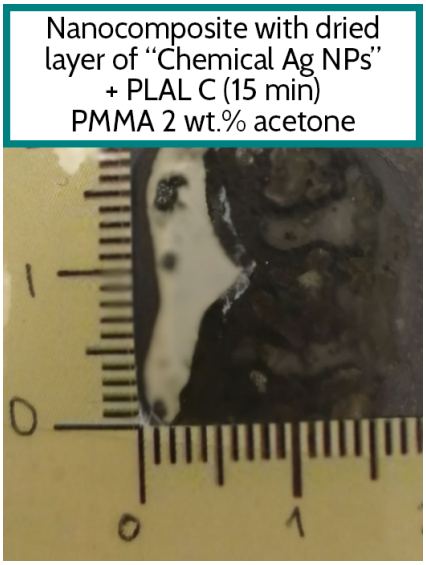

Figure 4.5: Polyynes-PMMA solid nanocomposite with Ag NPs dried from the aqueous colloid.

In the stability study, SERS spectra of the sample have been periodically taken from the moment it solidified up to 21 weeks after. Through the map aquisition mode, several spectra have been recorded in a small area around the measured point for each measurement with time. In order to have a reliable representation of the evolution of the nanocomposite vibrational properties over time, the mean intensities of the spectra aquired at different times have been computed and reported in Fig. 4.6. As already mentioned, the SERS effect is strongly dependent on the interaction between the incident laser light, the Ag nanoparticle and the adsorbed species, so the SERS spectra taken in adjacent spots of the defined map could be very different from each other. In order to take into account this fact, the standard error (SE) associated to the computed mean intensity has been introduced in the study and reported in form of the thin vertical lines crossing each SERS specrum. In particular, it can be noted that the higher SE of the mean has been achieved in the sp carbon region, proving the highly local dependence of SERS mechanism for the enhancement of signals coming from polyynes

adsorbed on Ag NPs surface.

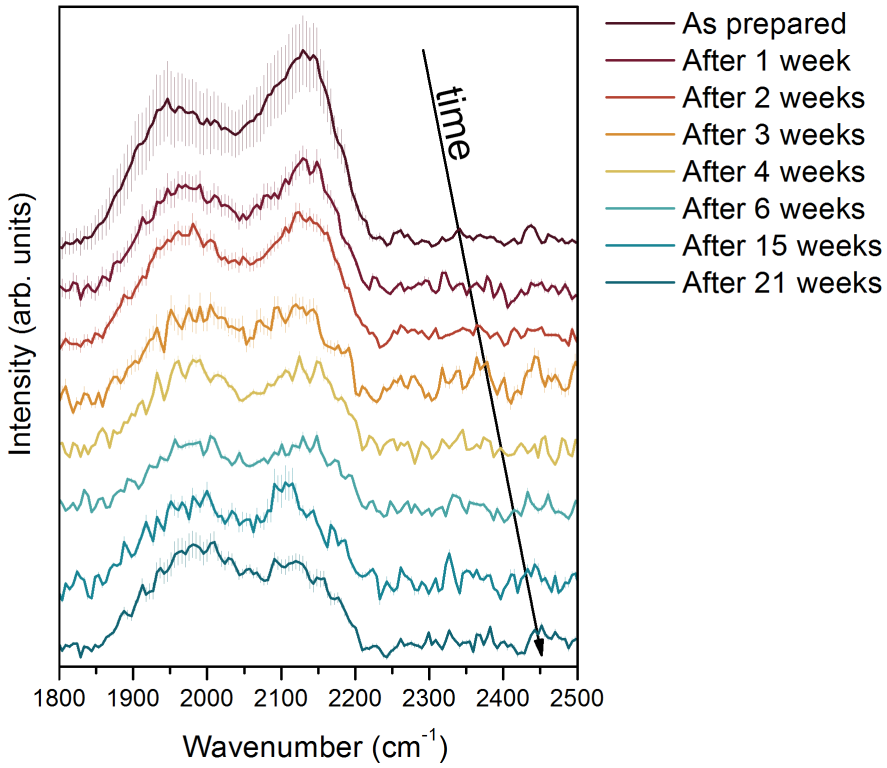

Figure 4.6: Stability study of the polyynes-PMMA film with Ag NPs from the aqueous colloid.

When using Ag NPs from the aqueous Ag colloid, the PMMA peak at 2951 cm^{-1} gets broadened and rumorously covered in the SERS characterization, probably because of the high concentration of Ag NPs or of the interaction between Ag NPs and adsorbed macromolecular chains, which could be mediated by the presence of surfactants and chemical species on NPs surface. The reported spectra have been normalized using as a reference the strong sp^2 carbon band peaked around 1570 cm^{-1}, taking into account that it might undergo changes with time due to cross-linking effects, which could promote an increase in the sp^2 carbon fraction at the expense of the more unstable sp carbon fraction.

The evolution of sp carbon signals at different times allowed us to verify the stability enhancement provided by the encapsulation of polyynes in the polymeric nanocomposite. The two strong polyynic features could be clearly distinguished even in the collected SERS spectra, allowing to assess polyynes

presence in the nanocomposite even at 21 weeks after the synthesis. After about 3 weeks, the SERS bands of sp carbon, originally peaked at 2135 cm^{-1} and 1965 cm^{-1}, have been subjected to modifications in shape and position with time, resulting slightly broadened and less defined as time passed. In particular, in the case of the sp band at higher wavenumbers, a red shift of about 20 cm^{-1} has been observed in the measurements performed after 15 weeks from the synthesis, together with a decrease of the relative intensity already after 3 weeks if compared to the band at lower wavenumbers. On the other hand, considering the band at lower wavelengths, a smaller change in shape occurred with respect to the other polyynic signal, together with a much lower reduction in its relative intensity. Furthermore, a blue shift of about 15 cm^{-1} has been observed. The most probable hypothesis for the observed shifts is related to a modification in the chemical interaction between Ag NPs and adsorbed polyynes over time, which could heavily affect the whole SERS enhancement process and the resulting highlighted peaks.

4.2 Nanocomposites of polyynes in a PMMA matrix with Ag NPs by *in situ* PLAL

In addition to the use of Ag NPs from the aqueous colloid, a completely different approach has been followed for the nanocomposite synthesis, in order to overcome the limitations of such NPs. In this method, the synthesis of Ag NPs by pulsed laser ablation in liquid (PLAL) has been performed exploiting the wide versatility of such physical method, which in this approach has been used not only for the synthesis of polyynes, but also for Ag NPs production, by the ablation of a Ag target in a sort of "all PLAL"-based process. Furthermore, the use of PLAL for the synthesis of both Ag NPs and of polyynes allowed us to design a novel process for the *in situ* synthesis of Ag/polyynes/PMMA nanocomposites. A great advantage of the use of PLAL is the possibility to produce the Ag NPs in a solvent different from water, whose presence was unavoidable when using the aqueous Ag colloid, and which presented solubility issues with PMMA, affecting both the introduction of Ag in the nanocomposite and the solidification step. Moreover, the absence of a chemical reduction method allowed to synthesize high purity NPs without the presence of surfactants and chemical byproducts, which could affect the interactions of Ag NPs with macromolecular chains and polyynes. Even though the concentration of Ag NPs synthesized by physical methods is much lower compared to the one achieved by means of chemical reduction processes, a SERS effect has been observed also with NPs

of this different nature, allowing to study the encapsulation of polyynes in the nanocomposite with a different synthesis route and their stability over time.

4.2.1 Synthesis of polyynes-PMMA nanocomposites with Ag NPs by *in situ* PLAL

The use of pulsed laser ablation in liquid for the synthesis of Ag NPs allowed to fabricate the nanocomposites in a different way compared to the strategy followed with aqueous Ag colloid. Indeed, the absence of water allowed to obtain a controlled single-step nanocomposite solidification by casting and leaving to dry over a Si substrate a PLAL solution, already containing both polyynes and Ag NPs. To do this, the nanocomposite solution has been achieved by performing the *in situ* synthesis of polyynes directly in a solution containing the Ag NPs.

In order to select a proper PLAL solvent, different Ag NPs solutions have been produced by laser ablation of an Ag target for 5 minutes with a fluence of 2 J/cm^2, the same used for the C target, using as liquid media both acetone and a PMMA 2 wt.% in acetone solution. Furthermore, to investigate the effects of the addition of PMMA after the Ag NPs synthesis, a third solution has been achieved by mixing a PMMA solution to a solution of Ag NPs in acetone just after their synthesis, up to reach a 2 wt.% concentration. The three different liquid samples have been characterized both as prepared and two days after the synthesis by means of UV-Vis absorption spectroscopy. The spectra are reported in Fig. 4.7.

In all the studied systems a strong absorption band around 400-430 nm has been observed, peaked in the expected region for the Ag NPs surface plasmon resonance (SPR) band. This allowed to prove the effective formation of Ag NPs by PLAL in different solvents. An indication of Ag NPs stability with time has been provided by the change in shape of the absorption spectra taken after two days. As time passes, NPs in solution tend to agglomerate, leading to a broadening of the absorption peak and to a shift towards higher wavelengths, due to the formation of larger clusters. It can be observed that among the studied samples, the NPs ablated in the PMMA 2 wt.% acetone solution were the ones characterized by a lower increase of size polydispersity after two days. In particular, their two spectra at $\lambda \geq 480$ nm were almost coincident, indicating an almost unvaried even after two days. This was an expected property since, as indicated in literature, the presence of a dissolved polymer in the PLAL liquid medium helps to maintain an almost constant size distribution with time, conferring steric stabilization and

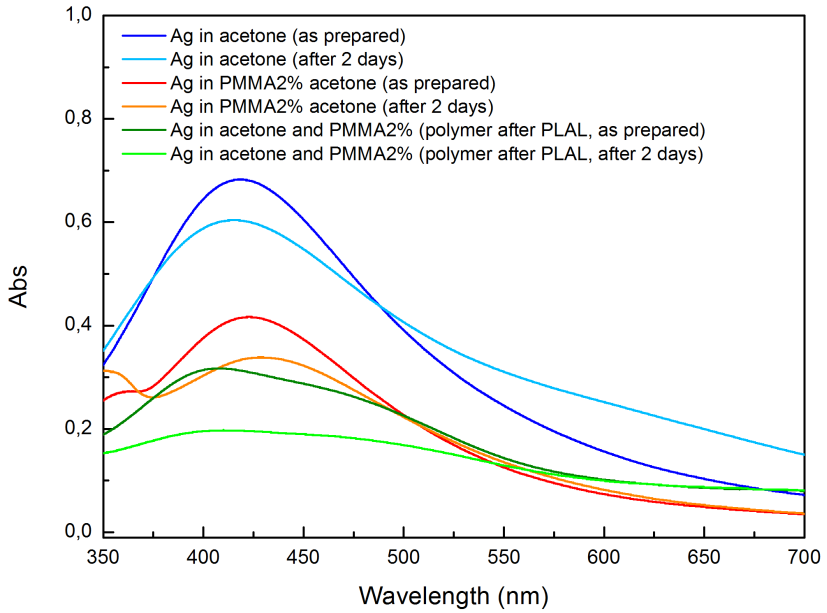

Figure 4.7: UV-Vis spectra of Ag NPs by PLAL in different solvents.

growth quenching on the generated nanomaterials [110].

Further details on the formation and morphology of the synthesized Ag NPs have been provided by means of scanning electron microscopy characterization. In Fig 4.8 are reported the SEM images of (a) Ag NPs and (b) Ag NPs in a PMMA film over a Si substrate, achieved after solvent evaporation of the Ag in acetone and Ag in PMMA 2 wt.% acetone PLAL solutions, respectively. Ag NPs with a diameter between 20-50 nm could be observed, in a much lower concentration compared to Ag NPs from chemical methods. In particular, the SEM characterization of Ag NPs in the polymeric film has been a non trivial analysis, since sample charging occurred due to the non-conducting nature of PMMA. Hence, in order to achieve reliable SEM images, a conductive Ag paste has been applied to the borders of the sample.

The preliminary analysis of ablated Ag NPs allowed us to select the solution of PMMA 2 wt.% acetone as initial PLAL solvent in the novel *in situ* synthesis process for the nanocomposites with Ag NPs. This new strategy involved the ablation of a Ag target for 5 min in a PMMA 2 wt.% acetone solution, followed by the ablation of a graphite target directly in the achieved Ag/PMMA/acetone solution, after having replaced the Ag target with the C one. Doing so, the achieved solution could be casted and dried on a Si

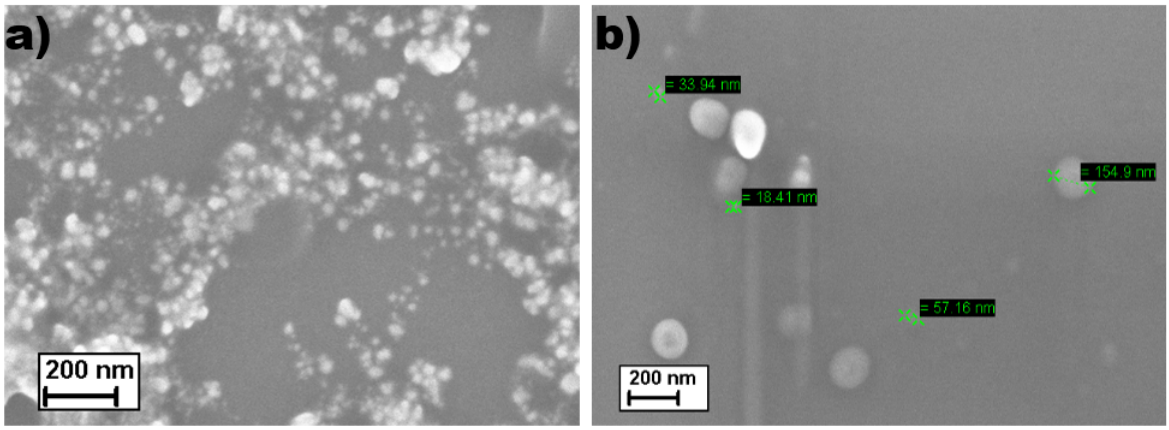

Figure 4.8: SEM images of (a) Ag NPs and (b) Ag NPs in PMMA by PLAL of Ag target.

substrate, leading to the formation of a thin PMMA film with immobilized polyynes and Ag NPs. Compared to the strategies followed when dealing with the aqueous Ag colloid, a single solidification step with already dispersed Ag NPs within the polymer matrix has been achieved. This has been possible by employing a physical method for Ag NPs synthesis, without the need of leaving to dry in two separate times first the aqueous Ag colloid and then the polymeric solution with polyynes. In this way, in the solid film a different physico-chemical interaction has been established between Ag, polyynes and PMMA.

After having ablated the Ag target for 5 min, two samples containing polyynes have been synthesized by PLAL of the graphite target at different ablation times using the produced Ag/PMMA/acetone solutions as liquid media. The UV-Vis spectra of the achieved solutions are reported in Fig. 4.9, where they have been compared also to the Ag/PMMA/acetone solution in which the C ablation was not performed.

Two competing phenomena can be observed looking at the shifts of the Ag NPs SPR band as the C ablation time increases from 0 (absence of polyynes) to 15 min. As the overall ablation time increases due to C ablation, the first phenomenon occurring is the fragmentation of the Ag NPs present in solution due to further laser irradiation, leading to a blue shift lower wavelengths of the SPR peak, from 424 to 405 nm, corresponding to a decrease of NPs mean size. Indeed, in absence of an Ag target, no further Ag mass is introduced in the system, and the already formed particles undergo a resizing process during the ablation of the C target. However, as the graphite ablation time increases from 5 to 15 minutes, a red shift of the SPR peak from 405 to 410 nm

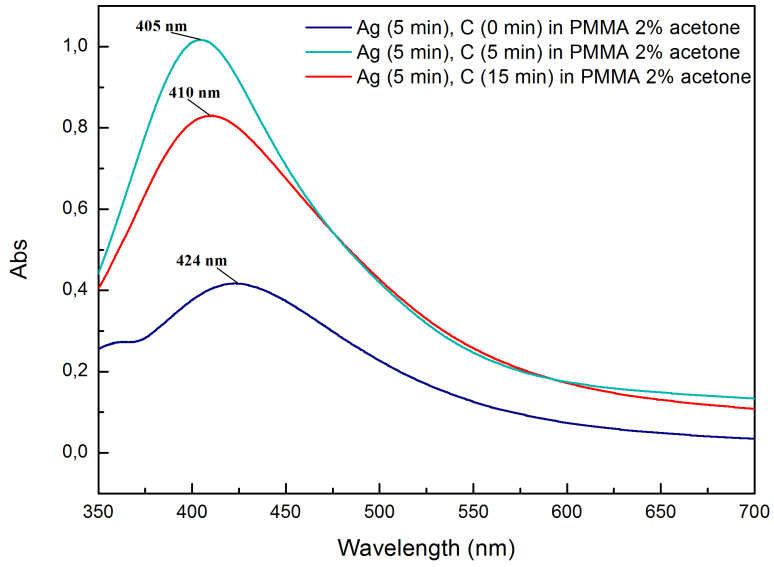

Figure 4.9: Effect of C ablation time in a Ag NPs solution.

is observed. This is related to a second competing phenomenon consisting of Ag NPs agglomeration, which becomes relevant and superimposes to the Ag fragmentation process, leading to an increase of Ag NPs mean size reflected by a shift of the SPR peak towards longer wavelengths. This tendency can be explained by the increase of polyynes concentration in the solution with a longer ablation time, as polyynes peculiar effect in presence of Ag NPs is to promote their aggregation by pinning on their surface. Even though polyynes absorption features can not be observed in presence of a solution of PMMA in acetone, due to the overlapping with solvent bands, this UV-Vis analysis allowed us to reinforce the hypothesis of successful polyynes synthesis, since the increase in the mean size of NPs has been probably promoted by the increase of polyynic concentration as the C ablation time increased.

Once the nanocomposite solution has been left to solidify on a Si substrate, an effective proof of polyynes presence in the nanocomposite has been provided by means of the SERS analysis of the solid film. By looking at the UV-Vis profiles in Fig. 4.9, we chose to perform the vibrational characterization on the sample corresponding to a Ag ablation time of 5 min in the PMMA 2 wt.% acetone solution, followed by a graphite ablation time of 15 min. Indeed, due to NPs agglomeration promoted by the polyynic presence, its SPR peak (410 nm) has broadened and the slight increase in the absorption in

correspondance to the Raman wavelength (532 nm) could improve the SERS ehnancement. Furthermore, as mentioned above, with the ablation time of 15 min a higher concentration of produced polyynes could be promoted. In Fig. 4.10 the Raman spectrum of the polyynes-PMMA nanocomposite film with Ag NPs produced by PLAL is reported, compared to the spectrum of an analogue solid film in which C ablation was not performed.

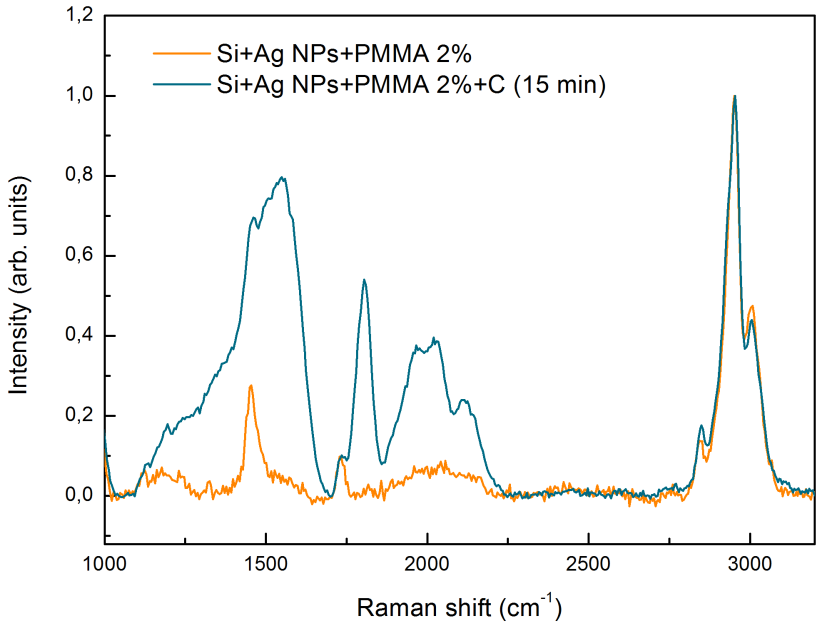

Figure 4.10: SERS spectrum of the polyynes-PMMA nanocomposite with Ag NPs by *in situ* PLAL.

The two spectra have been normalized using as a reference value the intensity of the peak corresponding to the CH stretching mode of PMMA at 2951 cm^{-1}. Considering the spectrum of the sample in which C has been ablated for 15 min, a broad and intense sp^2 carbon band around 1550 cm^{-1} has been observed. Moreover, three peculiar sp features have been detected, peaked at 2115 cm^{-1}, 2025 cm^{-1} and 1980 cm^{-1}, respectively. Polyynic signals have been observed thanks to the presence of Ag NPs by PLAL, which succeeded in providing the required SERS enhancement for the vibrational characterization. As a result, a polyynes-PMMA nanocomposite with entrapped Ag NPs has been successfully obtained, performing the laser ablation both to achieve Ag NPs and then to synthesize polyynes by changing the target in the

PLAL solution after the Ag NPs formation. Compared to the one provided by the aqueous Ag colloid, a different SERS mechanism has been observed when using Ag NPs. This may depend on the solidification method and on the nature of synthesized particles themselves, which heavily affects the way they interact with the other nanocomposite components. With this kind of NPs, three different sp peaks could be distinctly observed, while in the aqueous Ag colloid case only two peaks were found in the sp region (see Fig. 4.4). Moreover, a strong SERS enhancement of the typical PMMA peak at 2951 cm^{-1} has been observed, which did not occur using the other kind of Ag NPs. This may be related to the purity degree of NPs achieved by PLAL, which do not require the presence of surfactants and reducing agents, allowing a stronger interaction with macromolecular chains. A further feature in the SERS spectrum of the Ag/polyynes/PMMA nanocomposite film is the appearance of a strong band peaked at 1805 cm^{-1}. This wavenumber has been assigned in scientific literature to the C=O stretching vibrational mode [117]. Even though the carbonyl group is present both in acetone and in the PMMA repeating unit, a vibrational mode at that wavenumber does not belong to acetone or PMMA alone. Indeed, acetone should be absent in the solid system since its evaporation has been promoted to achieve the film, however if an unevaporated fraction would be present in the measurement taken just after film solidification, from Raman spectra in literature we assign a peak related to the carbonyl group at 1715 cm^{-1} with a feature at lower intensity at 1750 cm^{-1}. For what concerns PMMA, both the Raman spectra found in literature and the ones reported in Fig. 4.9 display a C=O feature only at 1732 cm^{-1}. Thus, the peak at 1805 cm^{-1} could be related to byproducts generated during the laser ablation of graphite in presence of an oxygen source, catalyzed by the presence of Ag NPs.

In order to explore the effects of the ablation sequence, a polyyne-based nanocomposite solution with Ag NPs by *in situ* ablation has been achieved by inverting the ablation steps while all the other process parameters have been kept constant. In this case, first a graphite target has been ablated for 15 min in a PMMA 2 wt.% acetone solution, then, in the achieved polyynic solution, the PLAL of a Ag target has been performed for further 5 min. In this way, Ag NPs in solution were not irradiated also during the 15 min of C ablation, but only for the 5 min of Ag ablation. At the same time, polyynes in PLAL solution have been irradiated for additional 5 min during the Ag ablation. However, while the UV-Vis analysis of the PLAL solution allowed to prove the formation of Ag NPs, very weak polyynic signals have been detected in the vibrational characterization of the solidified sample. Different hypothesis have been formulated in order to understand why polyynes were almost absent in the nanocomposite with the inverted ablation sequence. A

first reason could be that, being irradiated for further 5 minutes without the ablation of a carbon source, polyynes in solution may undergo faster degradation reactions due to the exposure to laser pulses. Moreover, the formation of Ag NPs after polyynes synthesis might be not as effective as in the case of original ablation sequence (first Ag, then C) in conferring stability on synthesized polyynes. Another possible phenomenon which might be occurred during the synthesis process is the adsorption of polyynes on the bulk Ag target surface as it was introduced in the PLAL vial, causing a reduction of the actual polyynes concentration in the PLAL solution. As a result, the more effective PLAL sequence was the one adopted in principle, with the PLAL of the C target for 15 minutes only after the 5 minutes ablation of the Ag target.

Up to now, all the ablations have been performed using the 532 nm green wavelength. In order to select an optimal nanocomposite for the long-term stability study, once that PLAL initial solvent and ablation sequence have been determined, a study on the effects of PLAL wavelength has been conducted, by changing from the second harmonic to the fundamental laser wavelength (1064 nm) for the nanocomposite *in situ* synthesis process. While the fundamental wavelength is not as common as the second harmonic one in polyynes synthesis, in literature is shown an increase of the ablation yield when the fundamental wavelength is used for metallic NPs production, making us expect a higher concentration of synthesized Ag NPs [106]. In order to work at the same fluence conditions adopted with the 532 nm wavelength ($2\ J/cm^2$), the lens-target distance has been reduced from 170 to 128.5 mm. In this way, a larger laser spot on the target compensated the increase in energy per pulse, which raised from 54 to 198 mJ/pulse with the 1064 laser. The ablation process has been conducted keeping the same PLAL parameters used for the nanocomposite obtained with the 532 nm, performing the ablation of Ag (5 min) followed by C (15 min) in the usual 2 mL solution of PMMA 2 wt.% acetone. The UV-Vis absorption profile of the solution achieved using the fundamental wavelength is shown in Fig. 4.11, compared to the one achieved with second harmonic wavelength.

In order to observe the Ag NPs SPR peak in the solution ablated with the 1064 nm wavelength, a dilution with PMMA 2 wt.% in acetone has been required to avoid the saturation of the absorption peak. This was an indication of the high Ag NPs concentration, as expected using the fundamental wavelength. Without dilution, indeed, the SPR peak would have been much more intense compared to the one characterizing the solution obtained using the 532 nm laser. The higher concentration of Ag NPs was reflected also by the coloration of the solution, which tended to a dark reddish-brown tonality just after few seconds after the beginning of the PLAL process, while in

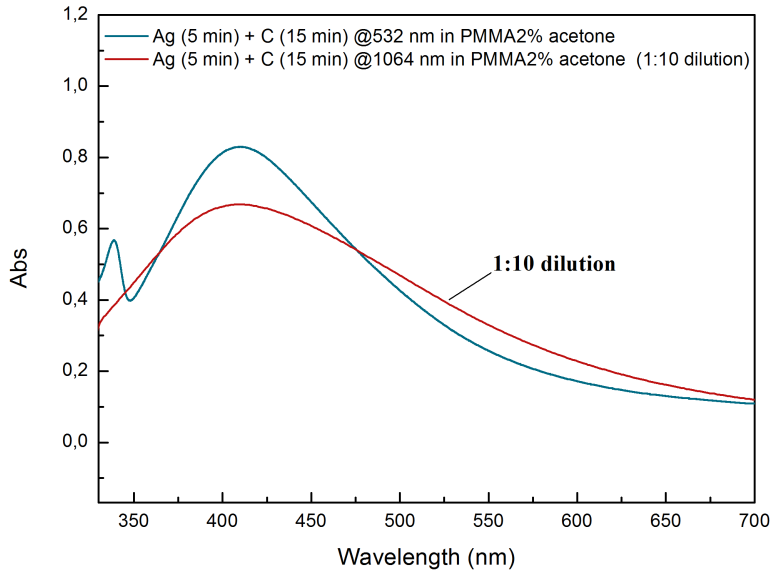

Figure 4.11: Effect of ablation wavelength in the synthesis of a polyynes-PMMA nanocomposite solution with Ag NPs by PLAL.

the case of lower concentrated Ag NPs produced with the second harmonic wavelength it was light yellowish. Both the solution presented a SPR peak at 410 nm, indicating a similar size distribution of Ag NPs. Furthermore, as in the case of 532 nm ablation wavelength, the absorption spectrum of the Ag NPs produced with the 1064 nm laser displayed a good absorbance value in correspondance of the Raman spectrometer laser wavelength (532 nm).

In order to prove the polyynes presence, Raman spectroscopy has been performed on a solid sample, which has been achieved by acetone evaporation after having casted the solution over a Si substrate. In Fig. 4.12 is reported the Raman spectrum from the analysis of the solid sample achieved with the ablation wavelength of 1064 nm, compared to the one related to the synthesis with 532 nm. The Raman spectra have been normalized using the intensity of the sp^2 carbon peak at 1560 cm^{-1} as a reference value. Differently from the film produced with the 532 nm laser, the one achieved with the fundamental wavelength presents only two broader and less defined polyynic features, peaked at 2155 cm^{-1} and 1970 cm^{-1}. Also in this case, the detection of such signals has been made possible by the SERS enhancement provided by the presence of Ag NPs in the nanocomposite. Compared to the intensity of the sp^2 band, the one of sp carbon bands is much lower in the case of the use

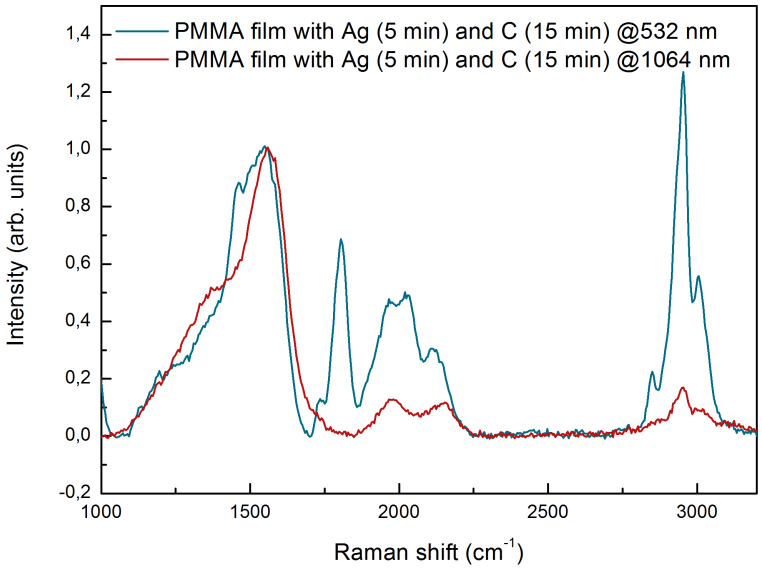

Figure 4.12: Effect of wavelength on SERS spectra of polyynes-PMMA films with Ag NPs by PLAL.

of fundamental wavelength. Furthermore, the PMMA peak at 2951 cm^{-1}, related to the CH stretching mode, is much weaker in the sample produced with the fundamental wavelength. As a result, the observed SERS features led us to hypothesize a much lower yield in the synthesis of sp carbon chains in the nanocomposite film with the 1064 nm. This might related to two different causes: firstly, the high concentration of Ag NPs does not allow the laser pulse to properly hit the graphite target during the polyynes synthesis step, due to the higher probability of scattering of incident light with Ag NPs. In this way, light reflection would lead to a reduction of the actual laser energy which reaches the C target. Moreover, the high energy achieved with the 1064 nm wavelength could lead to a faster PMMA degradation in the PLAL solvent, reducing the polyynic stabilization effect provided by the polymer. A further observation can be done on the absence of the 1805 cm^{-1} peak in the $\lambda_{abl} = 1064$ nm spectrum. It has been shown that this peak is strictly related to the presence of polyynes in a nanocomposite containing Ag NPs by PLAL, thus its absence might be related to the reduced synthesis yield of polyynes in the sample, since, except from PLAL wavelength, any other of the process parameters has been kept identical as in the case when the peak was detected using the 532 nm laser wavelength.

4.2.2 Stability of polyynes-PMMA nanocomposites with Ag NPs by *in situ* PLAL

After having tried different ablation and material parameters, it turned out that the nanocomposite film produced by PLAL (λ_{abl} = 532 nm) of Ag (5 min) and C (15 min), using acetone with dissolved PMMA 2 wt.% as initial liquid medium, was the one characterized by a stronger SERS profile in the expected sp carbon region. The nanocomposite studied in this stability investigation is reported in Fig. 4.13.

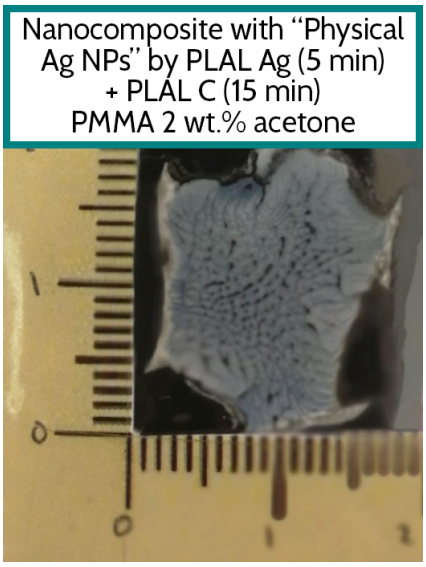

Figure 4.13: Polyynes-PMMA solid nanocomposite with Ag NPs by *in situ* PLAL.

The exploration of such features allowed us to select this sample in order verify the CAWs stability improvement, in analogy with what has been done with the selected polyyne-PMMA nanocomposite with Ag NPs from chemical methods (see Fig. 4.6). Hence, the same characterization route as been adopted also with the Ag/polyynes/PMMA film with Ag NPs from pulsed laser ablation. By means of the Raman spectrometer with the diode-pumped laser (532 nm) and the automatic translator, a point with strong and narrow sp signals has been identified and, by the application of a centimeter scale on sample's borders, it has been periodically analyzed using the map aquisition mode, from the moment it solidified up to 21 weeks after. Similarly to the vibrational analysis of the nanocomposite with Ag NPs from the aqueous colloid, due to the strong local dependence of SERS response, a statistical interpretation of measurements has been required. In Fig. 4.14 the stability

study of the nanocomposite with NPs from physical methods is reported. Each spectrum in the plot represents the mean intensity among the ones achieved by the map aquisition around the investigated point, together with the standard error (SE) of the computed mean.

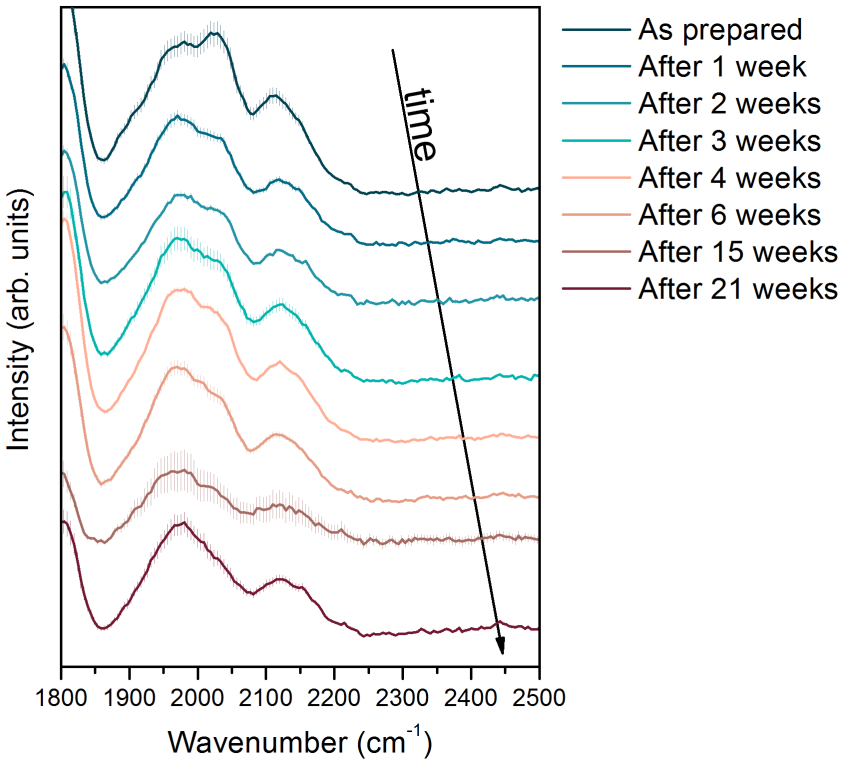

Figure 4.14: Stability study of the polyynes-PMMA film with Ag NPs by *in situ* PLAL.

From the investigation of this nanocomposite over time, the stability enhancement provided by the PMMA matrix as well as by the Ag NPs dispersed in the nanocomposite has been proved, as sp peaks have been clearly detected even at 21 weeks from sample preparation. Differently from the sample with Ag NPs from chemical reduction methods, which was characterized by two polyynic bands, this nanocomposite film displayed in principle three sp peaks, located at 2115 cm^{-1}, 2025 cm^{-1} and 1980 cm^{-1}. However, already after a few weeks, the peak at 2025 cm^{-1} started to change in shape and to decrease in intensity, initially becoming a shoulder of the band at 1980 cm^{-1}, up to being completely incorporated into a single broader band after 21 weeks. For what concerns the sp peak at 2115 cm^{-1}, an appreciable broadening has been

observed only after 15 weeks, without involving other changes in relative intensity and position. The spectra achieved in this stability study are less rumorous compared to the ones shown in the stability study of the sample containing Ag NPs from the aqueous colloid (Fig. 4.6), probably due to the lower concentration of Ag NPs from physical methods in the nanocomposite. Another difference with the stability behaviour observed in the nanocomposite with NPs from aqueous Ag colloid involves the shifts of polyynic peaks positions. Indeed, in that sample a red shift of the peak at higher wavenumbers and a blue shift of the one at lower wavenumbers have been observed, probably due to a possible change in the chemical interaction between the carbon wire and the Ag nanoparticle, which is responsible for a modification in the SERS enhancement. However, in the case of the film containing Ag NPs from PLAL, such shifts have not been observed. Their absence could be related to a more stable chemical interaction between polyynes and Ag NPs by physical methods. A further feature of this stability analysis is the presence of the C=O stretching peak at 1805 cm^{-1} even after 21 weeks: the detection of such peak even at longer times allows to exclude the one of the initial hypothesis involving the SERS of an unevaporated fraction of acetone, and to focus the attention on a mechanism of interaction between Ag nanoparticles and byproducts of graphite ablation.

As a result, a remarkable long-term stability of polyynes in the nanocomposite has been observed also in nanocomposites with Ag NPs synthesized by PLAL. However, it is not possible to already state a quantitative correlation between the polyynes stability enhancement and the nature of used NPs in the two studied samples, due to the differences in the solidification route of the nanocomposites, in the synthesis process of the Ag NPs as well as in their physico-chemical properties.

Conclusions and future perspectives

The initial aims of this thesis work were:

- Synthesis of polyynes in a PMMA matrix by means of pulsed laser ablation in liquid (PLAL) and subsequent characterization of the produced nanocomposites;
- Evaluation of polyynes stability enhancement provided by the embedding in a polymeric nanocomposite.

For what concerns the synthesis step, pulsed laser ablation in liquid revealed to be a versatile and effective production method for the synthesis polyynes-PMMA nanocomposites. Following the *in situ* synthesis concept, polyynes have been successfully produced in a PMMA matrix for the first time, performing the graphite ablation directly in a solution of PMMA in acetone. Then, different solidification methods have been investigated, among which the route of casting and drying the PLAL solution over a Si substrate allowed to achieve a more homogeneous and thin nanocomposite film. The addition of Ag NPs for surface-enhanced Raman scattering (SERS) purposes allowed to perform an effective characterization of the samples. Indeed, both kinds of used NPs (from an aqueous Ag colloid and from PLAL of Ag in the polymeric liquid before C ablation) provided an exceptional enhancement of the polyynic signals. In the samples containing Ag from PLAL directly in a step of the polyynes nanocomposites, UV-Vis absorption spectroscopy and scanning electron microscopy (SEM) have been used in order to characterize the plasmonic and morphological properties of synthesized Ag NPs. After having found a proper combination of material and process parameters, two nanocomposite films, achieved with the two different strategies for the entrapment of Ag NPs, have been selected for the stability study over time. In this analysis SERS measurements have been periodically performed around the same point in the nanocomposite. The typical *sp* signals have been detected in both samples, allowing us to observe the polyynic presence

at least for the first 21 weeks after the sample preparation. Thus, the steric stabilization effect provided by the polymer, together with the adsorption of polyynes on Ag NPs surface, allowed to improve the stability of polyynes immobilized in the nanocomposite.

The achieved results could be a possible starting point for further researches, as well as for other supporting studies to have a more complete comprehension of the observed phenomena. First of all, a natural continuation can be the stability study of the already presented nanocomposites at times even longer than 21 weeks, in order to determine the actual lifetime of CAWs in these nanocomposites. Secondly, it could be interesting to study the evolution of *sp* carbon signals during the laser ablation process by *in situ* SERS measurements directly by the immersion mode of a proper probe, either continously or by interrupting the synthesis process at fixed time intervals. In this way, information on the polyynic generation mechanism during PLAL could be achieved, allowing also to compare polyynes stability properties in the liquid solution and in the solid films. Furthermore, the same route followed to achieve the polyynes nanocomposites with Ag NPs from PLAL could be used for the solidification of the nanocomposite over a glass slide, which has been proven to be an effective method for PMMA solidification as a transparent, free standing film. In this way, by means of UV-Vis spectroscopy, the properties of Ag NPs in the solid state nanocomposite could be explored and compared to the ones achieved from the analyis of PLAL solution. A very common element in the researches involving CAWs is the use of high performance liquid chromatography (HPLC), a powerful tool which provides information on size distribution of produced polyynes and which is able to separate linear chains by size. In this thesis work it has not been used due to the high viscosity of the polymer, which is detrimental to the HPLC columns. Nevertheless, it could be interesting to separate polyynes in a proper solvent (e.g. acetone) and to add the polymer in a second time, in order to investigate the stability of polyynes of different lenght in polymeric nanocomposites. In addition to this, the effects of PMMA concentration in the PLAL solution on polyynes formation and stability could be deepen. These are only some of the possible future steps to expand the presented work, however, having regard to the obtained promising outcomes and to the lack of a complete treatment of polyynes-polymer nanocomposites in literature, there is a plenty of work to be done in the future in order to explore the field of polyynes-polymer nanocomposites, also trying new materials as well as process parameters, heading step by step to the exploitation of CAWs properties in future solid-state devices.

Bibliography

[1] Eduardo HL Falcao and Fred Wudl. Carbon allotropes: beyond graphite and diamond. *Journal of Chemical Technology & Biotechnology: International Research in Process, Environmental & Clean Technology*, 82(6):524–531, 2007.

[2] Andreas Hirsch. The era of carbon allotropes. *Nature materials*, 9(11): 868–871, 2010.

[3] Charles Letnam Mantell. Carbon and graphite handbook. 1968.

[4] Neil W Ashcroft and N David Mermin. Solid state physics. 1976.

[5] Donald R Askeland, Pradeep Prabhakar Phulé, Wendelin J Wright, and DK Bhattacharya. The science and engineering of materials. 2003.

[6] OA Shenderova, VV Zhirnov, and DW Brenner. Carbon nanostructures. *Critical reviews in solid state and material sciences*, 27(3-4): 227–356, 2002.

[7] Carlo S Casari and Alberto Milani. Carbyne: from the elusive allotrope to stable carbon atom wires. *MRS Communications*, 8(2):207–219, 2018.

[8] Harold W Kroto, James R Heath, Sean C O'Brien, Robert F Curl, and Richard E Smalley. C60: Buckminsterfullerene. *nature*, 318(6042): 162–163, 1985.

[9] Henry Ajie, Marcos M Alvarez, Samir J Anz, Rainer D Beck, Francois Diederich, K Fostiropoulos, Donald R Huffman, Wolfgang Kraetschmer, Yves Rubin, et al. Characterization of the soluble all-carbon molecules c60 and c70. *Journal of Physical Chemistry*, 94(24): 8630–8633, 1990.

[10] Sumio Iijima. Helical microtubules of graphitic carbon. *nature*, 354 (6348):56–58, 1991.

[11] Prabhakar R Bandaru. Electrical properties and applications of carbon nanotube structures. *Journal of nanoscience and nanotechnology*, 7(4-5):1239–1267, 2007.

[12] Kostya S Novoselov, Andre K Geim, Sergei V Morozov, D Jiang, Y_ Zhang, Sergey V Dubonos, Irina V Grigorieva, and Alexandr A Firsov. Electric field effect in atomically thin carbon films. *science*, 306(5696): 666–669, 2004.

[13] Salisu Nasir, Mohd Zobir Hussein, Zulkarnain Zainal, and Nor Azah Yusof. Carbon-based nanomaterials/allotropes: A glimpse of their synthesis, properties and some applications. *Materials*, 11(2):295, 2018.

[14] J Jansta and FP Dousek. Some aspects of existence of elementary carbon with sp-hybridized bonds. *Carbon*, 18(6):433–437, 1980.

[15] PPK Smith and Peter R Buseck. Carbyne forms of carbon: do they exist? *Science*, 216(4549):984–986, 1982.

[16] Th Henning and F Salama. Carbon in the universe. *Science*, 282(5397): 2204–2210, 1998.

[17] Carlo S Casari, Matteo Tommasini, Rik R Tykwinski, and Alberto Milani. Carbon-atom wires: 1-d systems with tunable properties. *Nanoscale*, 8(8):4414–4435, 2016.

[18] Robert B Heimann, Jacob Kleiman, and Norman M Salansky. Structural aspects and conformation of linear carbon polytypes (carbynes). *Carbon*, 22(2):147–156, 1984.

[19] Franco Cataldo. *Polyynes: synthesis, properties, and applications*. CRC Press, 2005.

[20] Rik R Tykwinski, Wesley Chalifoux, Sara Eisler, Andrea Lucotti, Matteo Tommasini, Daniele Fazzi, Mirella Del Zoppo, and Giuseppe Zerbi. Toward carbyne: Synthesis and stability of really long polyynes. *Pure and Applied Chemistry*, 82(4):891–904, 2010.

[21] Mingchao Wang and Shangchao Lin. Ballistic thermal transport in carbyne and cumulene with micron-scale spectral acoustic phonon mean free path. *Scientific reports*, 5:18122, 2015.

[22] Ying Zhu, Hongcun Bai, and Yuanhe Huang. Electronic property modulation of one-dimensional extended graphdiyne nanowires from a first-principle crystal orbital view. *ChemistryOpen*, 5(1):78–87, 2016.

[23] Mingjie Liu, Vasilii I Artyukhov, Hoonkyung Lee, Fangbo Xu, and Boris I Yakobson. Carbyne from first principles: chain of c atoms, a nanorod or a nanorope. *ACS nano*, 7(11):10075–10082, 2013.

[24] Pavel B Sorokin, Hoonkyung Lee, Lyubov Yu Antipina, Abhishek K Singh, and Boris I Yakobson. Calcium-decorated carbyne networks as hydrogen storage media. *Nano letters*, 11(7):2660–2665, 2011.

[25] Sara Eisler, Aaron D Slepkov, Erin Elliott, Thanh Luu, Robert McDonald, Frank A Hegmann, and Rik R Tykwinski. Polyynes as a model for carbyne: synthesis, physical properties, and nonlinear optical response. *Journal of the American Chemical Society*, 127(8):2666–2676, 2005.

[26] Thomas Gibtner, Frank Hampel, Jean-Paul Gisselbrecht, and Andreas Hirsch. End-cap stabilized oligoynes: model compounds for the linear sp carbon allotrope carbyne. *Chemistry–A European Journal*, 8(2): 408–432, 2002.

[27] Wesley A Chalifoux, Robert McDonald, Michael J Ferguson, and Rik R Tykwinski. tert-butyl-end-capped polyynes: Crystallographic evidence of reduced bond-length alternation. *Angewandte Chemie International Edition*, 48(42):7915–7919, 2009.

[28] Alberto Milani, Matteo Tommasini, Mirella Del Zoppo, Chiara Castiglioni, and Giuseppe Zerbi. Carbon nanowires: Phonon and π-electron confinement. *Physical Review B*, 74(15):153418, 2006.

[29] RE Peierls. Quantum theory of solids. *London, England*, page 108, 1955.

[30] Shujiang Yang and Miklos Kertesz. Linear C_n clusters: Are they acetylenic or cumulenic? *The Journal of Physical Chemistry A*, 112 (1):146–151, 2008.

[31] Miklos Kertesz, Cheol Ho Choi, and Shujiang Yang. Conjugated polymers and aromaticity. *Chemical reviews*, 105(10):3448–3481, 2005.

[32] Johanna A Januszewski and Rik R Tykwinski. Synthesis and properties of long [n] cumulenes. *Chemical Society Reviews*, 43(9):3184–3203, 2014.

[33] Franco Cataldo. Stability of polyynes in air and their degradation by ozonolysis. *polymer degradation and stability*, 91(2):317–323, 2006.

[34] Franco Cataldo. Polyynes from submerged electric arc. iv. hydrogenation to ene–ynes. 2004.

[35] C S Casari, A Li Bassi, L Ravagnan, F Siviero, C Lenardi, P Piseri, G Bongiorno, C Bottani, and P Milani. Chemical and thermal stability of carbyne-like structures in cluster-assembled carbon films. *Physical review B*, 69(7):075422, 2004.

[36] Franco Cataldo. Storage stability of polyynes and cyanopolyynes in solution and the effect of ammonia or hydrochloric acid. *Fullerenes, Nanotubes, and Carbon Nanostructures*, 15(3):155–166, 2007.

[37] Wesley A Chalifoux and Rik R Tykwinski. Synthesis of polyynes to model the sp-carbon allotrope carbyne. *Nature chemistry*, 2(11):967, 2010.

[38] C S Casari, Valeria Russo, A Li Bassi, C Bottani, F Cataldo, A Lucotti, M Tommasini, M Del Zoppo, C Castiglioni, and G Zerbi. Stabilization of linear carbon structures in a solid ag nanoparticle assembly. *Applied physics letters*, 90(1):013111, 2007.

[39] Shu Okada, Minoru Fujii, and Shinji Hayashi. Immobilization of polyynes adsorbed on ag nanoparticle aggregates into poly (vinyl alcohol) films. *Carbon*, 49(14):4704–4709, 2011.

[40] Kang An, Guotong Wei, Gongmin Qi, Leimei Sheng, Liming Yu, Wei Ren, and Xinluo Zhao. Stability improvement of c8h2 and c10h2 embedded in poly (vinyl alcohol) films with adsorption on gold nanoparticles. *Chemical Physics Letters*, 637:71–76, 2015.

[41] Ryutaro Matsutani, Fumiyoshi Ozaki, Riyo Yamamoto, Tomoe Sanada, Yutaka Okada, and Kazuo Kojima. Preparation of polyynes up to c22h2 by liquid-phase laser ablation and their immobilization into sio2 gel. *Carbon*, 47(7):1659–1663, 2009.

[42] Lei Shi et al. Confined linear carbon chains as a route to bulk carbyne. *Nature materials*, 15(6):634–639, 2016.

[43] Dieter Bäuerle. *Laser processing and chemistry*. Springer Science & Business Media, 2013.

[44] Vincenzo Amendola and Moreno Meneghetti. What controls the composition and the structure of nanomaterials generated by laser ablation in liquid solution? *Physical Chemistry Chemical Physics*, 15(9):3027–3046, 2013.

[45] Antonio Miotello and Roger Kelly. Laser-induced phase explosion: new physical problems when a condensed phase approaches the thermodynamic critical temperature. *Applied Physics A*, 69(1):S67–S73, 1999.

[46] Daniel Werner, Akihiro Furube, Toshihiro Okamoto, and Shuichi Hashimoto. Femtosecond laser-induced size reduction of aqueous gold nanoparticles: In situ and pump- probe spectroscopy investigations revealing coulomb explosion. *The Journal of Physical Chemistry C*, 115 (17):8503–8512, 2011.

[47] R Fabbro, J Fournier, P Ballard, D Devaux, and J Virmont. Physical study of laser-produced plasma in confined geometry. *Journal of applied physics*, 68(2):775–784, 1990.

[48] B Toftmann, Jørgen Schou, and JG Lunney. Dynamics of the plume produced by nanosecond ultraviolet laser ablation of metals. *Physical Review B*, 67(10):104101, 2003.

[49] Zijie Yan and Douglas B Chrisey. Pulsed laser ablation in liquid for micro-/nanostructure generation. *Journal of Photochemistry and Photobiology C: Photochemistry Reviews*, 13(3):204–223, 2012.

[50] Tetsuo Sakka, Shuji Iwanaga, Yukio H Ogata, Akira Matsunawa, and Tadashi Takemoto. Laser ablation at solid–liquid interfaces: An approach from optical emission spectra. *The Journal of Chemical Physics*, 112(19):8645–8653, 2000.

[51] Carsten Momma, Boris N Chichkov, Stefan Nolte, Ferdinand von Alvensleben, Andreas Tünnermann, Herbert Welling, and Bernd Wellegehausen. Short-pulse laser ablation of solid targets. *Optics communications*, 129(1-2):134–142, 1996.

[52] Takeshi Tsuji, D-H Thang, Yuuki Okazaki, Masataka Nakanishi, Yasuyuki Tsuboi, and Masaharu Tsuji. Preparation of silver nanoparticles by laser ablation in polyvinylpyrrolidone solutions. *Applied Surface Science*, 254(16):5224–5230, 2008.

[53] Dmitry G Shchukin and Helmuth Möhwald. Sonochemical nanosynthesis at the engineered interface of a cavitation microbubble. *Physical Chemistry Chemical Physics*, 8(30):3496–3506, 2006.

[54] Tatiana E Itina. On nanoparticle formation by laser ablation in liquids. *The Journal of Physical Chemistry C*, 115(12):5044–5048, 2011.

[55] M Tsuji et al. Formation of hydrogen-capped polyynes by laser ablation of graphite particles suspended in solution. *Chemical physics letters*, 355(1-2):101–108, 2002.

[56] Masaharu Tsuji, Shingo Kuboyama, Toshinori Matsuzaki, and Takeshi Tsuji. Formation of hydrogen-capped polyynes by laser ablation of c60 particles suspended in solution. *Carbon*, 41(11):2141–2148, 2003.

[57] Ryutaro Matsutani, Takuya Kakimoto, Kosuke Wada, Tomoe Sanada, and Hiromasa Tanaka. Preparation of long-chain polyynes c18h2 and c20h2 by laser ablation of pellets of graphite and perylene derivative in liquid phase. *Carbon (New York, NY)*, 46(7):1103–1106, 2008.

[58] Kohei Inoue, Ryutaro Matsutani, Tomoe Sanada, and Kazuo Kojima. Preparation of long-chain polyynes of c24h2 and c26h2 by liquid-phase laser ablation in decalin. *Carbon*, 48(14):4209–4211, 2010.

[59] Ryutaro Matsutani, Kohei Inoue, Tomoe Sanada, Noriyuki Wada, and Kazuo Kojima. Preparation of long-chain polyynes of c28h2 and c30h2 by liquid-phase laser ablation. *Journal of Photochemistry and Photobiology A: Chemistry*, 240:1–4, 2012.

[60] Giuseppe Compagnini, Valentina Mita, Rosario Sergio Cataliotti, Luisa D'Urso, and Orazio Puglisi. Short polyyne chains produced by pulsed laser ablation of graphite in water. *Carbon*, 45:2445–58, 2007.

[61] Ryutaro Matsutani, Takuya Kakimoto, Hiromasa Tanaka, and Kazuo Kojima. Preparation of polyynes by liquid-phase laser ablation using different irradiation target materials and solvents. *Carbon*, 49(1):77–81, 2011.

[62] Seung-Keun Shin and Seung-Min Park. Preparation of polyynes by the laser ablation of graphite in water and organic solvents. *Bulletin of the Korean Chemical Society*, 33(2):597–600, 2012.

[63] A Hu, J Sanderson, AA Zaidi, C Wang, T Zhang, Y Zhou, and WW Duley. Direct synthesis of polyyne molecules in acetone by dissociation using femtosecond laser irradiation. *Carbon*, 46(13):1823–1825, 2008.

[64] Peter Siemsen, Robert C Livingston, and François Diederich. Acetylenic coupling: a powerful tool in molecular construction. *Angewandte Chemie International Edition*, 39(15):2632–2657, 2000.

[65] Vincenzo Amendola and Moreno Meneghetti. Laser ablation synthesis in solution and size manipulation of noble metal nanoparticles. *Physical chemistry chemical physics*, 11(20):3805–3821, 2009.

[66] Hiroshi Tabata, Minoru Fujii, and Shinji Hayashi. Laser ablation of diamond nanoparticles suspended in solvent: synthesis of polyynes. *Chemical physics letters*, 395(1-3):138–142, 2004.

[67] Hiroshi Tabata, Minoru Fujii, Shinji Hayashi, Tatsuya Doi, and Tomonari Wakabayashi. Raman and surface-enhanced raman scattering of a series of size-separated polyynes. *Carbon*, 44(15):3168–3176, 2006.

[68] Tomonari Wakabayashi, Mao Saikawa, Yoriko Wada, and Toshie Minematsu. Isotope scrambling in the formation of cyanopolyynes by laser ablation of carbon particles in liquid acetonitrile. *Carbon*, 50(1):47–56, 2012.

[69] Alberto Milani, Matteo Tommasini, Valeria Russo, Andrea Li Bassi, Andrea Lucotti, Franco Cataldo, and Carlo S Casari. Raman spectroscopy as a tool to investigate the structure and electronic properties of carbon-atom wires. *Beilstein journal of nanotechnology*, 6(1):480–491, 2015.

[70] Alberto Milani, Matteo Tommasini, and Giuseppe Zerbi. Connection among raman wavenumbers, bond length alternation and energy gap in polyynes. *Journal of Raman Spectroscopy: An International Journal for Original Work in all Aspects of Raman Spectroscopy, Including Higher Order Processes, and also Brillouin and Rayleigh Scattering*, 40 (12):1931–1934, 2009.

[71] J Kastner, H Kuzmany, L Kavan, FP Dousek, and J Kürti. Reductive preparation of carbyne with high yield. an in situ raman scattering study. *Macromolecules*, 28(1):344–353, 1995.

[72] Roberto Pilot, Raffaella Signorini, Christian Durante, Laura Orian, Manjari Bhamidipati, and Laura Fabris. A review on surface-enhanced raman scattering. *Biosensors*, 9(2):57, 2019.

[73] Andrea Lucotti, Matteo Tommasini, Mirella Del Zoppo, Chiara Castiglioni, Giuseppe Zerbi, Franco Cataldo, Carlo Spartaco Casari, Andrea Li Bassi, Valeria Russo, M Bogana, et al. Raman and sers investigation of isolated sp carbon chains. *Chemical physics letters*, 417(1-3): 78–82, 2006.

[74] Ivano E Castelli, Paolo Salvestrini, and Nicola Manini. Mechanical properties of carbynes investigated by ab initio total-energy calculations. *Physical Review B*, 85(21):214110, 2012.

[75] Ovidiu Cretu et al. Electrical transport measured in atomic carbon chains. *Nano letters*, 13(8):3487–3493, 2013.

[76] Alberto D Scaccabarozzi, Alberto Milani, Sonia Peggiani, Stefano Pecorario, Bozheng Sun, Rik R Tykwinski, Mario Caironi, and Carlo S Casari. A field-effect transistor based on cumulenic sp-carbon atomic wires. *The journal of physical chemistry letters*, 11(5):1970–1974, 2020.

[77] Fanghao Hu, Chen Zeng, Rong Long, Yupeng Miao, Lu Wei, Qizhi Xu, and Wei Min. Supermultiplexed optical imaging and barcoding with engineered polyynes. *Nature methods*, 15(3):194, 2018.

[78] AL Ivanovskii. Graphynes and graphdyines. *Progress in Solid State Chemistry*, 41(1-2):1–19, 2013.

[79] Veena Choudhary and Anju Gupta. Polymer/carbon nanotube nanocomposites. *Carbon nanotubes-polymer nanocomposites*, 2011:65–90, 2011.

[80] Rupali Gangopadhyay and Amitabha De. Conducting polymer nanocomposites: a brief overview. *Chemistry of materials*, 12(3):608–622, 2000.

[81] Mingfa Zhang, Yang Li, Zhiqiang Su, and Gang Wei. Recent advances in the synthesis and applications of graphene–polymer nanocomposites. *Polymer Chemistry*, 6(34):6107–6124, 2015.

[82] Subhadip Mondal, Lalatendu Nayak, Mostafizur Rahaman, Ali Aldalbahi, Tapan K Chaki, Dipak Khastgir, and Narayan Ch Das. An effective strategy to enhance mechanical, electrical, and electromagnetic shielding effectiveness of chlorinated polyethylene-carbon nanofiber nanocomposites. *Composites Part B: Engineering*, 109:155–169, 2017.

[83] Orna Breuer and Uttandaraman Sundararaj. Big returns from small fibers: a review of polymer/carbon nanotube composites. *Polymer composites*, 25(6):630–645, 2004.

[84] Jijun Zeng, Bethany Saltysiak, WS Johnson, David A Schiraldi, and Satish Kumar. Processing and properties of poly (methyl methacrylate)/carbon nanofiber composites. *Composites Part B: Engineering*, 35(3):245–249, 2004.

[85] Mohammad Moniruzzaman and Karen I Winey. Polymer nanocomposites containing carbon nanotubes. *Macromolecules*, 39(16):5194–5205, 2006.

[86] Rodney Andrews, David Jacques, Mickael Minot, and Terry Rantell. Fabrication of carbon multiwall nanotube/polymer composites by shear mixing. *Macromolecular Materials and Engineering*, 287(6):395–403, 2002.

[87] S Bal and SS Samal. Carbon nanotube reinforced polymer composites—a state of the art. *Bulletin of Materials Science*, 30(4):379, 2007.

[88] Dongyu Cai and Mo Song. Recent advance in functionalized graphene/polymer nanocomposites. *Journal of Materials Chemistry*, 20(37):7906–7915, 2010.

[89] Xiao-Lin Xie, Yiu-Wing Mai, and Xing-Ping Zhou. Dispersion and alignment of carbon nanotubes in polymer matrix: a review. *Materials science and engineering: R: Reports*, 49(4):89–112, 2005.

[90] Hyunwoo Kim, Ahmed A Abdala, and Christopher W Macosko. Graphene/polymer nanocomposites. *Macromolecules*, 43(16):6515–6530, 2010.

[91] Florian H Gojny, Malte HG Wichmann, Bodo Fiedler, Wolfgang Bauhofer, and Karl Schulte. Influence of nano-modification on the mechanical and electrical properties of conventional fibre-reinforced composites. *Composites Part A: Applied Science and Manufacturing*, 36 (11):1525–1535, 2005.

[92] Bani H Cipriano, Arun K Kota, Alan L Gershon, Conrad J Laskowski, Takashi Kashiwagi, Hugh A Bruck, and Srinivasa R Raghavan. Conductivity enhancement of carbon nanotube and nanofiber-based polymer nanocomposites by melt annealing. *Polymer*, 49(22):4846–4851, 2008.

[93] ES Choi, JS Brooks, DL Eaton, MS Al-Haik, MY Hussaini, H Garmestani, D Li, and K Dahmen. Enhancement of thermal and electrical properties of carbon nanotube polymer composites by magnetic field processing. *Journal of Applied physics*, 94(9):6034–6039, 2003.

[94] Monika Tyagi and Dhruv Tyagi. Polymer nanocomposites and their applications in electronics industry. *Int. J. Electron. Electr. Eng*, 7(6): 603–608, 2014.

[95] Ray H Baughman, Anvar A Zakhidov, and Walt A De Heer. Carbon nanotubes–the route toward applications. *science*, 297(5582):787–792, 2002.

[96] JKWea Sandler, JE Kirk, IA Kinloch, MSP Shaffer, and AH Windle. Ultra-low electrical percolation threshold in carbon-nanotube-epoxy composites. *Polymer*, 44(19):5893–5899, 2003.

[97] Yonglai Yang, Mool C Gupta, and Kenneth L Dudley. Towards cost-efficient emi shielding materials using carbon nanostructure-based nanocomposites. *Nanotechnology*, 18(34):345701, 2007.

[98] L Kavan. Electrochemical carbonization of fluoropolymers. *Chemistry and physics of carbon*, 23:69–171, 1991.

[99] Sibananda Sana and Chandan Adhikary. Synthesis and entrapment of polyynes inside nano-pores of anodized alumina membrane: A linear allotrope of carbon. *International Journal for Science and Advance Research in Technology (IJSART)*, 3(9):400–406, 2009.

[100] R Sata, H Suzuki, N Ueno, Y Morisawa, M Hatanaka, and T Wakabayashia. Uv-polarizing linear polyyne molecules aligned in pva. *Chinese Journal of Chemical Physics*, 32(2):175–181, 2019.

[101] Sonia Peggiani, Anna Facibeni, Alberto Milani, Chiara Castiglioni, Valeria Russo, Andrea Li Bassi, and Carlo S Casari. In situ synthesis of polyynes in a polymer matrix by pulsed laser ablation in liquid. *arXiv preprint arXiv:2006.15025*, 2020.

[102] Zeena S Pillai and Prashant V Kamat. What factors control the size and shape of silver nanoparticles in the citrate ion reduction method? *The Journal of Physical Chemistry B*, 108(3):945–951, 2004.

[103] John A Young, Kieran T Lynch, Anton J Walsh, and Albert A Ruth. Generation of noble metal nanoparticles by laser ablation in liquids: the role of the molecular environment. In *Opto-Ireland 2005: Nanotechnology and Nanophotonics*, volume 5824, pages 138–148. International Society for Optics and Photonics, 2005.

[104] Vincenzo Amendola, Stefano Polizzi, and Moreno Meneghetti. Free silver nanoparticles synthesized by laser ablation in organic solvents and their easy functionalization. *Langmuir*, 23(12):6766–6770, 2007.

[105] Giuseppe Compagnini, Alessandro A Scalisi, and Orazio Puglisi. Ablation of noble metals in liquids: a method to obtain nanoparticles in a thin polymeric film. *Physical Chemistry Chemical Physics*, 4(12): 2787–2791, 2002.

[106] Dongshi Zhang and Stephan Barcikowski. Rapid nanoparticle-polymer composites prototyping by laser ablation in liquids. *Encyclopedia of polymeric nanomaterials*, 2131:2141, 2015.

[107] Dongshi Zhang and Bilal Gökce. Perspective of laser-prototyping nanoparticle-polymer composites. *Applied Surface Science*, 392:991–1003, 2017.

[108] NG Semaltianos, W Perrie, S Romani, RJ Potter, G Dearden, and KG Watkins. Polymer-nanoparticle composites composed of pedot: Pss and nanoparticles of ag synthesised by laser ablation. *Colloid and Polymer Science*, 290(3):213–220, 2012.

[109] AS Nikolov et al. Influence of the liquid level and ablation process duration on the characteristics of nanostructures created by nanosecond laser ablation of ag in water. In *19th International Conference and School on Quantum Electronics: Laser Physics and Applications*, volume 10226, page 102260C. International Society for Optics and Photonics, 2017.

[110] Philipp Wagener, Gudrun Brandes, Andreas Schwenke, and Stephan Barcikowski. Impact of in situ polymer coating on particle dispersion into solid laser-generated nanocomposites. *Physical Chemistry Chemical Physics*, 13(11):5120–5126, 2011.

[111] J Bosbach, D Martin, F Stietz, T Wenzel, and F Träger. Laser-based method for fabricating monodisperse metallic nanoparticles. *Applied physics letters*, 74(18):2605–2607, 1999.

[112] Luisa D'Urso, Giuseppe Grasso, Elena Messina, Corrado Bongiorno, Viviana Scuderi, Silvia Scalese, Orazio Puglisi, Giuseppe Spoto, and Giuseppe Compagnini. Role of linear carbon chains in the aggregation of copper, silver, and gold nanoparticles. *The Journal of Physical Chemistry C*, 114(2):907–915, 2010.

[113] A Kucherik, S Arakelian, T Vartanyan, S Kutrovskaya, A Osipov, A Povolotskaya, A Povolotskii, and A Man'shina. Laser-induced synthesis of metal–carbon materials for implementing surface-enhanced raman scattering. *Optics and spectroscopy*, 121(2):263–270, 2016.

[114] Kuk Ki Kim, Seung Keun Shin, and Seung Min Park. Aggregation of polyynes on metal nanoparticles. *Bulletin of the Korean Chemical Society*, 33(2):625–628, 2012.

[115] PC Lee and D Meisel. Adsorption and surface-enhanced raman of dyes on silver and gold sols. *The Journal of Physical Chemistry*, 86(17): 3391–3395, 1982.

[116] HA Willis, VJI Zichy, and PJ Hendra. The laser-raman and infra-red spectra of poly (methyl methacrylate). *Polymer*, 10:737–746, 1969.

[117] George A Pitsevich, Ekaterina Kozlovskaya, and Iryna Doroshenko. Analysis of the carbonyl group stretching vibrations in some structural fragments of poly-3-hydroxybutyrate. *arXiv preprint arXiv:1604.00815*, 2016.